UNIVERSITÀ
DEGLI STUDI
DI PADOVA

Sede Amministrativa: Università degli Studi di Padova
Dipartimento di Scienze Chimiche

Scuola di Dottorato di Ricerca in Scienza e Ingegneria dei Materiali
XXV Ciclo

Materials and methods for modular microfluidic devices

Direttore della Scuola: Ch.mo Prof. Gaetano Granozzi
Supervisore: Ch.mo Prof. Camilla Ferrante

Dottorando: Nicola Rossetto

Abstract (English version)

This thesis work concerns the investigation of materials and methods that can be applied to the realization of microfluidic devices (MFDs). In particular, the attention is placed on modular MFDs, as opposed to fully integrated ones. The reasons behind this choice are given in detail in Section 1.2 of this work, but they can be here summarized in the fact that while integrated MFDs offer great advantages in terms of portability, modular devices are more versatile, and so particularly well suited for research applications.

The first part of the work here reported describes the microfabrication techniques employed for the realization of single-function microfluidic modules. Devices have been fabricated through PDMS replica molding from SU-8 masters. Masters have been in turn realized through masked UV-lithography or one- or two-photon direct laser writing, depending on the resolution requirements. The replica molding method is a very fast and efficient way to realize MFDs, but suffers from some limitations in the structure shapes that can be successfully replicated. In light of this, a photopolymerizable hybrid organic/inorganic sol-gel blend is proposed and tested as alternative material for MFDs fabrication. The characterization results reveal that this material is biocompatible and features better mechanical properties than PDMS, but structures with more than one dimension exceeding a few micrometers tend to crack during fabrication, making this blend unusable as bulk material. Still, this material could be efficiently employed to fabricate sub-structuration inside PDMS channels.

Following this investigation on materials, a microfluidic mixing module is proposed and tested. Since laminar flow conditions dominate inside microchannels, efficient mixing in MFDs require the use of specifically designed mixers. The proposed module makes use of obstructions inside a microchannel to perturb the laminar flow and thus enhance mixing of two species. The most efficient geometries have been selected with the aid of numerical simulations, and two promising layouts have been fabricated and

experimentally tested by measuring the dilution of a fluorophore (mixing between a fluorophore solution and pure solvent) through confocal fluorescence microscopy.

Thirdly, the fabrication and characterization of an optofluidic light switching module is reported. This device employs a water/air segmented flow generated by a T-junction to alternatively transmit or total-reflect a laser beam. This deflection is proved to be periodical, and its frequency can be varied nonlinearly by adjusting the injection flow rates of air and water. The duty cycle of the module is also characterized, and a method to modulate it by increasing the water temperature is proposed and verified.

Finally, a number of attempts to generate a nanoporous, low refractive index PDMS are described. The identification of an efficient procedure to fabricate this kind of material would lead to the possibility of using common microfluidic channels as water-core waveguides. To date, these attempts have not been totally successful, but critical points are identified, and viable strategies for future works on the subject are proposed.

Abstract (Versione italiana)

Questo lavoro di tesi tratta dello studio di materiali e metodi che possono essere applicati alla realizzazione di dispositivi microfluidici (DMF). In particolare l'attenzione è rivolta ai dispositivi modulari, piuttosto che a quelli altamente integrati. Le ragioni dietro questa scelta sono spiegate in dettaglio nella Sezione 1.2 di questa tesi, ma possono essere qui sintetizzate nel fatto che anche se i DMF integrati offrono grandi vantaggi in termini di dimensioni finali, i dispositivi modulari sono più versatili, e quindi particolarmente utili per applicazioni nel campo della ricerca.

La prima parte del lavoro qui riportato descrive le tecniche di microfabbricazione utilizzate per la realizzazione di moduli microfluidici monofunzionali. I dispositivi sono stati realizzati per *replica molding* in PDMS a partire da master in SU-8. I master sono stati a loro volta fabbricati tramite litografia UV con maschera oppure per scrittura laser diretta ad uno o due fotoni, a seconda dei requisiti di risoluzione. Il *replica molding* è un metodo molto rapido ed efficiente per realizzare DMF, ma presenta alcuni limiti per quanto riguarda la forma delle strutture che è possibile replicare con successo. Alla luce di questo, un sol-gel fotopolimerizzabile ibrido organico/inorganico viene qui proposto e testato come materiale alternativo per la fabbricazione di DMF. I risultati della caratterizzazione rivelano che questo materiale è biocompatibile e presenta proprietà meccaniche migliori di quelle del PDMS, ma strutture con più di una dimensione eccedente i pochi micrometri tendono a sviluppare cricche, cosa che impedisce l'utilizzo di questo sol-gel come materiale massivo. Ciononostante, questo sol-gel potrebbe venir efficacemente impiegato per la realizzazione di sottostrutturazioni all'interno di canali microfluidici.

Dopo questo studio sui materiali, un modulo microfluidico per il mescolamento è proposto e testato. Dato che le condizioni di flusso laminare sono dominanti all'interno dei microcanali, per ottenere un mescolamento efficiente in un DMF è necessario includere nel dispositivo un miscelatore specificatamente progettato. Il modulo proposto

utilizza delle ostruzioni all'interno del microcanale per perturbare il flusso laminare e quindi favorire il mescolamento. Con l'aiuto di alcune simulazioni numeriche, le geometrie più efficienti sono state individuate, e due layout particolarmente promettenti sono stati realizzati e caratterizzati sperimentalmente misurando la diluizione di un fluoroforo (mescolamento tra una soluzione del fluoroforo e puro solvente) attraverso la microscopia confocale di fluorescenza.

A seguire, viene riportata la fabbricazione e caratterizzazione di un modulo optofluidico per la deflessione della luce. Questo dispositivo utilizza un flusso segmentato acqua/aria generato da una giunzione a T per trasmettere o riflettere (per riflessione totale interna) alternativamente un fascio laser. Questa alternanza è periodica, e la sua frequenza può essere controllata variando la portata dei flussi iniettati di aria e acqua. Inoltre, il *duty cycle* del modulo è stato caratterizzato, e viene proposto e verificato un metodo per modularlo attraverso un aumento della temperatura dell'acqua.

Infine, vengono descritti alcuni tentativi di generare un PDMS nanoporoso con basso indice di rifrazione. La messa a punto di una procedura efficiente per la fabbricazione di questo genere di materiale porterebbe alla possibilità di usare i classici canali microfluidici come guide d'onda. Al momento questi tentativi hanno avuto solo parziale successo, ma i maggiori punti di criticità sono stati identificati, e vengono proposte alcune strategie per il loro futuro superamento.

Contents

Introduction

Since their initial diffusion about 10 years ago, microfluidic devices (MFDs) have captivated much attention in both academic and industrial environments. This interest is due to the many advantageous characteristics of microfluidics for a number of different applications ranging from chemical synthesis to sensing to sample characterization. The inclusion of light exploitation inside microfluidic devices (optofluidics) further expanded the field of applicability, and thus the attention given to this branch of science.

Abreast with the design of progressively more complex MFDs, increasingly sophisticated fabrication techniques have been developed to allow the actual realization of such devices. To date, a vast range of materials can be microstructured with resolutions ranging from hundreds of micrometers to hundreds or even tens of nanometers. This possibility has in turn allowed the realization of extremely complex devices with thousands of channels and fluidic elements like valves, pumps or mixers. On the other end, such high integration is often tied to technical challenges that can require much work to overcome. Because of this, the very last years have seen the appearance of modular microdevices in which compactness and portability are slightly reduced in exchange for increased flexibility and ease of fabrication. Following this approach, instead of realizing a single, integrated microfluidic chip able to perform all the operations required to obtain the final result, a number of free-standing, single-function modules are connected to achieve the same end. The work reported in this thesis follows this modular philosophy, and proposes two single-function modules, along with the techniques to produce these and other microfluidic elements.

The **first chapter** (Overview on Microfluidics) offers a wide overview on the field of microfluidics, starting with its applications and proceeding to describe the elements most commonly present in a MFD along with the materials and fabrication techniques used to realize them. Finally, a section is dedicated to the field of optofluidics.

The **second chapter** (Microfabrication) explains the fabrication techniques used in this work. The first part of the chapter describes the main procedure employed to realize the modules shown in subsequent chapters, i.e. PDMS replica molding from masters obtained through UV photolithography and direct laser writing. Following that, the characterization of a new photopolimerizable hybrid organic/inorganic sol-gel material is performed. This second material has better mechanical properties and chemical resistance than PDMS, and is presented as a candidate for internal channel sub-structurations that require these improved qualities.

The **third chapter** (Microfluidic Mixer) introduces the problem of mixing inside microchannels. Due to the dominant laminar flow conditions, chaotic motion is strongly inhibited in microdevices. Without specifically designed mixers, mixing can only happen through free diffusion, a process too slow for many applications. A qualitative demonstration of this is given in the first part of the chapter, followed by the presentation of a mixing module based on a partially obstructed channel. The module design is optimized through the use of numerical simulations, and two promising layouts are experimentally tested using the dilution of a fluorescent molecule as indicator of mixing efficiency.

The **fourth chapter** (Optofluidic Optical Switch) presents a light-controlling module for optofluidic applications. This device exploits a water/air segmented flow to alternatively transmit and total-reflect a laser beam shone on the channel. The result is a periodic deflection of the light towards one of two well-defined directions. The response in terms of frequency of the device to varying injection flow rates is characterized, along with eventual variations in the duty cycle (fraction of the total period spent by the laser beam in the reflected state). Since the duty cycle appears to be constant at all tested flow rates, an alternative method to modulate it (a variation in water temperature) is proposed and verified.

The **fifth chapter** (Water-Core PDMS Waveguide) describes a series of attempts to realize a nanoporous, low refractive index PDMS. Such a material could be employed

as cladding for a water-core waveguide, and the direct consequence would be the possibility of using common microfluidic channels as optical waveguides. While these first attempts have not been entirely successful, the most critical point have been identified and discussed, and possible strategies for future works are presented.

Finally, the **Conclusions** offer a summary of the results obtained during this work, as well as observation concerning the drawbacks and limitations of these materials and modules.

Chapter 1

OVERVIEW ON MICROFLUIDICS

1.1 Microfluidic devices

Microfluidics can be defined as the field of science and technology concerning itself with devices that employ tiny volumes of fluids, on the order of 10^{-6} to 10^{-15} liters[1]. While its origins go back to the first studies on capillaries, it can be stated without any fear of denial that microfluidics enjoyed a true development only in the last 10 years. This recent evolution is both due to new microfabrication technologies that allow scientists to build complex devices and to the increasing awareness that the peculiar behavior of fluids on such a small scale can be exploited in a vast number of possible applications. All these particular features can be related to two characteristics of microfluidic devices (MFDs): a very high surface to volume ratio and a low Reynolds number.

Since MFDs (also known as “microfluidic chips”) work with such tiny amount of fluid, it is unavoidable that the channels inside which the liquid flows will be very thin. This directly translates into the high surface to volume ratio mentioned before. This characteristic can be a welcome boon for any application that requires very fine control over the fluid condition, since the small volume will ensure that any gradient present will be very limited in extent. Also, the large superficial area allows easy access to the fluid to support functions like heaters. Conversely, this also allows fast dispersion of any undesired heat produced, for example, during a chemical reaction. Another advantage related to using small quantities of fluid becomes evident when such fluid is toxic, unstable or dangerous in any other way: if an accident occurs, the volume of fluid involved is so minimal that the danger to the user is very limited. Finally, vast surfaces mean that capillarity and, more in general, interfacial forces will be dominant over volume-related ones like gravity. In other words, usually fluids inside MFDs do not freely fall and the device works just the same even upside down.

The second characteristic is somewhat less intuitive. Fluids inside microchannels usually benefit (or suffer, depending on the desired application) from a low Reynolds number (Re). This dimensionless quantity is defined as[2,3]:

$$\mathrm{Re} = \frac{\rho u L}{\mu} = \frac{u L}{\nu} \qquad (1.1)$$

where ρ is the density of the fluid, μ its (dynamic) viscosity, $\nu = \mu/\rho$ its kinematic viscosity, u its mean velocity and L the characteristic length of the system (i.e., in this case, the diameter or side length of the channel).

The Reynolds number quantifies the ratio between inertial and viscous forces inside the fluid in a given system. If Re is low, viscous forces are prevailing and the flow is said to be laminar. In laminar flow the fluid moves in parallel layers, and its velocity has only one vectorial component (parallel to the fluid layers planes). If Re is high, inertial forces are prevailing and the flow is turbulent (chaotic). When flowing inside a tube or channel, the fluid is characterized by laminar flow if Re < 2300 and turbulent if Re > 4000, with an intermediate region where both flows are possible. From equation (1.1) it can be seen that any fluid can be made to flow in the laminar regime if its velocity and the characteristic length of the system are small enough. How much small depends on the fluid viscosity.

In microfluidic devices, both kind of flows could be desired, depending on the intended application. Laminar flows inhibit mixing between two substances, since molecules can travel between flowing layers only by diffusion, which is a relatively slow process that can sorely limit the efficiency of any device that relies on the mixing of two reagents (e.g. microreactors for chemical synthesis). On the other hand, turbulent flows allow very fast mixing, but being chaotic they are very difficult to model or characterize, and so the conditions of the turbulent fluid inside the channels are largely unknown. Now, considering a typical microfluidic device with water (μ ~1 cP) flowing inside a 100 μm wide square channel, to achieve turbulent flow conditions (Re > 4000) the fluid should be flowing with a mean velocity of 40 m/s. This velocity is extremely high, equivalent

to a flow rate of 3.6 l/h, and this means that almost always the flow inside a microchannel will be laminar. Thus, the flowing conditions of fluids inside MFD are generally stable and often quite easy to predict. Unfortunately, laminar behavior also means that spontaneous mixing inside a microchannel is almost always strongly inhibited, and for many MFDs this can be a problem not easily solved (more on this subject in Section 1.3.3).

1.1.1 Microreactors

One of the first developed applications for MFDs are microreactors, i.e. devices for chemical synthesis. The reasons for this are quite straightforward, once considered the characteristics of microdevices: the reaction conditions can be finely tuned and the small volumes handled allow minimizing the danger of hazardous reagents or reactions. Because of this, MFDs have been particularly studied for chemical processes that involve explosive reagents or intermediates, or for reactions that synthesize toxic products (e.g. chemotherapeutical drugs). As an example of handling potentially dangerous reactions, deMello et al. have realized a microfluidic device for the conversion of α-terpinene into ascaridole[4]. This synthesis requires the use of strong light to excite a sensitizing dye which in turn generates singlet oxygen from air or pure oxygen. The gas reacts then with α-terpinene (in methanol solution) to give ascaridole. Unfortunately, oxygenated organic solvents are explosive, which means that in macro-scale synthesis large volumes of dangerous reagents are formed during the process. In the MFD oxygen, dye and α-terpinene are all flowed inside a microchannel which is placed under a light source. In this way only a tiny volume of oxygenated sample is generated in any given moment, essentially removing safety concerns. Another example comes from Zhang et al. and regards the use of ethyl diazoacetate[5]. This reagent is flammable, and releases gaseous N_2 if heated, resulting in an explosive behavior. The authors proposed a microfluidic device for the ring-expansion reaction shown in Figure 1.1. This reaction is not only strongly exothermic, but also releases gaseous nitrogen as

Figure 1.1: ring expansion reaction requiring ethyl diazoacetate. The explosive behavior of this reagent, added to the exothermic nature of the reaction makes microreactors the preferable vessel to handle this synthesis.

a secondary product, maximizing the risk of vessel overpressure and possibly explosion. Once again, these hazards are greatly reduced due to the small volumes of reagents (which minimize the amount of reactive involved in case of incident) and to the high surface to volume ratio of the microchannels, which provides rapid dissipation of generated heat. In general, it is worth of note that in principle a microfluidic device can be a network of channels completely isolated from the external environment, which makes MFDs the best solution for user safety not only in case of incident, but also for day-to-day operations involving toxic reagents. Of course, small volumes also mean small throughput, but this limit can be overcome by using multiple MFDs in parallel. In this way, all the beneficial characteristics are maintained for every single device, but the final throughput is multiplied by the number of MFDs used.

Another useful characteristics of MFDs for chemical synthesis is the possibility of generating dangerous reagents directly *in situ*. Since in a microdevice the reagents flow along microchannels until they meet other substances, react and are then collected as products, it is easy to imagine that a parallel channel on the same device can be used to synthesize the dangerous or unstable substance that is then injected into the main channel where the other reagents for the main reaction are flowing. Once again, this approach can maximize operator safety. Kim et al. used a similar approach to perform a series of reactions involving diazomethane[6]. Diazomethane is an extremely dangerous gas, being toxic, carcinogenic and explosive (as well as odorless). The authors realized a MFD featuring two parallel channels separated by a thin gas-permeable membrane. The diazomethane is generated *in situ* in the first channel by reacting N-methyl-N-nitroso-p-toluenesulfonamide (Diazald) with a strong base in aqueous solution. While

reagents and secondary products continue along the channel and are collected as waste, the gas migrates through the membrane to the adjacent channel, ready to react. The authors tested various reactions by flowing different precursors in the second channel and measuring the product yield at the outlet. As in the previous examples, risks for operators are minimized by working (at any given moment) with only small quantities of dangerous reagents, and in this case the hazardous species is created and reacted inside the isolated environment of the MFD.

Microfluidic reactors also offer potential advantages from an industrial point of view. Currently, most of the synthesis are done in large batch reactors. This poses several disadvantages. First of all, it is difficult to maintain the exactly same conditions (temperature, concentration, etc.) across all the reactor. MFDs can help solve this problem, as already mentioned above. Also, batch reactors are necessarily discontinuous processes, since the reactor must be filled with reagents, allowed to perform the reaction and finally emptied of all products. On the contrary, a MFD is intrinsically continuous, since reagents are pumped at the inlet, react as they flow and are finally collected at the end of the channels network. From the industry point of view, the advantages of continuous processes over discontinuous ones are quite evident: much less automation is required and unproductive time losses are essentially eliminated.

An almost inescapable limitation of MFDs for chemical synthesis is their vulnerability to channel clogging. Since typical microfluidic channels sport dimensions on the order of hundreds of micrometers, any solid impurity that manages to get inside a MFD will usually dam one of the channels, effectively ruining the device. While this problem is usually not severe enough to require solvent filtration, it will bar any chemical reaction that generate precipitate from being performed in MFDs. In theory, small amounts of solid matter can be carried by the liquid flow without harm to the device, but this practice is risky, since any unexpected increase in precipitate generation will probably ruin the chip. Also, safeguards must be included in the pumping system, since a clogged

channel will cause a strong overpressure inside the MFD, possibly to the point of leakage of (potentially dangerous) reagents if not outright chip explosion.

1.1.2 Micro total analysis systems

Another field that has been vastly explored by microfluidic applications is that of sample characterization. The interest for this kind of systems is so huge that "micro total analysis system" (μTAS) has basically become a synonym for "microfluidic device". These MFDs can be roughly divided in two broad categories: devices for quality control and devices for the detection or characterization of analytes. The principles behind both kind of devices are mostly the same, but the required characteristics for such MFDs can be markedly different. The base idea upon which all these systems are founded is that of creating a platform where the sample is injected at the inlet, analyzed while it flows along the channels network and finally collected or disposed of (depending on the destructiveness of the analysis) at the outlet.

Devices for quality control give their best when thought of in association with microfluidic reactors. It is very easy to imagine a MFD where the product is synthesized and immediately characterized just by adding the analysis system at the end of the synthesis channel(s). More importantly, a feedback system can be implemented so that any imperfection detected by the analysis translates immediately into a modification of the reaction conditions until the proper product is once again synthesized. As before, from an industrial point of view the advantages of these systems are noteworthy. As an example, McMullen and Jensen realized a device composed of a first channel network for chemical synthesis followed by an HPLC set-up to analyze the reaction products[7]. An automated optimization routine checks the characterization results and if necessary modifies reaction parameters (solvent concentration, reaction time and temperature). This device was used in particular to optimize the yield of intermediate benzaldehyde in the benzyl alcohol to benzoic acid conversion.

The main requirement from this kind of characterization devices is that the analysis performed must be non-destructive, since it will be performed on the totality of the product. Another important point is that the analysis should be fast. Even time-consuming characterizations can be implemented in a MFD simply by increasing the analysis channel length (and thus the time required for the fluid to pass through), but in this case the feedback system will suffer from a possibly large delay, strongly decreasing its efficiency. In light of these requirements, most of the quality control devices are based on spectroscopic techniques. In the overwhelming majority of the cases, the light is generated, collected and analyzed outside of the MFD due to the difficulty of integrating such functions into a microdevice (but see Section 1.5). This translates into the necessity for non-miniaturized equipment surrounding the device, but this is typically of little consequence for an industrial set-up where these devices are not meant to be moved. Alternatively, chromatographic systems, while more time-consuming than spectroscopic ones, can double as purification steps and as such are also object of frequent investigation.

Devices for detection or sample characterization feature a different set or requirements. First of all they do not need the analysis to be either fast nor non-destructive. Both qualities would be an add-on, but they are no longer a strict requirement since there is no need for fast feedback, and only a part of the sample will be analyzed. This opens the door for an enormous range of possible characterizations that can be implemented, from electrochemical to chromatographic to colorimetric and so on. However, most of these devices are intended to be moved quite often, and so need to be portable. This immediately excludes light-based characterizations unless light source and detector can be integrated into a chip (or are available everywhere, e.g. the sun as source and the eye as detector). Obviously, in a portability contest MFDs have by their own nature a lead start over most other devices, and so much of the research effort has gone into realizing compact and portable μTAS. Such a platform would be of great values for many analysis (e.g. environmental) that currently are often made by collecting the sample on

the field, transporting it to a lab and performing the analysis there. The possibility to complete all the required steps directly on the field would be a great advancement in terms of costs and time. On this subject, Beaton et al. realized a MFD for the quantification of nitrite in seawater for environmental purposes[8]. The chip exploited a colorimetric method (the Griess assay) to measure the analyte concentration. All the device, including supporting instrumentation like power sources or detectors, was included in a 16x30 cm cylinder, and its capabilities were demonstrated by a 57-hours field test in ocean water.

There is another advantage of microdevices related to their small dimensions: only tiny volumes of sample are required. This is of great importance when the analyte is potentially dangerous or available only in small quantities, and makes MFDs particularly interesting for forensic and medical applications (especially when portability is added). It is also worth noting that if the analysis requires the addition of reagents other than the sample, those too will only be required in small quantities. This could be important when such additions are costly or, once again, potentially dangerous. As an example, Liu et al. realized a MFD for forensic DNA analysis[9]. While the device is not easily portable, its small channel volumes minimizes the amount of sample needed to perform the analysis. Also, since most of the process is performed inside the chip, operator interaction with the sample is almost eliminated. This has the great advantage of reducing the risk of sample contamination.

1.1.3 Kinetic studies in microchannels

The high stability (and tunability) of reaction conditions inside microdevices makes MFDs ideal systems for kinetic studies. Also, the flowing nature of these platforms greatly simplifies the collection of data. Assuming that all involved reagents meet at a certain point along a channel, the reaction will proceed while they are brought along by the flow. This means that different places along the channel correspond to different reaction times. This peculiar characteristic allows the implementation of an array of

detectors to monitor the reaction progress, a much simpler method than the analysis of samples extracted from the reaction batch at different times. In a MFD with an array of detectors (e.g. photodiodes for light absorption measurements) at fixed distances from one another, the sampling frequency (i.e. how much time elapses between successive measurements) depends exclusively on the flow velocity inside the channel. By flowing the reagents at high speed the sampling rate can in theory be extremely high (on the order of hundreds of nanoseconds of reaction time between measurements or even less, depending on the device).

The greatest drawback of microfluidics for this kind of application is related to the laminar flow that dominates at these channel dimensions. The above description stems from the assumption that all reagents are perfectly and instantaneously mixed at time zero. Since in laminar conditions mixing can only be achieved through diffusion (a slow process), real devices usually sharply diverge from this hypothesis. A common answer is to include in the MFD a mixer (see Section 1.3.3), but in this case the dead volume of the mixer reduces the time resolution of the device (that is, species start to mix when they enter the mixer and are completely mixed when they exit; the time the flow needs to clear the mixer degrades the time resolution of the device). Another solution is to perform measurements only at the interface between the flows carrying the reagents. Around the interface, mixing by diffusion is effectively instantaneous and the previous assumption can be held. However, this method require the sampling probe (e.g. the light beam for absorption measurements) to be small enough to sample only the neighborhood of the interface.

An example of device for kinetics studies is provided by Voicu et al. in the form of a MFD for the polymerization of *N*-isopropylacrylamide[10]. The chip is fitted to perform attenuated total reflection Fourier transform infrared spectroscopy (ATR-FTIR) along the channel just after the mixing step. This set-up allowed the authors to monitor the effect of a vast range of reaction condition on the polymerization kinetics.

1.1.4 Microfluidics for biology

The very last years have shown a previously unknown increase in interest by physicists, chemists and engineers towards biology, and the field of microfluidics is no exception. A staggering number of publications has appeared proposing various devices for cells culturing and investigation. Once again, the small dimensions of microfluidic channels come to aid. Tiny volumes mean that the environment conditions of the cell culture can be finely determined and, if necessary, tuned. A continuous flow along the channels can be used to bring nutrients to the cells while at the same time drawing away waste that could in time poison and kill the culture. This function can be very easily automated, reducing the time the scientist needs to devote to keeping the system viable. Finally, if the cells must be subjected to treatment (e.g. staining, transfecting or lysing), only a small amount of reagent is needed. Since chemicals for these applications are usually quite expensive, this reduction can be quite advantageous.

Once the cells are grown and possibly treated, their analysis can be performed on the chip. The most common methods of analysis in this field are optical ones, fluorescence imaging above all, and they can be readily applied to a MFD. Even if direct integration of optical instruments in the chip can be problematic at best, devices for cell culture and analysis don’t usually require portability, so external optical system can be applied to the MFD. Since cells are of the same order of dimension than microchannels (i.e. tens of micrometers), they can be manipulated inside microdevices with relative ease. For example, a suitably dimensioned channel can be used to assure that cells flow inside it in a single file, ready to be analyzed one at a time.

A very common limitation of cells studies in macro is related to the fact that different cell culture (even from the same cell line) cannot be always considered equivalent. This is due to potential differences during their growth and multiplication, and has dramatic repercussions for the researcher that desires to subject the same cell type to different condition or reagents. In this case, the only macroscopic solution would be to grow a large culture and then divide it between various isolated wells to treat them with

different reagents. Obviously, such a procedure would be quite convoluted, and would probably damage the culture. In a MFD, the solution is (once again) much simpler. A cell culture can be grown along a network of channels and then, with the help of a rationally designed system of inlets, only part of it can be subjected to every given reagent. If necessary, the characteristic laminar flow featured by microdevices can be invoked to ensure that different reagents can even travel along the same channel with minimal mixing between them. As an example of this last method, Sun et al. realized a MFD for the study of calcium signaling between cells[11]. In this device, cells were seeded and grown inside a microchannel and then a laminar flow was established in the channel between a buffer and a calcium-emission-stimulating reagent (ATP). Only a part of the channel was exposed to ATP, which means that only some of the cells started to emit calcium ions (see Figure 1.2). By quantifying (through fluorescent labeling) the amount of calcium ions that reached the non-emitting cells, the authors investigated calcium-based intercellular signaling.

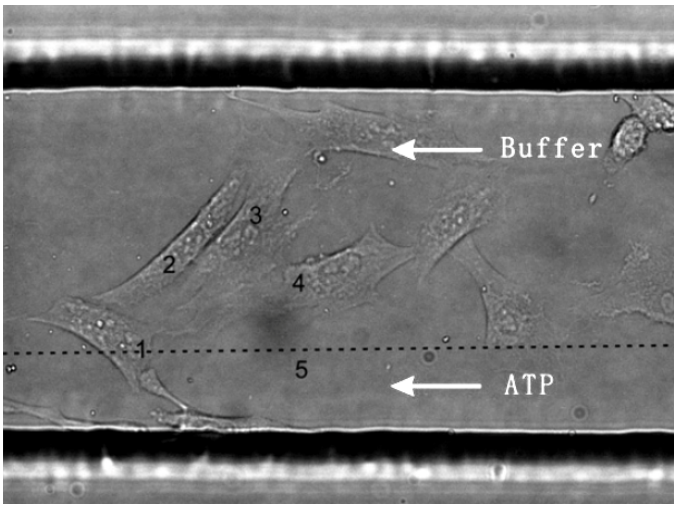

Figure 1.2: optical image of cells grown inside a microchannel. Both buffer and ATP solution are injected in the channel. Laminar flow ensures that only cell 1 comes into contact with ATP. (adapted from [11])

1.2 Integrated vs modular devices

The previous chapter showed that microfluidic devices can be developed for an enormous number of possible applications spanning among very different fields of science. Of course, most of these fields are often inevitably interconnected: a device for biological investigation will usually necessitate a characterizing method to observe the

system, just as a microreactor for chemical synthesis will benefit from on-line product analysis. Thus, the categorization of microfluidics by their field of application is rough at best and meaningless at worst. However, another kind of division can be considered, one based not on the final purpose of the MFD but on how complex devices are designed: integrated or modular microfluidics.

1.2.1 Integrated microfluidics

The integrated approach to microfluidics stems from the very captivating dream of realizing a small, portable and monolithic device able to perform its designed function without the need for any external equipment. The advantages of such a device are quite evident: it can be used wherever and whenever needed, possibly even by untrained personnel. Unfortunately, these undoubtedly desirable features come with a number of disadvantages that must be considered, and challenges that must be overcome. First of all, realizing a monolithic device able to perform complex operation is quite difficult, especially if the dimensions of the various elements are on the order of micrometers. This difficulty steeps even higher if the different functions needed by the final device require different materials (e.g. metal for high pressure or glass for optical transparency) that must be kept in airtight contact to prevent leakage. Another limitation is that if part of the device stops working for any reason (e.g. a clogged channel, a quite likely outcome if the device is used “on the field”), all the device must be replaced. Depending on the fabrication process, this replacement could be quite expensive in terms of both time and money. Finally, from the researcher point of view, it is not uncommon for a prototype device that has been tested for some time to be scrapped in favor of a similar one, usually because only one of several elements must be redesigned (e.g. a different kind of mixer in a complex device for synthesis and characterization). When this happens, there is a substantial chance that *all* the device must be redesigned to accommodate the changes, especially if the modified element requires a different material.

In spite of these difficulties, the overwhelming majority of papers published on the subject of microfluidics dwell on integrated devices (or towards them). This is of course understandable, since if those limitations could be overcome the payback would be worth the effort, with the achievement of all the advantages described above. Lin et al. published a review on such systems[12], with particular focus on chips for chemical synthesis. The degree of complexity of such devices is impressive, as can be seen for example in Figure 1.3. It must be noted, however, that the photograph doesn't show the external equipment that surrounds the microfluidic chip. This is the greatest limitation of current integrated microdevices: they still must be supported by external (macroscopic) instruments, mainly pumps but also voltage generators or light sources as needed. While this restriction can be of no consequence for synthesis microreactors (which are conceived not for portability but for all the advantages described in Section 1.1.1), it means that the dream of a portable, "black box" microsystem is still somewhere further in the future.

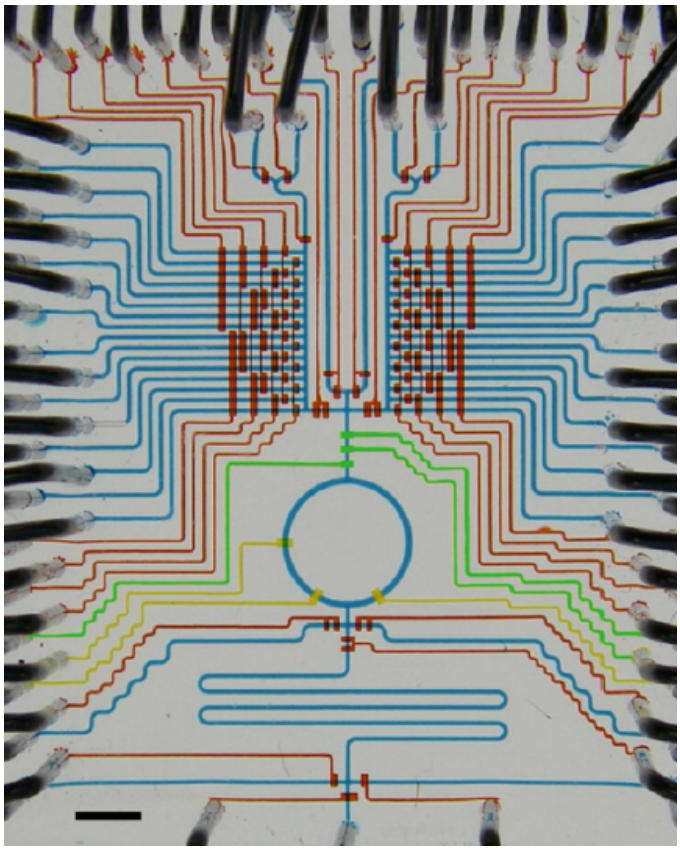

Figure 1.3: photograph of a highly integrated microreactor able to perform 1024 different *in situ* click chemistry reactions. The tubing connected to the various inlets and outlets lead to external equipment (off image) like pumps or drains. (reproduced from [12])

1.2.2 Modular microfluidics

Modular microfluidics is the other side on the MFD coin. In this approach, for every elementary function needed in the device a free standing module is realized, and

multiple modules are then connected to obtain the desired final result. The complete device will be somewhat less compact than an integrated one, and the single modules must be connected between them, adding a new challenge to the realization of the final device, but the advantages are noteworthy. First of all, from the practical point of view, if any module breaks down it can be singularly substituted, without the need to trash all the device. Also, the design and actual realization are greatly simplified. Each module can be designed without constrains due to functions present in other modules, and the best material can be selected for each one while still avoiding the engineering nightmare of integrating so many different materials in a single pseudo-monolithic piece. More in general, each module can be designed without any regard for other modules, as long as a suitable connection can be later established. This possibility is a boon for industrial and/or scientific collaboration projects, since it allows every research unit to work on his module without been affected by what happens in other units until the very end of the project. The advantages for project coordination are self-evident, especially with the added benefit that if unforeseen complications plague the work of one research unit, the others can still proceed and, at worst, the final device will only lack one module. Another good feature of modular microfluidics is that during device testing it is relatively easy to change one element (by redesigning the specific module) while leaving all the others intact, instead of been forced to recreate the whole device. Finally, once a suitable "toolbox" of single-function modules (like pumps, mixers, reactors, and so on) has been prepared, it is just a matter of connecting any number of them as needed to realize hundreds of different devices.

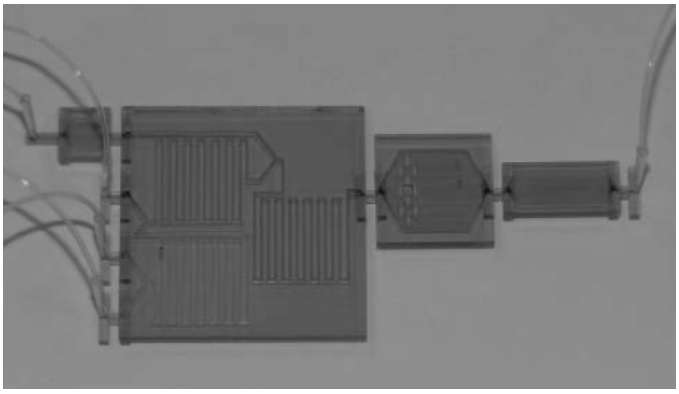

Figure 1.4: photograph of a modular microfluidic device obtained by connecting different modules, each serving one specific function like reaction chamber or mixing step. (adapted from [13])

As an example of modular approach to microfluidics, P. K.

Yuen created a platform where various functional elements (modules) can be freely combined for a huge number of possible applications[13] (see Figure 1.4). In this work the challenge of module connection was solved with a LEGO-like system in which modules feature protruding outlets that leaklessly fit corresponding holes (inlets) in adjacent elements. In addition to research works, a number of patents have been granted in the last years concerning modular microfluidic devices[14–16].

1.3 Microfluidic elements

Whether a microfluidic device is made with a modular or integrated design, it will necessarily consist of various functional elements. In the modular approach those elements will be individual modules, and as such physically separated from one another, while in an integrated device they will coexist in a single chip, but their function will otherwise be the same. What follows is a description of the state of the art concerning the most frequently used microfluidic functional elements, that is valves, pumps and mixers.

1.3.1 Microfluidic valves

In any complex channel network valves are needed to control the direction of flow, and microdevices are no exception. This is especially true with integrated devices, but also modular ones often benefit from (or require) valves. Valves can be roughly divided in two categories: active and passive. Active valves are operated by an external stimulus, and are usually employed to bar the fluid from entering certain zones of the device at the wrong time. Passive valves, on the other hand, work without any external input, and are commonly used to allow flow in one direction but prevent backflow or to allow one particular fluid to pass while rejecting another. One of the first passive valve was proposed by the Whitesides group in 2002 and consisted in an elastomeric flap that could be pushed open by a liquid flowing in the right direction but effectively closed the

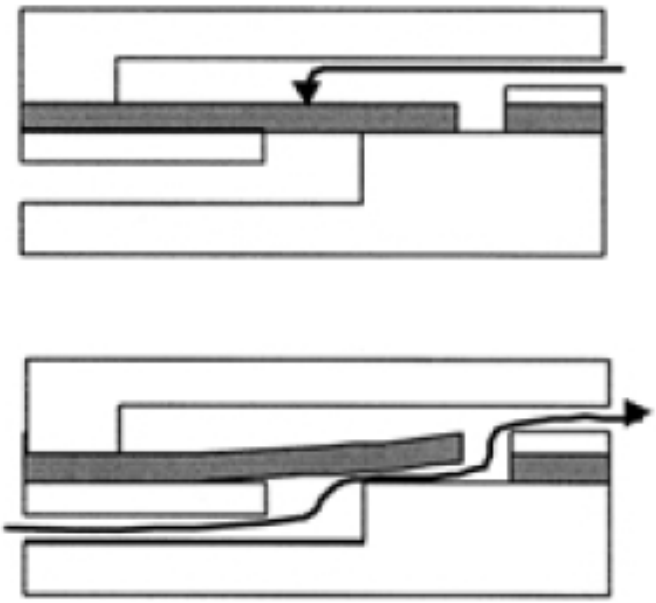

Figure 1.5: schematic reproduction of a passive flap valve. The darkened area is a thin, flexible PDMS membrane. When the fluid comes from the right (upper sketch) the flap blocks the channel. When the fluid comes from the left (lower sketch) the flap is bent by the liquid pressure and the fluid flows through. (adapted from [17])

channel if the liquid flowed in the opposite direction[17] (see Figure 1.5). This kind of valve can be used to prevent backflow in a MFD, and also allows the realization of simple pumps (see Section 1.3.2). A different type of passive valve, one that differentiate between fluids instead of direction of flow, has been proposed by Y. S. Song[18]. This element consists in a microfluidic channel filled with an agarose hydrogel doped with carbon nanotubes (to improve mechanical properties). This porous material will allow mineral oil to flow through undisturbed. However, if water is flowed instead, the hydrogel will swell, sealing the pores and blocking the channel. The modification is reversible, as long as the valve is allowed to dry once swelled.

While passive valves have their applications, most of the recent MFDs rely on active ones. The reason for this is that active valves are easier to fabricate and can be controlled much better than passive ones, at the price of dependency on off-chip controls and instrumentation. Among active microfluidic valves, the so-called “Quake valves” are by far the most popular[19]. Proposed by the Quake group in 2000, they consist of two microchannels, a flow channel and a control channel (channel layout represented in Figure 1.6). The flow channel is where the liquid to be controlled by the valve flows. The control channel is placed orthogonally slightly above the flow one, separated by a thin elastomeric membrane. When compressed air is sent into the control channel, the higher pressure causes the membrane to bulge inside the flow channel,

effectively blocking it. Easy to fabricate and to use, Quake valves enjoy a (well-deserved) enormous popularity among microfluidics researchers, especially those that work on highly integrated devices, since active valves are critical to control complex multi-functional devices. It is far from uncommon to see highly integrated MFDs featuring tens if not hundreds of these valves[12].

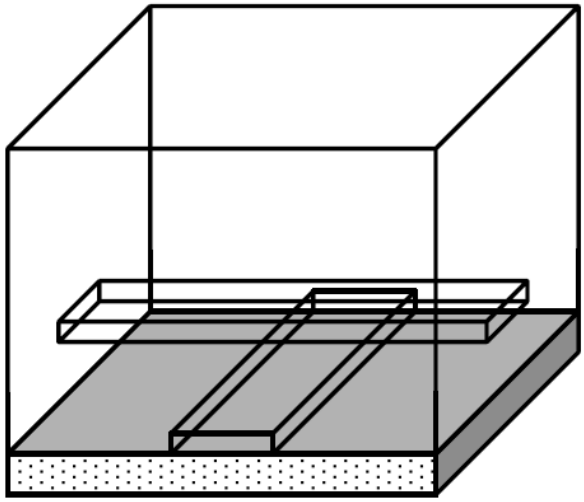

Figure 1.6: layout of a "Quake valve". When compressed air is forced in the upper channel, it will deform and bulge in the lower, sealing it. (adapted from [19])

In addition to those described, a great number of different valves have been proposed for use in MFDs with varying success. Additional information can be found for example in a comprehensive review article by K. Oh and C. Ahn[20].

1.3.2 Microfluidic pumps

All MFDs need a way to flow liquids inside the channels network. Most of the time this requirement is accomplished by off-chip pumps that push fluids in the device through an inlet. However, it would be greatly advantageous to transform the pumping system from external support equipment to actual part of the MFD. The simplest method to achieve fluid movement is to fabricate the channels with a material that is wetted by the fluid, attach a reservoir at the beginning of the device and let the channels be filled through capillarity. The drawback is immediately clear: once the channel is completely filled, no additional flow is generated. Thus, this method can be readily implemented for certain applications (e.g. throw-away devices for simple chemical analysis) but is insufficient for many other. A similar, more versatile method is to place the device on a rotating platform, place the inlet (and reservoir) at the center of the device and allow centrifugal forces to spread the fluid from the inlet towards the border of the chip.

Centrifugal microfluidics[21] have the advantage that the flow will continue even if the channels are already filled (as long as an outlet is provided), and fluid flow speed can be controlled by adjusting the rotation speed. This offers the possibility for additional control. If the device is realized in a material that is not wetted by the fluid, to enter a given channel the fluid will have to prevail against a force inversely proportional to the channel diameter. Thus, smaller channels will be accessed only if the centrifugal force (i.e. the rotation speed) exceed a certain minimum. A clever chip designer can exploit this phenomenon to control how and when certain areas of the device are reached by the liquid[22]. An even greater control can be exerted taking Coriolis force into account, as demonstrated by Kim and coworkers[23]. In a rotating MFD, Coriolis force is always perpendicular to the flow, but its direction depends on whether the device is rotating clockwise or counter-clockwise. Considering this, if a microchannel is designed to split in two, one of the two branches will be preferentially filled. Which one depends only on the direction of rotation of the whole device (see Figure 1.7).

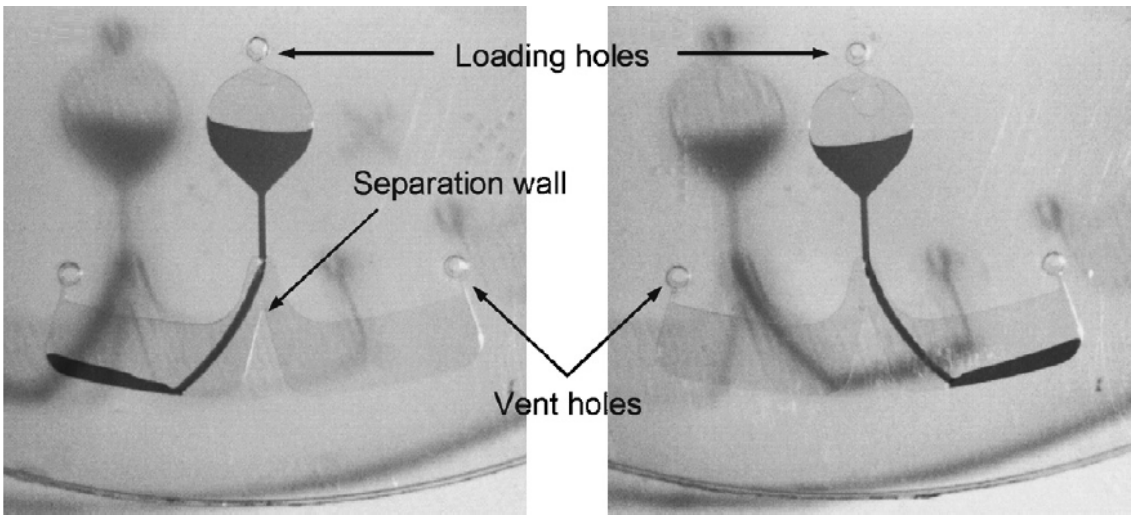

Figure 1.7: a centrifugal MFD that exploit Coriolis force to control the flow. Fluid is injected from the inlet marked "Loading hole" and moved by rotating the device. Which of the following chambers is filled depends exclusively on the verse of rotation: counter-clockwise (left) or clockwise (right). (adapted from [23])

While microdevices with centrifugal pumping are certainly not unknown, most of the pumps used for microfluidics exploit a mechanical action to push the fluid. One way[17] to design one is to create a deformable chamber connected to the channels network

through two opposing flap valves (see Section 1.3.1). The method of operation is shown in Figure 1.8. An external force is applied to compress the chamber, expelling the fluid through the outlet valve. Then the chamber is returned to its original volume (or slightly expanded) to pull in fluid through the inlet valve, returning the pump in the starting state. A vast number of forces have been proposed to manipulate the chamber, from piezoelectric to electrostatic to magnetic[24]. It is also worth of notice that such a pump can easily be designed to be man-powered, i.e. compressed with a finger push. Another, related, solution is the peristaltic pump[19]. In this element, a series of valves are closed in succession to propel the fluid along the channel (see Figure 1.9). A very simple way to create an air-actuated peristaltic pump is to equip a straight channel with a succession of at least three Quake valves. These kind of pump is slightly more complex than the deformable chamber one, but has the added advantage of being bidirectional: the operator only needs to invert the order of valve actuation to reverse the flow direction.

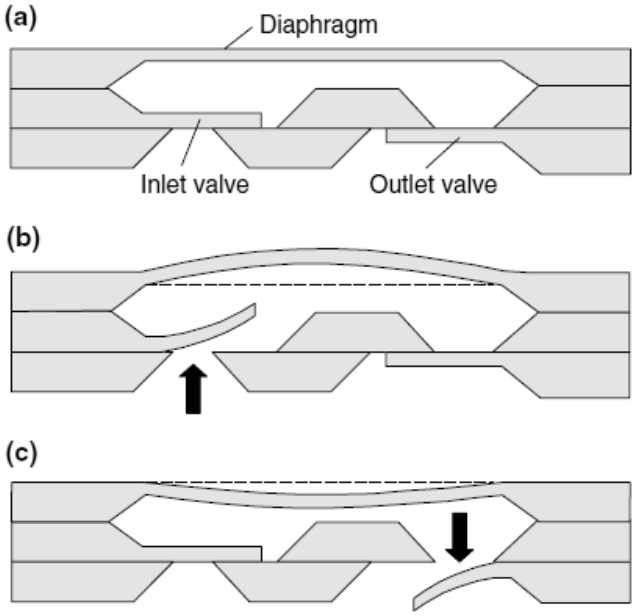

Figure 1.8: (a) simple pump made form two flap valves and a deformable diaphragm. The pump pulls fluid during the expansion phase (b) and expels it during compression (c). (adapted from [17])

Deformable chamber and peristaltic pumps are commonly used in MFDs, but both share a potential disadvantage: they generate a pulsed flow. While for many applications this is not a problem, in some cases a continuous flow would be desirable. When such a flow is needed, microfluidic chips with integrated pumping systems typically employ electroosmotic flow[25] (EOF). Devices using this kind of pumping strategy are usually realized in glass or fused silica, since when these materials come in contact with an electrolytic solution they will develop a negatively charged surface (due to spontaneous

deprotonation of surface silanol groups, as long as the pH of the solution is not too low). Consequently, positive ion present in the solution will be attracted to the channel walls, creating a positively charged layer. At this point, if an electric field is generated along the channel (positive at the inlet, negative at the outlet), the positive layer will start to flow, and all the fluid in the channel will be dragged along due to viscous forces. The resulting flow speed is continuous and mostly constant across all the channel. The main disadvantage of EOF is that it will not work when the channel is filled with a non-polar liquid with low conductivity, effectively ruling out many organic solvents. Another limitation is that the effective flowing speed is proportional to the applied field, but fields too strong incur in the risk of electrolysis or other reactions at the electrode. Thus, the maximum flow velocity applicable must be carefully estimated to avoid undesired reactions.

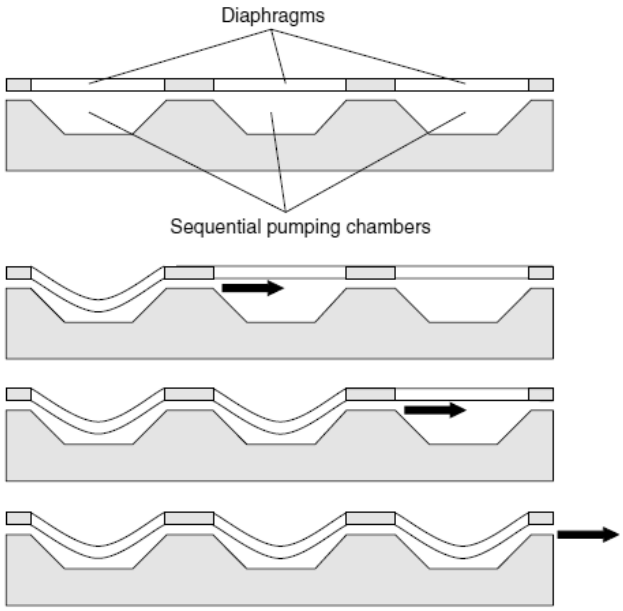

Figure 1.9: a peristaltic pump. In this design a series of valves are closed in succession to generate a flow in the desired direction. (adapted from [19])

Those presented are the most thoroughly studied microfluidic pump up to date, but many other have been proposed, different in design or operating principle. Once again, the reader is referred to a comprehensive review article for any additional information[24].

1.3.3 Microfluidic mixers

Since almost all MFDs feature (and often rely on) laminar flow, forcing different reagents to mix faster than through simple diffusion can be a very tough challenge. Thus, the realization of efficient mixers is a very hot topic in microfluidic research. Just

as valves, mixers can be divided in active and passive ones. Active mixers exploit an external force to achieve mixing, while passive ones work without off-chip intervention. The most conceptually simple way to mix two fluids is to include inside the channels a mechanical stirrer (like a paddlewheel). Unfortunately, the tiny dimensions of MFDs greatly complicate the practical realization of such an element. A micrometric paddlewheel can be created with any of the various microfabrication techniques (see Section 1.4), but realizing a miniaturized system able to actually rotate the wheel is a much more difficult undertaking, one often not worth the effort.

Most active mixers rely instead on inducing perturbation in the laminar flow through repeated perturbation in the pumping system. As an example, if the relative flow rates of two fluids flowing together in the same channel is repeatedly varied, mixing between them is enhanced[26]. Of course, the degree of enhancement is dependant on the nature and magnitude of the perturbation. Another, usually more efficient solution is to generate the perturbation only locally at the place where mixing is desired. An example of such system is given by Ahmed et al. and is based on an effect known as acoustic streaming[27]. In this work, the two fluids to be mixed are injected into a channel featuring a horseshoe-shaped microstructure (see Figure 1.10). As the channel is filled, an air bubble will spontaneously remain trapped inside the microstructure. To activate the mixing effect, a piezoelectric transducer is used to send an acoustic wave to the device. The effect of the wave on fluids and bulk material is negligible, but the membrane of the trapped air bubble will start to oscillate. This movement will be transmitted to the

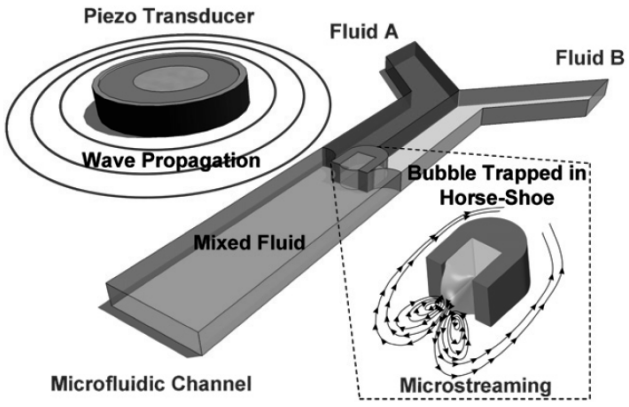

Figure 1.10: bubble acoustic streaming micromixer. The acoustic wave generated by the piezo transducer induces a fluctuation in the bubble membrane, which in turn generates recirculation in the channel, greatly enhancing mixing. (adapted from [27])

fluids as fluctuations in velocity and pressure, resulting in strong recirculation and consequent mixing. The effect can be very intense if the frequency of the acoustic wave is near the resonance frequency of the bubble. This resonance frequency *f* depends on the fluids involved and on the radius of the trapped bubble following[27]:

$$f^2 = \frac{1}{4\rho\pi^2 a^2}\left[3k\left(p + \frac{2\sigma}{a}\right) - \frac{2\sigma}{a}\right] \qquad (1.2)$$

where ρ is the density of the surrounding liquid, σ is the surface tension, *k* is the polytropic exponent of the gas, *p* is the fluidic pressure and *a* is the radius of the bubble. It should be noticed that this equation assumes spherical bubbles, so small differences in resonance frequency are expected for slightly oblate bubbles such as those trapped in this device. With this arrangement, mixing across a 240 μm wide channel was estimated to complete within 10 ms.

Active mixers share the advantage that they can be turned on or off as needed, improving device versatility, but unfortunately all require additional external equipment (e.g. power sources) limiting portability. Passive mixers, on the other end, are always "on", but once fabricated do not require any additional instrumentation. Mostly, passive microfluidic mixers are based on one of two approach. The first strategy is to reduce the lateral dimension of the fluid streams so that mixing by diffusion becomes feasible. A conceptually simple way to obtain this is to divide both inlet streams that have to be mixed in multiple, much smaller, sub-stream and then recombining them in a single channel alternating one liquid and the other. The result is a high number of very thin (few micrometers) streams in which mixing by diffusion can be accomplished in a matter of seconds[28]. Another possibility is to use two lateral flows to "compress" a central stream through an effect known as hydrodynamic focusing. As before, once the stream lateral dimension is so reduced, free diffusion will spontaneously perform the mixing[29].

A different strategy to obtain mixing is to induce pseudo-turbulent behavior in the flow. Obstacles, bends and bottlenecks are all viable methods to introduce transversal

components in the flow velocity, perturbing laminar flow and allowing parallel streams to compenetrate, achieving mixing. Another solution along the same principles has been proposed by Whitesides and coworkers[30] and is showed in Figure 1.11. A series of parallel ridges is engraved on the floor of the channel at an oblique angle with respect to the flow direction. These microstructures introduce an asymmetry along the transversal axis of the channel, effectively favoring the (lateral) movement along the engraved lines of the fluid near the channel floor. This movement will in turn displace the fluid near the lateral wall that will be forced to move toward the ceiling of the channel displacing the fluid there, and so on until an helical flow in generated. This kind of flow is clearly highly non-laminar, and induces turbulent mixing of the liquids in the channel.

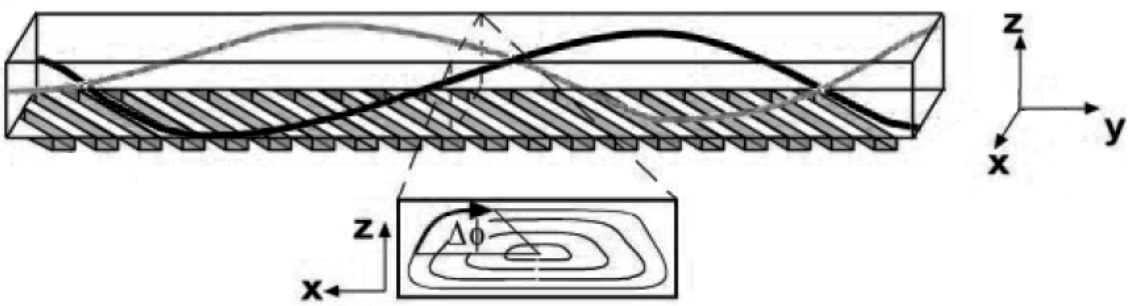

Figure 1.11: oblique ridges micromixer. The internal structuration of the channel induces an helical flow in the fluid that strongly perturbs laminar conditions. A cross-section of the streamlines of the flow is reproduced below the channel. (adapted from [30])

A number of different mixing strategies have been proposed for both active and passive mixers. As with valves and pumps, additional information can be found in a recent review article[31].

1.4 Materials and fabrication techniques

Considering the extremely wide range of applications at which MFDs are aimed, it shouldn't be a surprise that a number of different materials have been exploited to make microdevices. Clearly, any given material is well suited for some functions but performs

poorly for others, so different applications require different substrates. Moreover, it is not unknown (though fairly uncommon) for a single device to be fabricated using two or more different substances[32,33]. This variety in materials necessarily translates into a variety of microfabrication techniques that have been established or developed since the genesis of microfluidics. To report a complete list of materials and techniques would be quite pointless, but a description of the most common (or interesting) is beyond doubt useful, and as such will be given in the following.

1.4.1 Hard materials: glass and steel

In ultimate analysis microfluidics originally stems from earlier work on glass capillaries, so it's no surprise that glass is one of the most popular MFD material[34–36]. The reason is not only historical, since glass is an excellent substrate for any chemical application. These MFDs can be filled with almost any chemical without fear of adverse reaction, and can be heated to high temperature. Additionally, glass is transparent, making it a good substrate also for optical applications, and is biocompatible, allowing cells to attach and proliferate on a glass MFD. Apart from being somewhat fragile, glass has not any real disadvantage as substrate. Its true drawback lies in the fact that glass is quite difficult to microfabricate or more in general to work with. To answer this limitation, steel MFDs have been proposed and successfully employed[37,38]. Steel is chemically resistant to many solvents, able to withstand high temperatures and pressures and much easier to work than glass. Clearly steel is not transparent, a fact that rules out (off-chip) optical applications. It is also incompatible with some classes of reagents (mainly strong acids), and it is not biocompatible, but industrial metal microfabrication techniques are very well developed. This last fact assures that most commercial MDFs (especially those for chemical synthesis) are made of steel[*].

[*] See for example the microreactors proposed by Syrris (syrris.com/flow-products) or Flowid (www.flowid.nl/products)

1.4.2 Soft materials: polymers

While polymers cannot usually compare with glass or steel in terms of mechanical properties or chemical resistance, these materials are often cheap and much easier to work with. Interest in polymer MFDs is currently stronger in academic environment than in industrial facilities, but some commercial plastic MFDs are nonetheless available on the market[39]. Polymers from microdevices come most often from one of two categories: photopolymerizable materials and elastomers. Photopolymers, also called resists, are a well developed class of materials that owes much of its popularity to microelectronics, since resists are instrumental in the fabrication of microchips. When used as bulk materials in microfluidics, these substrates allow the fabrication of devices through photolithography (see Section 1.4.7) without the need for subsequent etching and resist removal.

In a microfluidic context, "elastomer" is almost guarantied to mean "polydimethylsiloxane" (PDMS). The chemical structure of polymerized PDMS is shown in Figure 1.12. This thermosetting polymer has become one of the most popular materials for MFDs fabrication, at least among scientific researchers[40–43]. PDMS is transparent, allowing optical applications, and its elastomeric nature allows the device a certain freedom (e.g. it can be bent, compressed or stretched). This polymer is also biocompatible, so that MFDs that require cell to be grown inside channels can be made from it. Finally, PDMS is the ideal material for the replica molding fabrication technique (see Section 1.4.9). The enormous popularity of this method is probably the main reason for this material to be so widespread. Notwithstanding all these favorable features, PDMS is not without limitations[44]. First of all, its mechanical properties and thermal resistance are not those of steel or glass, a fact that can limit

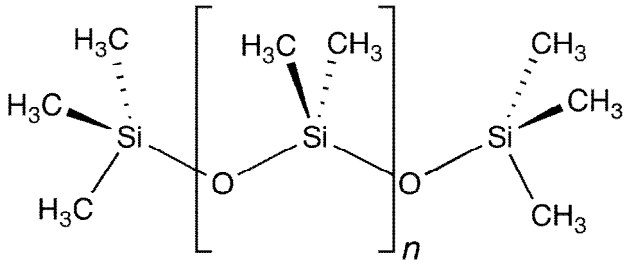

Figure 1.12: chemical structure of polymerized PDMS.

applications. Particularly problematic are devices that require high pressure, since (elastomeric) PDMS channels will swell noticeably at pressures far below those required to actually burst open the device. This polymer is also fairly incompatible with most organic solvent, since they will be absorbed and eventually lead to material delamination[45]. Finally, PDMS is permeable to most gasses[46], a fact that can be regarded as a mixed blessing, since its actual consequences depend on the purpose of the device: in a cell culturing MFD, oxygen and CO_2 permeability ensure that the cells can survive inside channels. On the other hand the same oxygen can be harmful for certain chemical reactions with unstable reagents.

1.4.3 Hybrid materials

A sort of middle ground between hard and soft materials is occupied by hybrid materials, i.e. substrates in which organic and inorganic components coexist. This peculiar composition confers to these materials hybrid characteristics that share the advantages of both polymers and harder substances like glass or silica[47]. Typically, the result will be a substrate with better mechanical properties than pure plastics, but less brittle and much more workable than ceramics[48]. The blend of organic and inorganic parts can be made in a number of different ways, the simpler of which is to physically mix them. As an example, silica nanoparticles dispersed in a polymeric matrix contribute to increase the elastic modulus of the whole substance[49]. While these "mixed" materials can surely be used in microfluidic applications, most or the research work in the field concentrate on materials that are hybrid on the molecular level, that is whose single molecules share organic and inorganic moieties. Most commonly, these hybrids present on one end a functional group that can react with other identical molecules to generate an inorganic Si-O-Si network, and on the other end an organic moiety. Exactly which organic moiety depends on the application, the rationale being that while the inorganic network confers mechanical stability to the whole, the organic half can be used to introduce the desired functionalities in the material. A wide variety

of different hybrids have been proposed in the literature. As an example, organic moieties have been used to tune the wettability of the surface[50,51]. Also, the optical properties of functional organic groups have been exploited for a number of applications ranging from very simple (e.g. colored glass) to quite complex (e.g. photochromic materials for optical storage or non-linear absorbers for optical limiting)[52].

One of the most interesting applications of hybrid materials is to include as organic part a photopolymerizable moiety. In this case, the material maintains its typical characteristics (most importantly better mechanical properties than pure polymers), but also becomes easily patternable via photolithographic methods (see Section 1.4.7), opening the way for hybrid material microfabrication[53,54].

1.4.4 Micromachining

One of the first developed method for the creation of microdevices is micromachining. There are several different machines that can engrave a network of channels in a steel or polymer slab, ranging from CNC (computer numerical control) milling machines to electrical discharge machining (EDM). All these machines share some features: they are large and possibly expensive, but very well known to the industry. The greatest advantage of these techniques is that patterns with arbitrary geometry can be realized with good precision in an almost completely automated way. Unfortunately, "good" precision is not always enough. CNC milling on metal can create channels of a few hundred microns (or down to about 80 μm with specifically designed equipment)[55]. EDM (with a machine specifically tuned for micromachining) can achieve resolution around 100 μm or (many) tens of micrometers[56]. If the base material is soft (polymers), resolution for CNC milling is strongly reduced because of material deformation, while EDM is downright impossible, since plastics are (usually) nonconductive. Whether these numbers are good enough or not depends of course on the final application of the

device, but a number of MFDs require channels dimension on the order of 10 micrometers, ruling out micromachining.

1.4.5 Focused ion beam milling and electron beam lithography

Focused ion beam milling (FIBM) can be considered as the evolution of micromachining. Instead of removing material from the sample with a rotating cutter, a focused ion beam is exploited to sputter atoms from the sample surface[57]. The maximum lateral resolution obtainable depends on the dimension of the focused beam, which is in principle limited only by the diffraction limit (i.e. about one half of the beam wavelength). Thanks to the fact that the beam is made of ions, which have an extremely small wavelength, experimental resolutions down to tens of nanometers have been reported[57–59]. Depending on the ion energy, some of the ions can be implanted in the sample. This effect can be beneficial or not, depending on the final application, and can be controlled by the operator through modulation of the impact energy. FIBM also has some disadvantage. First of all, it requires complex and expensive instrumentation to generate, focus and control the required ions. The fact that all the machine must be kept in (ultra) high vacuum only adds to complexity. Also, this fabrication technique is slow and serial, thus requiring a long time to realize large structures.

Electron beam lithography (EBL) is very similar to FIBM, with the difference that a beam of electrons, instead of ions, is employed[60,61]. The result on the sample is different, since electrons lack the mass to efficiently sputter material. Instead, the targeted area undergoes a chemical modification that makes it soluble in a suitable solvent, while the rest of the sample remains unaffected (see Section 1.4.7 for more examples of lithographic processes). Apart from these differences, EBL shares almost the same advantages and disadvantages of FIBM, only trading the possibility of ion implantation for an increased resolution (down to few nanometers). This increase is due to the fact that while ions can in principle be focalized much tighter (due to their smaller

wavelength), the sputtering process is less controllable, and often involves all the neighboring area.

1.4.6 Wet etching and reactive ion etching

Another way of creating MFDs is through chemical (wet) etching. In this technique, the starting material is partially covered with a mask (typically realized with photolithography, see Section 1.4.7) featuring holes shaped like the desired channel network. All the sample is then submerged in an aggressive chemical solution able to dissolve (etch) the starting material but not the mask. The result is that trenches will be created in the bulk material corresponding to the mask holes geometry[62]. This method is simple, and its resolution is in principle only limited by that of the mask. Unfortunately, etching is an isotropic process. This means that once the very first layer of material is removed, the etching process will proceed in every direction, including under the mask. The result will be rounded channels with internal diameters greater than the mask dimensions (decreased resolution). Notwithstanding this limitation, wet etching is a much favored technique, especially when the required channels are not too deep. When high resolution or deep channels are required, a modified etching technique can be used. Reactive ion etching (RIE) works along similar principles, but instead of a chemical solution, a plasma of positive reactive ions is employed[63]. This plasma is subjected to an electrical field perpendicular to the sample surface that forces the ions to move towards the (mask covered) sample. Where the ions impact, sample material is removed both through a sputtering effect and due to the chemical reactivity of the plasma. The presence of the electric field introduces a strong anisotropicity to the process, ensuring that lateral etching is much slower than vertical one. Thus, deep channel with mask-limited resolution can be obtained.

Both kind of etching are commonly used to create MFDs, especially those made of materials difficult to work otherwise, like glass. This technique has the great advantage of being able to work large areas at the same time, allowing the realization of large

devices. Wet etching is also quite simple and cheap, since the most expensive component is usually the mask, which can often be reused many times. With RIE, the instrumentation is a bit more expensive, since it must include a reaction chamber kept in low vacuum, and while the masks are almost immune to chemical etch from the plasma, the sputtering process damages them, compelling the user to replace them after a few cycles.

1.4.7 Photolithography

Photolithography is an extremely popular technique to create microdevices. It owes much of this popularity to the fact that this technique is instrumental in the realization of electronic integrated circuits and as such has been studied and developed more than any other technique in the last decades. A photolithographic fabrication starts with the deposition of a layer of photosensitive material (often called photoresist or simply resist) on a substrate. All the sample is then covered with a mask similar to those used for etching or RIE processes and exposed to a source of UV light. The part of the resist that is not covered by the mask undergoes a photoinduced modification whose precise nature depends on the specific resist. Most commonly (negative resist), the native material is an unpolimerized blend of some monomer whose polymerization reaction is activated by light

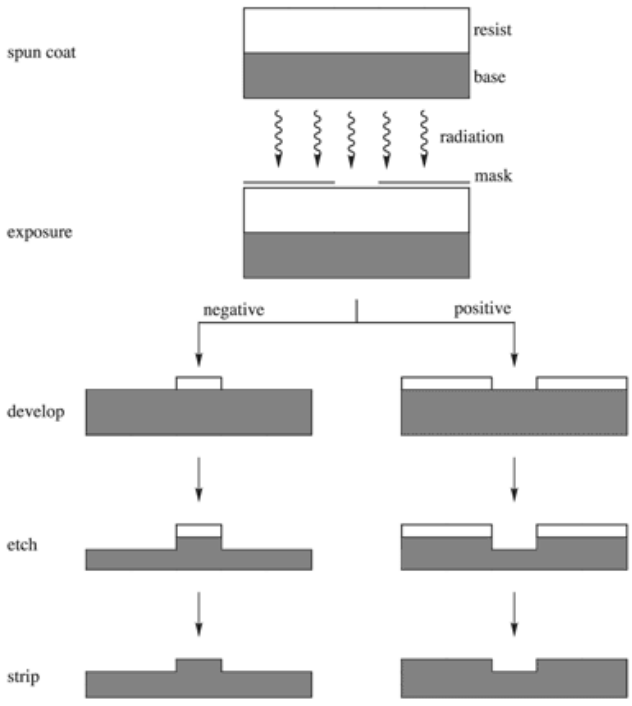

Figure 1.13: schematic representation of masked photolithography process with both negative and positive resist. The etch and strip steps are only performed if the desired MFD bulk material is the "base" one. (reproduced from www.sigmaaldrich.com)

absorption. If this is the case, the exposed material undergoes crosslinking and becomes resistant to a number of solvents able to dissolve the monomer form. The unpolimerized resist is then removed with said solvents (a process known as development) to obtain the desired microstructures. In other resists (positive resist), the material is already crosslinked and UV light actually breaks down the connection between monomers. If this is the case, the selected solvent will wash the exposed material, while that under the mask will be unaffected. Both these processes are exemplified in Figure 1.13. Regardless of what kind of resist is used, the result will be a microstructure supported on a substrate that feature a positive or negative reproduction of the mask. This microstructure could be the desired device, or in other cases the substrate is the material of interest and the polymer structure is just the mask for the following etching process.

Photolithography is a very well developed technique, quite simple in principle but with some limitations. First of all, the resolution of the final structure is limited by that of the mask, which must be created by other methods. However, such masks are only subjected to light exposure and not to aggressive chemicals, so each mask can be used indefinitely. Also, if the final device does not require resolutions exceeding a few hundred micrometers, masks can be created very cheaply by printing them in black ink on a transparent sheet[40]. Even if the mask is exceptionally resolved, the use of light imposes a further limitation on the maximum resolution (diffraction limit). Since the smallest feature obtainable is proportional to the wavelength of the radiation used, many attempt have been made to develop a photolithographic process that exploits light with shorter wavelength (deep UV or X-rays). With these techniques structures smaller than 100 nm have been created[64], but the difficulty in handling photons so energetic poses a strong limitation to the diffusion of this processes.

1.4.8 Direct laser writing

Direct laser writing (DLW) is the natural evolution of masked photolithography. Instead of using a mask and a wide light source, a laser beam is focalized on the sample and

moved to directly write the desired pattern in point-by-point fashion. The greatest advantage of this technique is that there is no longer need for a mask. This fact greatly simplifies the process, since it eliminates all the mask microfabrication steps that can be quite challenging for masks featuring complex patterns. The resolution of DLW is in principle equal to the smallest focal radius obtainable (i.e. the diffraction limit) but in practice lens aberrations and other hidden processes (e.g. polymerization propagation outside the actually exposed area) mean that the smallest feature obtainable is on the order of some micrometer (with soft UV light, that is wavelengths around 350-400 nm). The greatest drawback of this technique is that, being serial, it can take quite a long time to produce large patterns. However, with high laser powers the writing speed can be quite high (some millimeter per second or even more) and the process is easily automated, meaning that this is more a drawback for laboratory research than for industrial application.

A further evolution of DLW is the use of two-photon absorption processes to induce resist polymerization. Two-photon absorption is a process in which a molecule, instead of absorbing a photon of the appropriate energy to make a transition, absorbs two photon each of half the required energy to obtain the same result[65]. These kind of transitions are much less probable than classic, one-photon ones, so this process has two requirements. First of all, the number of photons impacting on the sample must be high (to account for small interaction probability), which means high light intensity. Secondly, linear (one-photon) absorption processes must be absent at the selected wavelength or, being much more probable, they will completely drown non-linear ones. In practice, for common UV-photoresist that absorb linearly at wavelength around 400 nm, the selected exposure wavelength will be around 800 nm, where the resist does not absorb through one-photon processes but only via two-photon absorption. The advantage in using non-linear processes is that the efficiency of two-photon absorption and subsequent resist polymerization is strongly (quadratically) dependant on the light

intensity. The reduction in light intensity *I* due to absorption as the beam travels inside a material in the z direction can be expressed as:

$$\frac{dI}{dz} = -\alpha I - \beta I^2 \qquad (1.3)$$

where α and β are respectively the first- and second-order absorption coefficients. In general, $\alpha \gg \beta$ and so second-order contributions are usually hidden by the much higher linear absorption unless extremely intense beams are used. However, both absorption coefficients vary with wavelength, so it is possible to choose a radiation for which $\alpha \sim 0$ and thus eliminate linear processes. From equation (1.3) it can be seen that non-linear absorption is indeed strongly dependant on the incident light intensity. Thus, in two-photon DLW absorption and subsequent polymerization can be selectively confined in the focal volume. This doesn't only mean a better lateral resolution than with one-photon photopolymerization. In one-photon DLW the laser light polymerizes the resist all along the optical axis (z axis), i.e. the whole thickness of the resist layer. This is because even in tight focusing conditions, the variation in light intensity along the z axis is quite small, and since one-photon polymerization depends linearly in intensity, it is all but impossible to tune the overall power so that only the focal volume is polymerized. On the other hand, two-photon processes depend on the square of the light intensity, that is they respond strongly to even small variations. In this case a

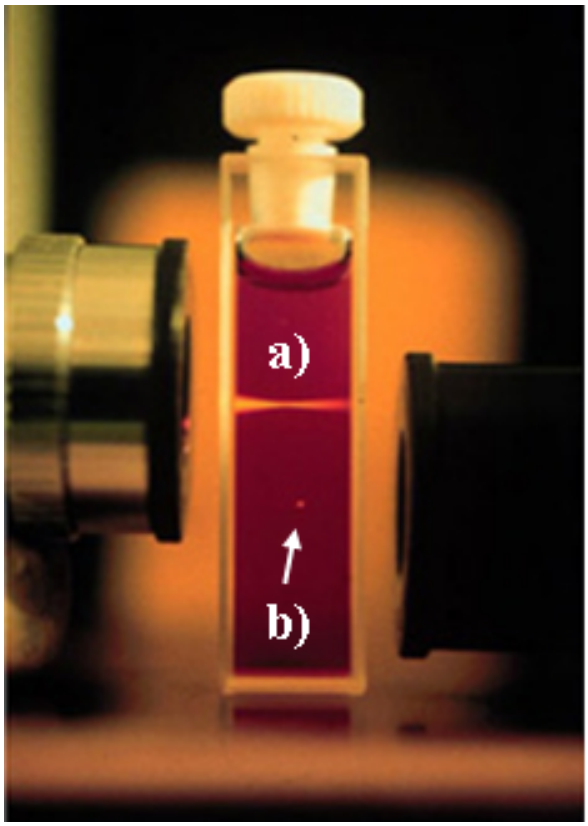

Figure 1.14: fluorescence in a rhodamine B solution induced by a) one-photon absorption and b) two-photon absorption.

careful adjustment of the laser power can create a situation where only in the focal volume the light intensity guarantees enough absorption to trigger polymerization, while in the rest of the optical axis the resist suffers no modification. The difference in absorption between one- and two- photon processes can clearly be seen in Figure 1.14. Thanks to this feature, two-photon DLW shows a unique characteristic among all the described microfabrication techniques: since at every given moment only a small dot (the focal volume) is polymerized, by moving the focal point along all three axis 3D pattern of arbitrary geometry can be created[66–69].

This technique has also another peculiar feature. Even if only the focal volume is polymerized, the resolution is still limited by the smallest focal volume obtainable (i.e. the diffraction limit). However, two-photon DLW can be used to fabricate structures even smaller than that. To explain why that is possible, one must consider that typical laser beams do not have a constant intensity profile along the beam cross section. Instead, they usually show a Gaussian profile which follows:

$$I(r) = I_0 e^{-\frac{2r^2}{w^2}} \qquad (1.4)$$

where $I(r)$ is the light intensity across the beam cross section, r is the distance from the beam center, I_0 is the light intensity at the center and w is the beam radius.

This means that the intensity is maximum at the center of the beam, and progressively decreases along the radius. This modulation is maintained when the beam is focalized, which means that in the focal volume different areas have different intensities. This variations are quite small, but the quadratic dependence of two-photon processes means that even small variations can have marked effects. The result is that if the total power of the laser beam is very finely tuned, it is possible to trigger polymerization only in the inmost part of the focal volume, effectively eluding the diffraction limit[67,69–71].

It should be noticed that, while the dimension of the absorption area is the most important parameter for microstructures dimensions, other phenomena concur to degrade the actual resolution. The most important of these are photoinitiator diffusion

and/or polymerization propagation outside the exposed area and thermally induced polymerization outside the focal volume[69]. Notwithstanding these effects, DLW remains an extremely powerful and versatile technique, able to realize 3D structures with resolution as good as a few tens of nanometers.

1.4.9 Replica molding

While PDMS shows a number of interesting features (see Section 1.4.2), the one reason that made it one of the most widespread materials for microfluidic is the replica molding technique[44]. This process (summarized in Figure 1.15) requires first of all a master bearing the desired network of channels in relief. Such a master is usually created through UV-photolithography or DLW, but any fabrication method can be employed. This master is then covered with unpolymerized (liquid) PDMS, and the whole is subjected to a thermal treatment that triggers PDMS polymerization. This process results in a solid slab of PDMS bearing the negative of the master relief (i.e. the channel network) engraved on the surface. The elastomeric nature of the polymer allows for easy detachment from the master, giving a network of open channels. To obtain a closed device, the replica is treated with ozone-UV or oxygen plasma along with a flat slab of PDMS or a cover glass. This treatment breaks the Si-O-Si bonds on both surfaces, activating them and ensuring that once brought into contact with one another an irreversible sealing is obtained[72].

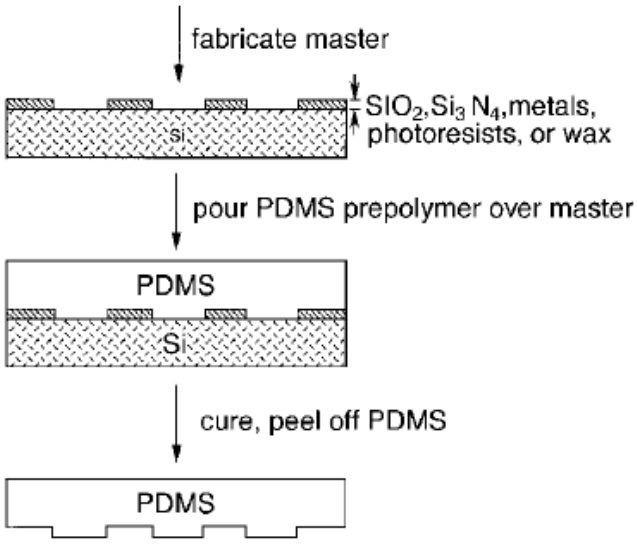

Figure 1.15: replica molding process. A microfabricated master is covered with liquid, unpolymerized PDMS. The following thermal treatment solidifies the polymer, allowing master removal and giving the PDMS replica. (adapted from [44])

This fabrication technique is fast and very cheap, since a single master can be used to generate a great number of replicas. The fact that PDMS is an elastomer allows the replica of complex structures where a stiffer material would break while being detached from the master. The greatest limitation to replica molding versatility is that it cannot replicate most three-dimensional structures. If the 3D part is limited to some overhanging feature, replica molding can still (in some cases) be employed, one again thanks to the elastomeric nature of PDMS that allows the replica to bend or stretch as needed to break free from the master[73]. However, structures with closed loops are completely off-limits, since there would be no way to separate the master from the PDMS, unless a master is sacrificed for every replica.

1.5 Optofluidics

Originally, the field of microfluidics concerned itself only with fluids. However, a great number of chemical reactions and characterization techniques are enhanced by the suitable application of light, so many researcher have explored the possibility of including optical elements inside MFDs. This new field, dubbed “optofluidics”, has given rise to a high number of publications in the last few years[74–76]. The main aims of optofluidic devices and a selection of proposed optical elements are reported in the following.

1.5.1 Photochemistry in microchannels

The most straightforward way to include light inside MFDs is simply to expose the entire device to an appropriate source of radiation. This approach is the natural evolution of batch (macroscale) photochemistry which is commonly used in chemical synthesis to obtain greater yields or selectivity. Once again, the use of microfluidic channels can enhance the performances of such devices[77]. One of the greatest limitation of macroscale apparatuses for photochemistry is that the radiation is

progressively absorbed by the reagents while propagating from the borders to the center of the reaction vessel. This translates into an inhomogeneity in terms of effective exposure which usually leads to decreased product selectivity. Microchannels, on the other hand, are very thin, allowing the radiation to be effectively constant along all the optical path. Another advantage of MFDs stems from the fact that a number of photoinduced reactions perform better at very high light intensities. While a macroscale system must strike a balance between large area of exposure and high radiation intensity, the whole width of a microchannel can be easily covered by a slightly focused (and very intense) laser beam. It should also be noticed that beyond providing high intensity, the use of a laser also guaranties monochromatic light, which is usually very beneficial for selectivity purposes. All these advantages have caused a very wide number of reactions to be tested in microchannels, usually with positive results in terms of product selectivity and yield, especially since these benefits add up to those typical of all MFDs (see Section 1.1.1). A recent review article from Oelgemölle and Shvydkiv[77] summarizes a number of these studies, offering a wide view on the literature concerning this subject.

Optofluidic devices have also been used for photoinduced polymerization. In the most common configuration, a microchannel is filled with flowing liquid monomer, and a suitable light is used to induce photopolymerization. If a focused laser is used, polymer microfibers can be realized by flowing the monomer under the fixed laser spot. If the laser light is intermittent (e.g. modulated with a chopper), dots or rods can be created. Alternatively, if the light is shone through a mask before reaching the channel, it is possible to obtain microparticles of arbitrary shape. In a further evolution of this system, considering the laminar flow conditions that dominate in microdevices two different liquid monomers can be flowed side by side. This allows the realization of microstructures made of two different polymers, each spatially localized in a very precise way (e.g. a disc with one half made of one polymer and the other made of another). One of these devices can be found, for example, in the work from Chung et al.

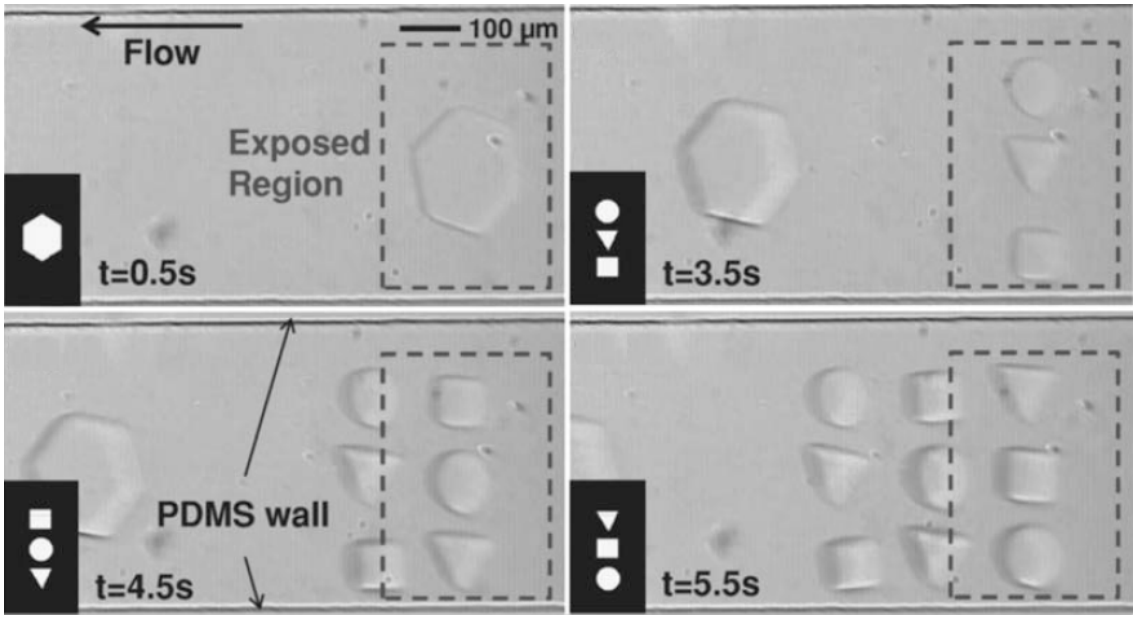

Figure 1.16: generation of arbitrary shaped polymer microparticles. Liquid monomer is flowed in the channel, and UV light is used to locally induce polymerization. The black insets show the photomask being used for each frame, and the dashed square identifies the corresponding exposure region. (adapted from [78])

where it is used to generate polymer particles of various composition and arbitrary shape (see Figure 1.16)[78].

1.5.2 Optofluidic detection and characterization

Considering how many characterization techniques rely on optical means (from spectroscopic to diffractive to plasmonic), it isn't particularly surprising that most optofluidic devices deal with these. On-line monitoring of reaction products has been already discussed in Section 1.1.2, and a number of other applications have been proposed and realized. Among these, sensing and/or characterization based on surface enhanced Raman spectroscopy (SERS) is probably the most common line of research[79]. Raman spectroscopy is a very powerful characterization technique, with high selectivity and the possibility to detect molecules invisible to similar methods like IR spectroscopy. The greatest limit of this techniques is that Raman spectroscopy relies on a process (inelastic scattering) that is fairly improbable, requiring high light intensity and high analyte concentrations. Luckily, it has been observed that molecules in the

proximity of a suitable metal surface exhibit a strong enhancement in their Raman response. To achieve this enhancement, the analyte molecules must be very close (a few nanometers at the farthest) to a metal nanoparticle or a metal surface with nanometric roughness. Notwithstanding these stringent requirement, SERS is very popular nowadays, due in no small part to the fact that in the right conditions the signal enhancement can be very high, up to a 10^{14}-fold increase, although routinely signal enhancement fairs around a 10^{5}-10^{6} fold increase[80]. This powerful technique has been repeatedly exploited in microfluidics. In most cases, these MFDs mix nanoparticles (brought by a liquid carrier) with a solution of analyte, and then apply a number of different methods to force the target molecules to came into close contact with the metal[81–83]. More complex devices integrate a synthesis step so that the required nanoparticles can be produced *in situ*, removing the need to worry about the stability of the colloidal suspension[84].

Another, related, method of detection is that based upon surface plasmon resonance (SPR). Plasmons are collective electrons oscillations on the surface of a thin metal film which can be excited by a light beam of a specific wavelength impacting on said surface with the correct angle (that is, the momentum of the inbound photons must equate that of the plasmon wave)[85]. Since the wave propagates on the surface, its momentum is strongly affected by whatever is surrounding the metal, including any adsorbed molecule. This fact is exploited for sensing purposes. The plasmon-carrying surface is functionalized with molecules able to selectively bind the analyte to be detected. When the binding occurs, the plasmon wave momentum gets modified, and the wavelength of maximum excitation (resonance wavelength) change accordingly. The main drawback of this method is that only the analyte very close to the surface (a few nanometers) can bind and thus be revealed. All the volume beyond that very short distance is lost to the sensor. Once again, the small dimensions of microfluidics helps to minimize the lost volume. A number of MFDs have been developed following these principles by

fabricating a microchannel above a functionalized metal surface to flow the analyte solution and bring it in close contact with the binding sites[86–88].

Many other optofluidic detection and/or sensing strategies have been proposed, but in general while all these devices are "optofluidic" in the sense that they combine light with microfluidics, all light handling (aside from the actual interaction) is usually made off-chip. This of course delegates complex supporting functions like light generation to external equipment, limiting compactness and portability.

1.5.3 Light generation

Including a generic light generation functionality inside a microfluidic device is not particularly difficult, since cheap and small LED sources are available to be integrated inside a MFD. Depending on the application, such inclusion could even be unnecessary if external ambient light is sufficient to work the device. However, many optofluidic modules need intense, coherent and/or monochromatic light and thus require the inclusion of a laser source. One simple way to achieve this is to integrate a laser diode in the device. While this solution has its merits (chief among them the fact that laser diodes are pumped electrically and not optically), it also has a number of drawbacks.

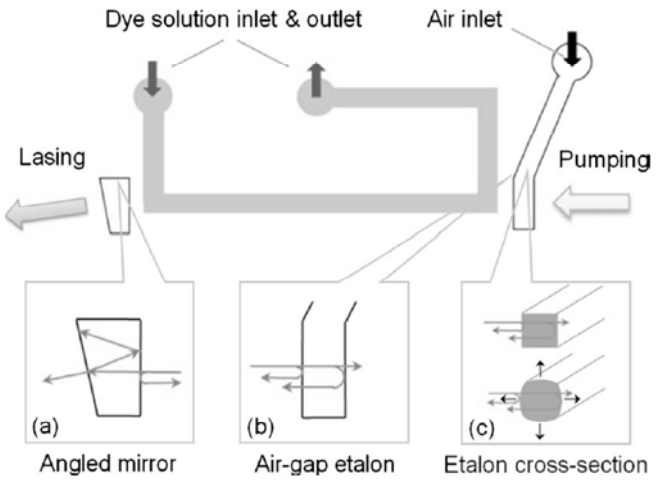

Figure 1.17: tunable microfluidic dye laser. Two air chambers act as cavity mirrors, and the etalon doubles also as wavelength selector. By injecting more air in the etalon, the chamber swells and the lasing wavelength is changed. (adapted from [90])

Diodes are made of semiconductors (mostly gallium or indium arsenide)[89], which are not typical bulk materials for microfluidics, posing the problem of integrating different materials in the same device (unless a modular approach is selected). Also, laser diodes are not tunable, limiting their versatility, and while enough different

diodes exist to cover almost all the visible and near infrared range, certain spectral region (e.g. blue light) still require devices that are quite expensive.

Another solution is to integrate a dye laser inside the MFD. Such lasers blend very well with microfluidics, since they rely upon a flowing dye solution as the active medium. Also, through the judicious choice of dyes any wavelength can be obtained, and the wide emission spectrum of any given dye allows laser tunability (as long as the cavity length can be modified accordingly). Resonant cavities in optofluidic dye lasers are usually realized in one of two ways. The first is to use a channel filled with dye solution and include two semireflecting surfaces along the channel axis. An example of such arrangement (with "mirrors" outside the channel) is reported in Figure 1.17. The bulk of the device is transparent polymer (PDMS), and two properly designed air-filled chambers provide a high enough refractive index step to ensure partial reflection. The chamber on the right doubles as a Fabry-Perot etalon that select the lasing wavelength. This design also exploits the elastomeric nature of PDMS to provide tunability: by

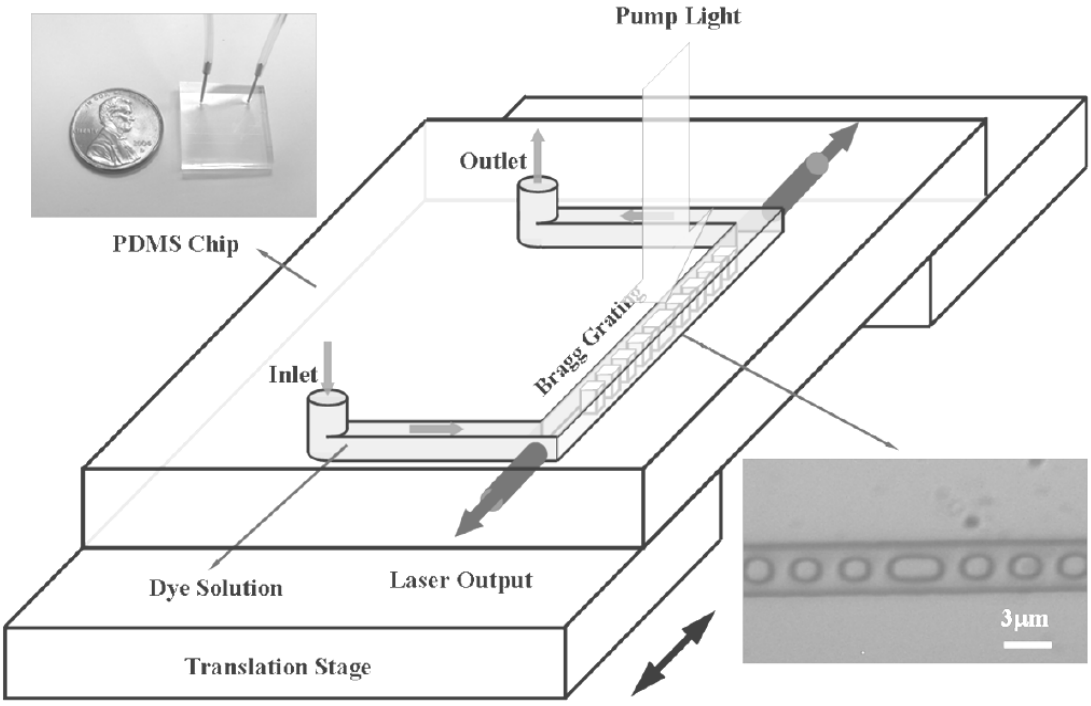

Figure 1.18: tunable DFB dye laser. The elastomeric nature of PDMS allows lasing wavelength tunability by stretching the whole device and thus changing the grating period. (adapted from [91])

forcing more air in the etalon chamber, the increased pressure causes the chamber to swell, effectively changing the length of the etalon and thus the lasing wavelength. With this arrangement, the authors reported a tunability range of 14 nm centered at 588 nm[90].

The second possibility is to realize a distributed feedback (DFB) laser by fabricating pillars inside the dye channel to generate the periodic refractive index modulation needed to confine and amplify light. Figure 1.18 shows the scheme of such a device[91]. Once again it is realized in PDMS, and as in the previous example, the elasticity of this material is exploited to achieve tunability. In this case, the whole device is mechanically stretched to modify the period of the refractive index modulation and consequently change the lasing wavelength. Using a combination of two dyes as the gain medium, the authors reported a 60 nm modulation of the emission with a 5% stretching of the device. It is worth of notice that the elasticity of PDMS is such that the limiting factor in lasing tunability is the emission spectrum of the selected dyes and not, as could be expected, the maximum deformation achievable by the material.

1.5.4 Light guiding

Regardless of whether the light is generated on- or off-chip, to be used for the desired application it must be guided to a specific location inside the device. For the simplest MFDs, simply pointing the beam from the source towards said location is enough. More complex devices might require additional care, especially if the target location is beneath layers of materials that could reflect, refract or scatter the light. The issue is even more sensitive if the light must not be brought to, but collected from said location and conveyed to (for example) a detector. The typical situation of this kind would be weak, highly divergent light emitted from some point inside the device that must be guided somewhere else. The only way to do this efficiently is to employ waveguides. Conventional optical waveguides (silica fibers) can be integrated in a MFD, or the bulk material of the device can be locally modified to increase its refractive index, allowing

it to guide radiation. This methods are straightforward, but for many applications a better solution would be to make the microfluidic channels themselves work as a waveguide. This would allow light-fluid interaction along all the channel length, providing long optical paths. Unfortunately, the most common materials for MFDs production (PDMS and glass) have a higher refractive index than water, the most common fluid flowed inside microchannels. This means that a water-filled channel cannot work as a conventional, total-reflection-confined waveguide. However, a number of alternative methods for confining light inside microchannels have been proposed[92]. Two of the most interesting are the liquid core/liquid cladding (L^2) waveguide, and the so-called ARROWs. Starting with the latter, antiresonant reflecting optical waveguides (ARROWs) have been known by the scientific community since the late eighties[92–95], but until a few years ago they have been only applied to whole-solid systems. In this waveguides, a low refractive index core is surrounded by layers of a higher-index material whose thicknesses are carefully adjusted (and depend on core dimension and both core and layers refractive indexes). The result is an antiresonant effect that prevents the light from escaping the waveguide[†]. It should be noticed that differently from conventional waveguides, the ARROW core is of *lower* refractive index than the "cladding". Exploting this effect, in microfluidic applications any channel filled with a fluid of known refractive index can be surrounded with suitably engineered cladding layers and thus be made into a waveguide[96]. The greatest drawback of these structures is that the surrounding layers have very strict requirements on both refractive index and thickness. This not only means that the fabrication process must be very precise, but also that a number of different materials will have to be integrated in the final device. Notwithstanding these limitations, ARROWs have been repeatedly (and successfully) employed inside microfluidic devices.

[†] More precisely, the propagation mode is leaky, but very low-loss. Also, the light is actually confined in the surrounding layers, but the propagation modes have a very strong overlap in the low-index core, justifying the approximation of core-bound light. A more rigorous mathematical treatment on the subject can be found in references [92] and [95].

The second kind of light-guiding microchannels are the L^2 waveguides. In this design, the laminar flow typical of MFDs is exploited to generate a stratified flow in which a core fluid is sandwiched between two layers of a lower refractive index liquid. In this way, all the waveguide (core and cladding) is inside the channel, and the light is confined in the inmost layer by total internal reflection regardless of the refractive index of the bulk material in which the channel is engraved[97]. This method is quite simple to implement, but also shows some limitations. First of all, if the selected fluids are miscible, diffusion will progressively blur the boundary between core and cladding, degrading the guide properties. Even if the liquids are not miscible, any molecule in the core layer will usually in part migrate to the cladding, decreasing its own concentration and thus reducing the sensitivity (for detection application) or the yield (for photochemical synthesis) of the device. Still, L^2 waveguides have been subjected to intense study, and a number of MFDs that make use of this technology have been proposed[97,98].

1.5.5 Light control

Even the simplest optofluidic devices, those that can dispense with waveguides or integrated light sources, will in most case require some element that manipulates or controls the light (e.g. a lens). This requirement can be met through the use of external equipment, but this solution reduces device portability and compactness. For this reason, many research groups have proposed a wide array of optofluidic elements able to manipulate light once it has been injected inside the device. The greatest part of the work has been dedicated to the design and realization of *tunable* optical elements[75,76]. Among these, variable focal length lenses are probably the most thoroughly investigated.

One of the most successful design for a tunable lens is a sealed cylindrical chamber which contain two immiscible liquids (water and a high refractive index oil)[99]. Both fluids are transparent to visible light. The lateral walls and the ceiling of the chamber

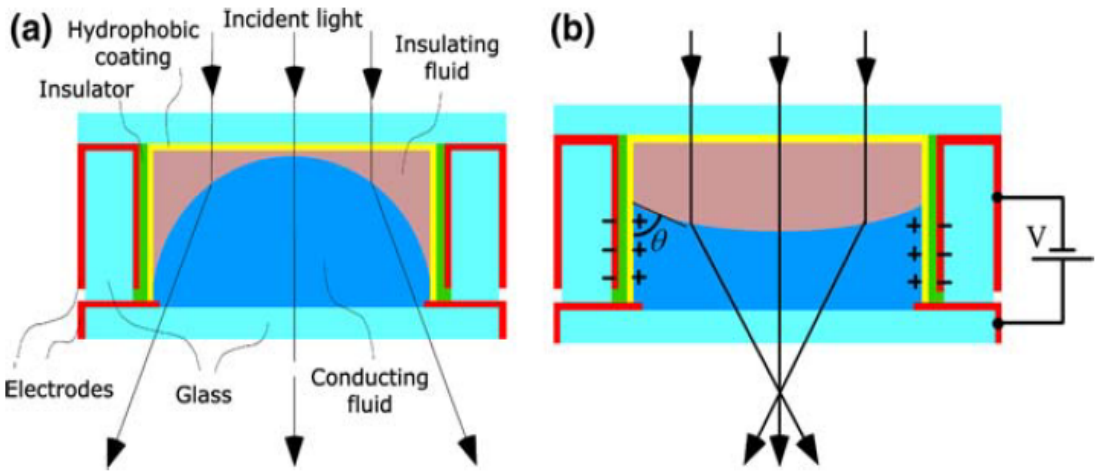

Figure 1.19: tunable optofluidic lens; a) the hydrophobic walls force the water phase to assume a hemispherical shape which works as a diverging lens; b) applying a voltage changes the wettability properties of the walls, modifying the shape of the water phase and changing the focal length of the lens. (reproduced from [99])

are functionalized to be hydrophobic, forcing the hydrophilic phase to assume a hemispherical shape (see Figure 1.19). The meniscus between the two fluids act as the lens interface, and in this configuration the whole chamber works as a divergent (negative focal length) lens. Applying a suitable voltage to the chamber walls, their hydrophobicity can be progressively reduced (a phenomenon known as electrowetting). This will cause a modification of the drop shape, which will in turn cause a variation in the lens focal length. This design has been particularly successful, to the point that commercial applications based on this element are already available on the market[‡]. Another kind of tunable lens exploits a lens-shaped empty chamber engraved in bulk PDMS. Since this material is elastic, forcing compressed air inside the chamber causes it to swell, changing the curvature of the walls and thus the focal length of the lens[100]. Another optical element that has been successfully realized is a tunable diffractive grating[76]. Once again the elastic behavior of PDMS is exploited to achieve tunability. The scheme of this element is shown in Figure 1.20. By increasing the pressure inside two of the four chambers, the engraved grating can be made to vary its period. The

[‡] See for example Philips FluidFocus lenses (www.research.philips.com/technologies/fluidfocus.html).

result is that once a laser beam is shone through the grating, the angle(s) of diffraction will vary accordingly, increasing as the grating period decreases.

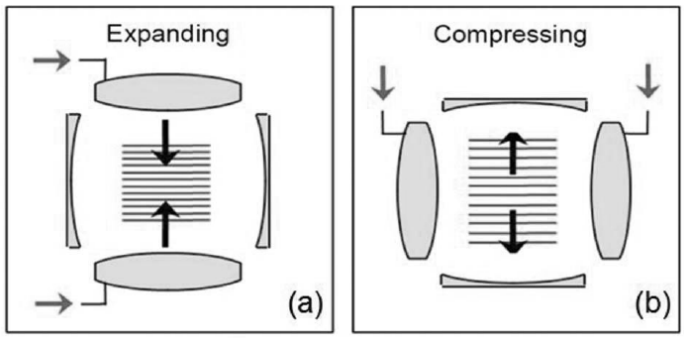

Figure 1.20: tunable PDMS diffraction grating. Forcing air inside two of the four chambers causes a deformation that a) contracts or b) stretches the grating. This results in a higher or lower diffraction angle, respectively. (adapted from [76])

A considerable number of other optofluidic elements have been proposed, but at the same time many of the optics that are typically featured on a macroscopic optical table remain to be fully developed. In particular, elements like polarizers, choppers or irises still have few, if any, optofluidic equivalents.

Chapter 2

MICROFABRICATION

2.1 Microfabrication with SU-8 and PDMS

The study and characterization of microfluidic devices (MFDs), starts with the techniques used to fabricate them. As summarized in Section 1.4, there are a lot of different processes to realize MFDs, and the choice of one or another depends on many factors like resolution requirements or materials constraints. The first objective in this work has been that of selecting a "default" fabrication method (and associated default materials) to be used whenever the device characteristics do not require a specific, different process. This preferred technique was chosen to be PDMS replica molding from masters obtained through UV photolithography or direct laser writing (DLW).

2.1.1 Master fabrication via UV photolithography

The selected photosensitive materials (resists) for master realization have been Microchem SU-8 2025 and 2050. These are two similar prepolymer blends differing only in the amount of solvent (cyclopentanone) present in the mixture, which in turn influences the viscosity of the whole and defines the range of film thicknesses that can be achieved through spin coating. SU-8 is a negative photoresist, which means that the part exposed to UV radiation will polymerize, while the rest will be washed away during development (see chapter 1.4.7). Figure 2.1 shows the chemical structure of the two main components of this material, as well as the polymerization reaction pathway[101]. SU-8 is composed by an epoxy-rich monomer that generates a highly crosslinked final material due to the high number of reticulating moieties available in each molecule (eight epoxy groups for each monomer molecule). The ring aperture reaction is catalyzed by fluoroantimonic acid generated by the UV-induced cleavage of a triarylsulfonium hexafluoroantimonate salt which acts as the photoinitiator. The resulting material has very good mechanical properties and is highly resistant to most

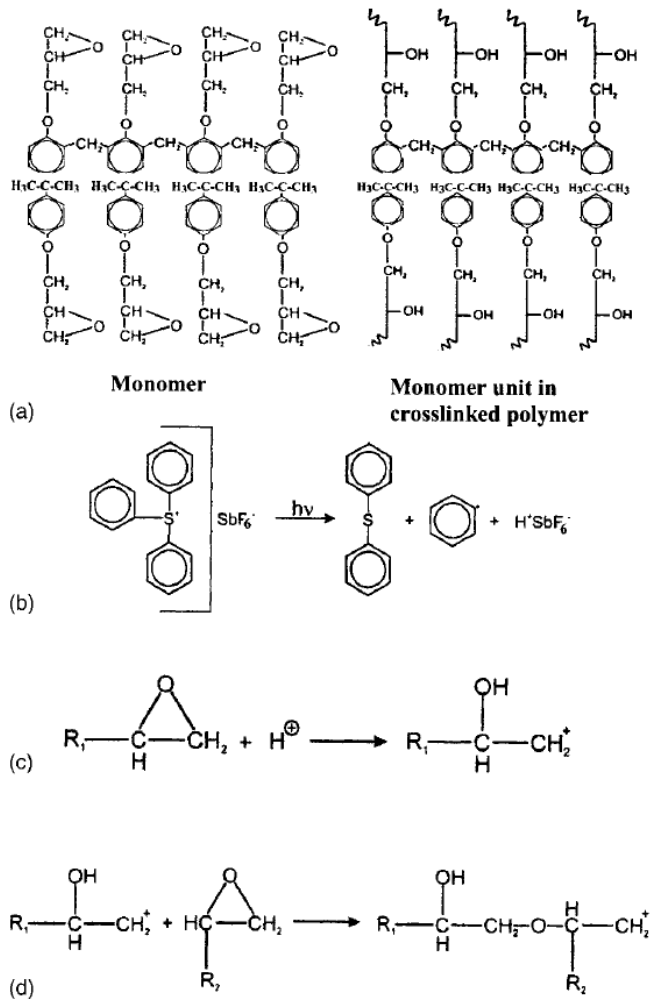

Figure 2.1: a) chemical structure of one SU-8 monomer unit in unreacted (left) and polymerized (right) form. The high number of epoxy moieties in each monomer ensure extended crosslinking between different molecules; b) photoactivation reaction of SU-8 initiator; c) polymerization initiation by means of H^+ catalyzed ring aperture; d) cationic polymerization propagation. (reproduced from [101])

solvents, allowing the realization of resistant masters which if needed can also feature structures with high aspect ratio (e.g. very high and thin pillars)[101–103].

The standard sample preparation is adapted from Microchem guidelines*, and is summarized in the following. A silicon substrate is thoroughly cleaned with deionized water and 2-propanol, and is placed in a UV-ozone (UVO) cleaner (Jelight model 42) for at least 10 minutes. This step is required to activate the sample surface by forcing the creation of dangling bonds in the native oxide surface that will enhance the adhesion of the SU-8 microstructures to the substrate. Without this extra step, there is a strong possibility that the photogenerated structures will detach from the silicon during the following processes. Once the substrate is ready, a thin film of SU-8 is deposited on the silicon via spin coating. The selected film thickness depends on the desired thickness of the final structures. Using SU-8 2025 and 2050, thicknesses between 20 μm and 70 μm have been routinely obtained. If greater thickness is required, two spin coater depositions (separated by a thermal treatment as

* Microchem guidelines are available at http://microchem.com/Prod-SU82000.htm.

described below) can be performed on the same sample to increase the thickness up to about 150 μm. Regardless of film thickness, the sample is then subjected to a thermal treatment to remove the excess solvent from the monomer. This is done in two steps, increasing the temperature first to 65°C and then to 95°C to reduce thermal stress. The exact duration of both steps depends on the film thickness (following Microchem guidelines), but it must be kept well in mind that while a greatly overlong time can compromise the following development, an incomplete solvent evaporation will surely lead to a number of complications like decreased resolution, structure deformation or detachment from the substrate. Once this treatment is complete, the sample is exposed through an appropriated mask to the UV light to induce polymerization. The light source used is a collimated UV lamp (Reinraumtechnik Lanz UV400) equipped with a timer to ensure precise exposure time. Once again the exact time depends on the film thickness. The masks are realized with a plotter by cutting holes in a black vinyl adhesive and than attaching it to a microscope slide. Exposure is followed by another thermal treatment with the same parameters of the first. This second bake is needed to actually polymerize the material, since the initiator is generated during the exposure, but the mobility of the involved chemical species at room temperature is too low to ensure reticulation in timely fashion[104]. Finally, the sample is submerged in SU-8 Developer (Microchem) under stirring until all the unexposed material is removed. The final sample is rinsed with 2-propanol and is now ready to be replicated. Masters with features down to 500 μm have been realized with this technique. The cutting process used to realized the masks leaves a slight roughness on the mask holes borders, which is replicated on the structures during photolithography. However, this roughness never exceeded 1-2 μm.

2.1.2 Master fabrication via direct laser writing

While UV photolithography is a fast and efficient technique, some devices require better resolution or greater flexibility. When this is the case, DLW has been employed

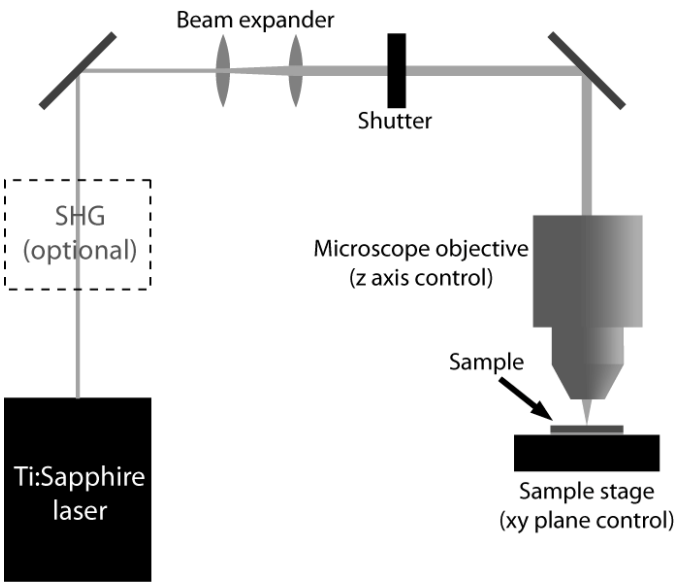

Figure 2.2: schematic representation of DLW set-up. The light produced by a pulsed Ti:Sapphire laser oscillator (780 nm, 130 fs) is expanded by two lenses and focalized on the sample by an objective microscope. Objective and sample stage can be moved to control the position of the focal volume on the sample. For one-photon DLW a second harmonic generation (SHG) module is added to the set-up.

(see chapter 1.4.8 for an overview on the principles and advantages of this technique). The procedure for master creation is the same as for UV lithography, with two differences. First of all the lamp exposure is replaced with direct laser writing, i.e. a focalized laser beam is shone on the sample to induce polymerization in a point-by-point fashion. Secondarily, the second (post-exposure) thermal treatment is skipped or greatly reduced in time, since the laser generates enough heat to complete the polymerization during exposure[105]. The experimental set-up that has been used for DLW is schematized in Figure 2.2. The light source is an ultrafast Ti:Sapphire laser (Coherent Mira 900-F) which generates laser pulses of 130 fs with a repetition rate of 76 MHz. The wavelength of the emitted light is tunable between 700 and 1000 nm, and for two-photon DLW it has been selected to be 780 nm. For one-photon DLW, a second harmonic generating crystal (Type I BBO) has been added on the light path to extend the available radiation to the 350-500 nm range. After exiting the laser, the beam is slightly expanded by a pair of lenses, sent through a computer-controlled shutter and finally focalized on the sample by a 20x (NA 0.46) microscope objective (Olympus UMPLFL20X). The objective is mounted on a piezoelectric holder that can change the z position of the focal point by up to 200 μm. The sample is placed on a stage made from two twin linear stages (Steinmeyer FMD PMT-160) able to translate the sample in the

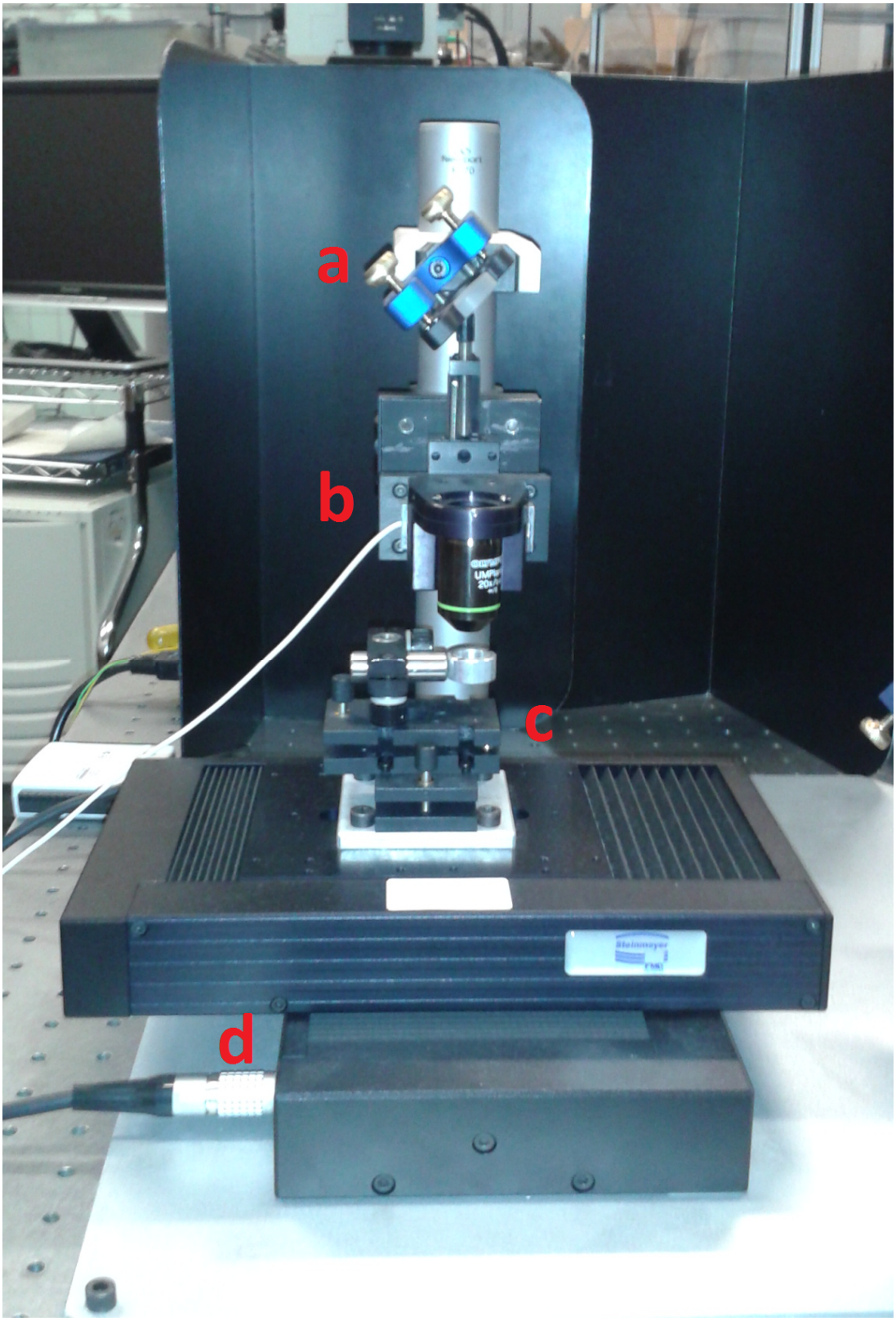

Figure 2.3: photograph of the stage area of the experimental set-up; a) mirror to direct the laser beam to the objective; b) objective mounted on a piezoelectric holder (z axis control); c) sample holder with tilters to ensure laser perpendicular incidence; d) couple of linear translators (xy plane control).

xy plane within a 100 cm^2 square area with 0.5 μm resolution. A photograph of the stage area is shown in Figure 2.3. Sample stage, objective holder and shutter are all connected to a computer. As part of this work, a labView program has been developed to integrate control for all three elements, allowing the automated fabrication of structures ranging from simple dots to complex figures delimited by segments or circular arcs. If two-photon DLW is employed, three dimensional structures can be made in a plane-by-plane fashion. This sort of automation is extremely useful since DLW is a serial process, and as such can be quite time-consuming if the required structures cover a large area.

2.1.3 Replica molding

Once the master structure have been created, the final device is realized through the replica molding technique[44] (see chapter 1.4.9). PDMS prepolymer and iniziator (Dow Corning Sylgard 184) are mixed in a 10:1 ratio and then degassed in mild vacuum to remove trapped air bubbles. The mixture is then poured over the master and subjected to a thermal treatment in oven at 120° C for 1 hour. The sample is then brought back to room temperature and the replica is peeled off from the master. Inlet and outlet holes are punched through the PDMS. Finally, the replica and a flat slab of PDMS or glass (e.g. a microscope slide or a coverglass) are treated with a UVO cleaner for 3 minutes to create surface dangling bonds that can react with one another when the two surfaces are brought into contact and kept at ~120°C for at least 1 hour. The result is a permanent sealing that completes the device.

2.2 Beyond PDMS

It has been mentioned before (see Sections 1.4.2 and 1.4.9) that while PDMS and replica molding are excellent ways to cheaply and rapidly produce MFDs, both suffer from certain limitations. The one drawback that most strongly influences microfluidic devices production is the limit imposed over microstructures shapes: replica molding

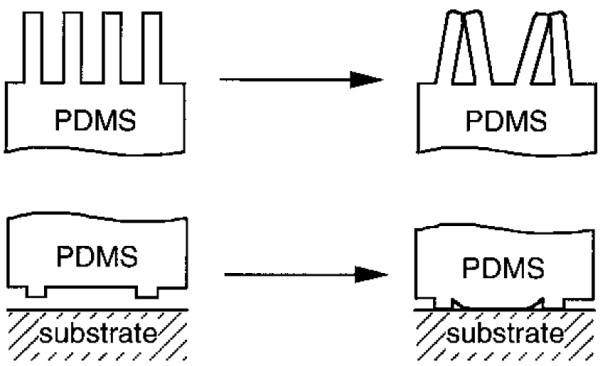

Figure 2.4: examples of how PDMS replicas featuring structures with high aspect ratio will usually collapse due to the elastomeric nature of this material. (adapted from [44])

cannot replicate masters with overhangs or closed loops. Also, the low Young modulus of PDMS means that structures with high aspect ratio will usually fold or collapse under their own weight[44]. Figure 2.4 shows some example of this behavior. Considering this fact, it would be extremely useful to investigate also some other material or technique able to complement PDMS replica molding, so that when the latter fails, the other would be ready to step in.

2.2.1 Hybrid sol-gel

The first candidate that has been tested is a hybrid organic/inorganic sol-gel blend[54]. This material is made from a mixture of zirconium butoxide, methacrylic acid and 3-methacryloxypropyltrimethoxysilane (MPTMS) in 3:6:5.5 molar proportions. Tetrahydrofuran (THF) is used as a solvent to reach the desired concentration (170 grams of SiO_2 groups per liter). MPTMS is a hybrid molecule, featuring both an inorganic part and an organic moiety (see Figure 2.5). Through condensation reactions, the inorganic groups (including Zr-butoxide) can reticulate and form the Si-O-Si network typical of most sol-gels. However, this molecule also contains an organic (methacrylic) moiety that can, with the aid of a suitable photoinitiator, polymerize to form an organic network. The selected photoinitiator is 4,4'-bis(diethylamino)benzophenone (in 1% concentration with respect to the acrylic units), which can absorb light with wavelength in the range 320-400 nm and thus promote polymerization[106,107]. The advantageous characteristics of this material are those typical of hybrid sol-gels: better mechanical properties and solvent resistance than most polymers, but reduced stiffness with respect to completely inorganic blends.

Samples for sol-gel microfabrication are prepared as follows. The sol-gel solution is spin coated (1500 RPM for 30 s) on UVO-treated silicon or glass, and then thermally treated at 100°C for 10 minutes to initiate Si-O-Si condensation. The resulting thin film is then exposed as needed through UV lithography or DLW. Development of unexposed material is achieved by submersion in hot (60°C) 2-propanol for approximately 1 minute. To quantify the film thickness, a series of samples have been exposed to the UV lamp for 1 hour (to ensure complete polymerization), scratched with a blade and measured with a profilometer (Tencor p-10). These measurements resulted in a average thickness of 2.5 μm for fully polymerized films. It should be noted that the polymerization/condensation process induces a moderate shrinkage in this material, which means that the measured value is less that the original, as-spinned thickness. However, since all the realized microstructures undergo this process, the measurement of shrunk films has been deemed more significant.

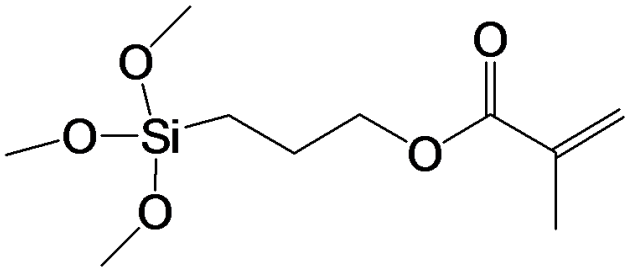

Figure 2.5: chemical structure of MPTMS, featuring both an inorganic group (left side of the molecule) and an organic moiety (right side).

2.2.1 Nano building blocks

Besides MPTMS, a second hybrid material has been tested: nano building blocks (NBB)[54]. This blend shares zr-butoxide and methacrylic acid with the previous solution, but substitutes MPTMS with the so-called nano building blocks. These nanostructures are chemically similar to MPTMS, but are already partially condensed to create a cage-like shape. A representation of NBB can be found in Figure 2.6. This material behaves in a way similar to the previous, meaning that the methacrylic "tails" that dangle from the cage vertices can polymerize when exposed to suitable light in the presence of 4,4'-bis(diethylamino)benzophenone (photoinitiator). However, it is

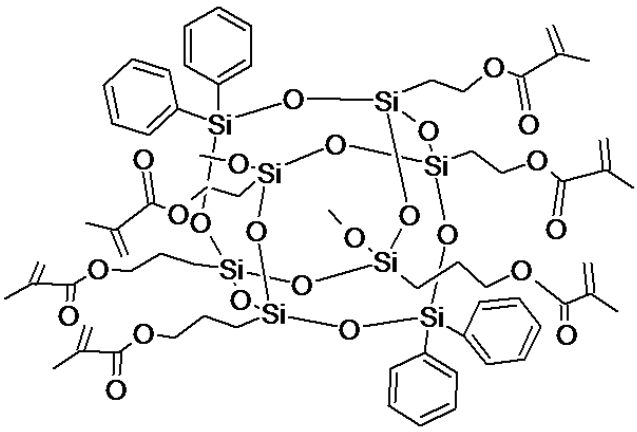

Figure 2.6: chemical structure of NBB. The cage-like Si-O-Si structure is surrounded by protruding photopolymerizable methacrylic groups.

expected that the presence of unit structures instead of single molecules will have an effect on the final properties of the material (e.g. in terms of fabrication resolution and mechanical properties). To qualify these features, a series of samples have been realized also for this blend. The preparation procedure is the same, except for the thermal treatment step that is skipped. This modification of the procedure is due to the fact that this material is already partially condensed. The high temperature would cause additional inorganic reticulation, bringing the film to the point that it would resist development even where it hasn't been exposed to light.

2.2.2 Differences between the two materials

To test the different behavior of the two materials (MPTMS and NBB blends) concerning DLW, linear structures have been realized through one-photon DLW on both substrates. Exposure have been performed with laser power on the sample ranging from 5 μW to 2.3 mW. The sample has been moved under the laser beam in a straight line with a speed of 100 μm/s. The resulting structures have been characterized through scanning electron microscopy (SEM) imaging.

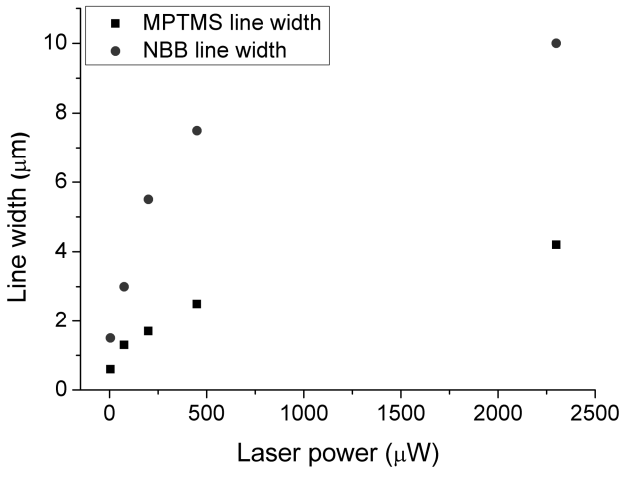

Figure 2.7: comparison of line width for MPTMS and NBB blends at different laser powers. All lines were realized through one-photon DLW (exposure wavelength 390 nm, scanning speed 100 mm/s).

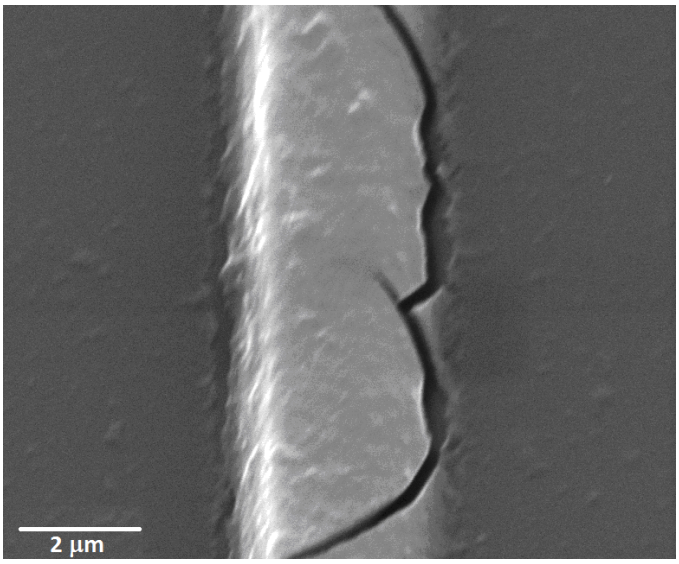

Figure 2.8: example of NBB structure showing cracks. The increased rigidity of this materials cannot sustain the stresses due to shrinkage even for thin structures like this one.

The results show a clear superiority of the MPTMS blend with respect to the NBB. The first material features a better resolution (i.e. smaller line width for the same laser power, see Figure 2.7). Also, NBB lines are often cracked (see for example Figure 2.8). This mechanical failure is attributed to an increased stiffness of the material, which is in turn ascribed to the rigidity of the cage-like nanostructures. During photopolymerization the blend undergoes a shrinkage process, which causes cracks in the structures where the material is too stiff to accommodate the reduction in volume. Both these drawbacks strongly limit the applicability of this blend for microfluidic devices fabrication. In light of this, the NBB blend has been discarded in favor of exclusive use of MPTMS as hybrid sol-gel material.

2.3 Direct laser writing with MPTMS

Once identified MPTMS as the preferred material to substitute PDMS where needed, a series of photopolymerization tests have been performed. Characterizations concentrated on the material response to two-photon DLW, ranging from single point exposure to lines generation to the fabrication of two-dimensional structures. Large-area structures have also been compared to similar structures realized through one-photon polymerization to identify limits and merits of both techniques.

2.3.1 Single point exposure characterization

The first characterizations for two-photon DLW on MPTMS aimed at investigating the material response to variation of laser power or exposure time. To begin, single point exposure was employed. This means that the laser beam has been allowed to hit the photosensitive film for a well-defined time without moving the sample. The result of this kind of exposure is a cylindrical or egg-shaped unit of polymerized material. Since this is the base unit of which any complex structure is made, it is usually called a voxel, by analogy with two dimensional pixels[†]. The diameter of the voxels depends on many factors, including objective numerical aperture and laser wavelength (that define the dimensions of the focal volume), laser power and exposure time[108]. In this work, objective NA and laser wavelength have been kept fixed at 0.46 and 780 nm, respectively. The effect on voxels diameter of varying laser power (from 1.5 mW to 6 mW) and exposure time (from 0.2 s to 2 s) is showed in Figure 2.9. The data have been collected through fluorescence imaging, exploiting the natural fluorescence of this material. Fully developed samples have been placed on an upright confocal microscope (Olympus FV300) equipped with a water-immersion 60x (NA 1.4) objective (Olympus UPLSAPO60XW) used both to focus a 488 nm Argon laser and to collect the fluorescence generated by said laser. At this excitation wavelength the material absorption is quite low, but enough to induce fluorescence in the 500-600 nm range that is

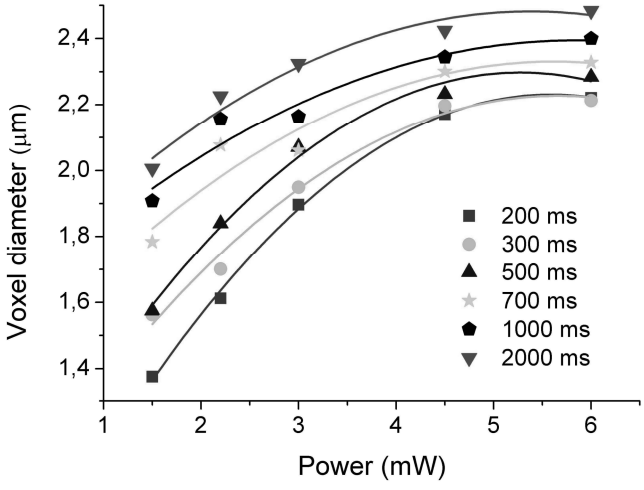

Figure 2.9: voxel diameter vs laser power (on sample) and exposure time. A clear saturation behavior can be seen at powers higher than 4 mW. Lines are only a guide to the eye.

[†]The word "pixel" is a contraction that stands for "picture element". A "voxel" can then be rendered as "volumetric pixel" or simply as "volume element".

recorded by the detector (photomultiplier tube). The confocal geometry (100 μm pinhole) ensure that out-of-focus fluorescence is not revealed. The error on voxel dimension measurements is estimated to be ±0.3 μm.

Observing Figure 2.9 progressive increase of voxel diameters with increasing laser power and/or exposure time can be easily seen. This behavior is expected, since only the beam area that exceeds a specific threshold intensity can promote photopolymerization. The radius w_0 of the focal area on the sample can be deduced from Gaussian optics laws[109]:

$$w_0 \approx \frac{2\lambda}{\pi NA} \qquad (2.1)$$

where λ is the laser wavelength and NA is the numerical aperture of the focalizing objective. Considering NA = 0.46 and λ = 780 nm, a focal radius of 1.08 μm is obtained. Considering that the spatial intensity distribution of the laser beam on the sample follows a Gaussian profile, it can be predicted that a reduction in overall laser power will cause a smaller polymerized area (see Section 1.4.8). A similar reasoning can be made for exposure time, taking into account the fact that even below-threshold intensity can interact with the photoinitiator and, in due time, generate enough reactive species to trigger polymerization. The trend of voxel diameter d with laser power and exposure time can be expressed as[108]:

$$d = w_0 \left[\ln\left(\frac{\sigma_{eff} N_0^2 f \tau t}{C} \right) \right]^{\frac{1}{2}} \qquad (2.2)$$

where f is the repetition rate of the pulsed laser, τ is the pulse duration, t the exposition time and σ_{eff} is the product of the initiator two-photon absorption cross section σ_2 and the efficiency η of the initiation process ($\eta < 1$). N_0 is the photon flux, which can be expressed as:

$$N_0 = \frac{P}{f \tau h \nu \pi w_0^2} \qquad (2.3)$$

where P is the average laser power on the sample and ν is the frequency of the involved photons. Finally, C is defined as:

$$C = \ln\left(\frac{\rho_0}{\rho_0 - \rho_{th}}\right) \tag{2.4}$$

where ρ_0 is the initial density of (unreacted) photoinitiator molecules and ρ_{th} is the minimum density of activated photoinitiator molecules able to trigger polymerization. Using equation (2.3), equation (2.2) can be rewritten as:

$$d^2 = w_0^2\left[K - \ln\left(w_0^4\right) + \ln\left(P^2 t\right)\right] \tag{2.5}$$

where

$$K = \ln\left(\frac{\sigma_{eff}}{Ch^2\nu^2\pi^2\tau f}\right) \tag{2.6}$$

Plotting the data in Figure 2.9 as a function of P^2t, the values of K and w_0^2 can be estimated (Figure 2.10). From the fit, $w_0 = 0.93 \pm 0.02$ μm, a value in good agreement with that estimated from Gaussian optics ($w_0 = 1.08$ μm). Unfortunately, nothing can be said about K, since both σ_{eff} and ρ_{th} (and thus C) are unknown.

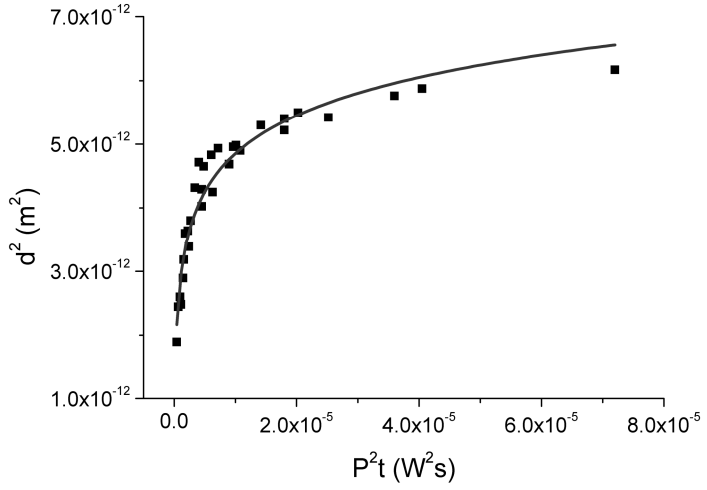

Figure 2.10: squared voxel diameter vs the product of exposure time and squared laser average power. Squares are experimental data point, while the line is a fit following equation (2.5).

Observing Figure 2.10 it can be seen that for high values of P^2t the data point indicate a smaller voxel diameter than that indicated by equation (2.5). This difference can be explained considering that equation (2.5) simply accumulate the photoinitiator radicals generated by every laser pulse, neglecting the

radicals lost between pulses[108]. For long exposure times, this neglected contribution can possibly become high enough to justify smaller voxels.

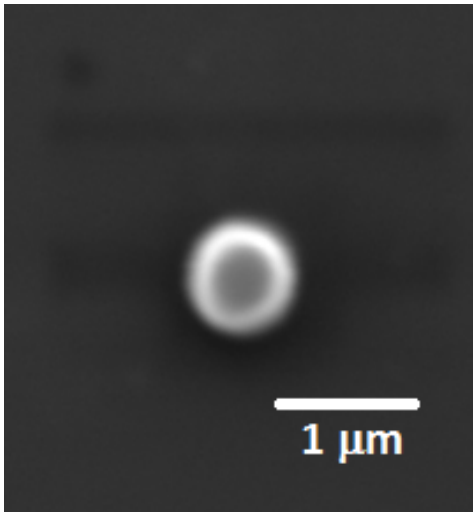

Figure 2.11: SEM image of one of the smallest voxel retrieved after development. The structure is approximately 600 nm in diameter.

Further experiments have been performed with the aim of quantifying the resolution available to this material, i.e. the tiniest structure achievable. The smallest voxel reproducibly retrieved after development had a 600 nm diameter and was obtained with a laser power of 0.5 mW and an exposure time of 500 ms (see Figure 2.11). This and similarly dimensioned structures are too small to characterize through fluorescence imaging, and so they were imaged with a SEM instrument.

2.3.2 Line exposure characterization

The second type of features that have been characterized are linear structures obtained by moving the sample with a controlled speed in a straight line under the laser spot. After development, the dimensions of the resulting lines have been quantified in the same way as before (fluorescence and SEM imaging). These data are reported in Figure 2.12. As with single point exposure, the line width increases with increasing laser power. Also, higher movement speeds of the sample stage cause the generation of smaller lines. This is to be

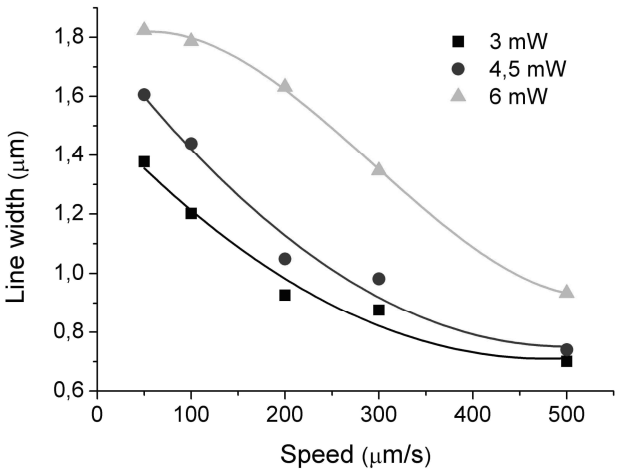

Figure 2.12: line width vs stage speed at increasing (squares to triangles) laser powers on sample. Differently from Figure 2.9, no saturation is observed. This is due to the exposure times being one to two order of magnitude shorter than in the single voxel case. Lines are only a guide to the eye.

expected, since stage speed is (inversely) proportional to exposure time, i.e. higher speeds correspond to shorter exposure times for each point of the line. The width of the smallest line reproducibly retrieved after development is around 700 nm, a value comparable with that of the smallest voxel (600 nm). Differently from the previous experiments (Figures 2.9 and 2.10), no clear saturation behavior can be seen in Figure 2.12. The reason for this appears clear once considered the effective exposure times corresponding to the speeds used in the experiments (50 μm/s to 500 μm/s). As an example, at a speed of 50 μm/s, the exposure time for the focal spot of 2 μm diameter is 40 ms. This means that the typical exposure times used for line writing are from one to two orders of magnitudes smaller than those used for single point exposure.

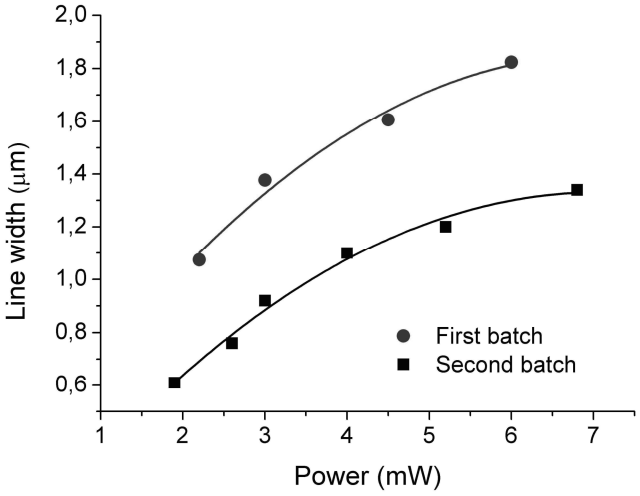

Figure 2.13: comparison of structures realized with two different batches of the same MPTMS sol-gel blend. Reproducibility is insufficient for structures requiring sub-micrometric resolution. Lines are only a guide to the eye.

To test the reproducibility of this process, a series of lines has been written with a constant 50 μm/s speed and laser power increasing from 2 mW to 7 mW on samples prepared with two different batches of the same sol-gel blend. The comparison between the two is reported in Figure 2.13. As can be seen from the graph, reproducibility between different batches can be achieved within ~500 nm. Thus, if resolutions below the micrometer are required, each batch will have to be singularly calibrated.

2.3.3 Two-dimensional structures: grids

Having fully qualified the relationship between exposure time (or stage speed), laser power and polymerized area dimensions, the attention was moved to the realization of

more complex structures. In particular, the possibility of realizing grids by intersecting multiple parallel lines was investigated. By using 90° angle intersections, regular square grids can be realized. Based on previous measurements, a laser power of 3 mW was selected, and the sample stage was moved with a speed of 50 μm/s. The step between adjacent lines was varied from 3 μm to 10 μm. An example of the resulting structures is reported in Figure 2.14. The measured line width for all grids is 1.1 ± 0.1 μm, meaning that there is no coalescence between adjacent lines even for the smallest-step grids. All the realized structures have good morphological quality and show no sign of cracks. This absence is proof of the reduced stiffness of this hybrid material compared to fully inorganic ones. This blend can sustain the tensile stresses that are generated during polymerization due to material shrinkage, and so the final structure is crack-free even in the points of maximum strain (i.e. the corners at lines intersections).

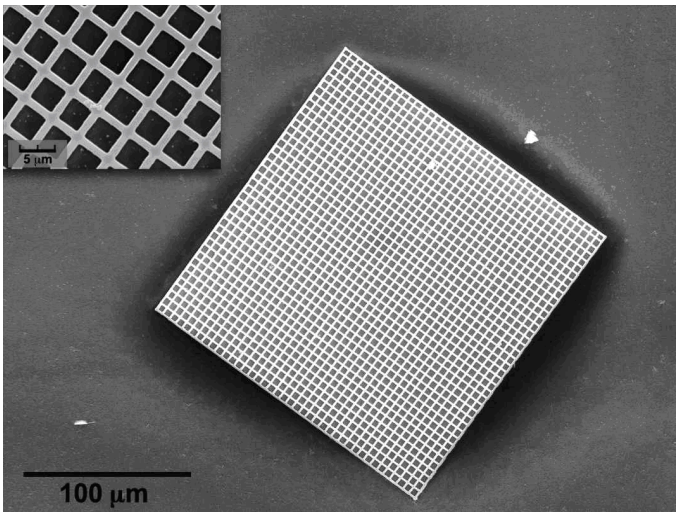

Figure 2.14: SEM image of a grid realized by two-photon DLW on MPTMS sol-gel. Inset: a detail showing the good quality of the microstructure, without any sign of cracks.

While two-photon DLW produces good quality structures, it suffers from a non-negligible drawback. Since the material must be polymerized point-by-point, DLW is a serial process. Even more aggravating is the fact that the extremely low two-photon absorptions cross-sections mean that long exposure times are required to activate enough photoinitiator to actually initiate polymerization. All considered, this translates into the fact that to create large area structures, very long times are necessary. As an example, realizing a 1x10 mm^2 rectangle would require over 100 hours of continuous

laser operation. Thus, the possibility of generating grids through one-photon DLW was explored.

2.3.4 One-photon microfabrication

The absorption (and corresponding polymerization) efficiency of one- and two-photon processes can be markedly different. As already mentioned in Section 1.4.8, intensity reduction due to absorption can be quantified as:

$$\frac{dI}{dz} = -\alpha I - \beta I^2 \tag{1.3}$$

where I is the light intensity and α and β are respectively the first- and second-order absorption coefficients. Separating the two contributes leads to:

$$\left(\frac{dI}{dz}\right)_{first\ order} = -\alpha I \tag{2.7}$$

$$\left(\frac{dI}{dz}\right)_{second\ order} = -\beta I^2 = -(\beta I) I \tag{2.8}$$

While linear absorption efficiency is constant for all intensities, nonlinear efficiency increases at high light intensities. Thus, for any comparison it is necessary to choose a specific intensity value. In the work here reported, the average laser power P on sample for two-photon DLW is on the order of 1 mW. Since the laser output is pulsed with a frequency ν of 76 MHz and a pulse duration τ of 120 fs, the peak power P_{peak} during exposure is:

$$P_{peak} = \frac{P}{\nu\tau} \approx 100\ \text{W} \tag{2.9}$$

The radius w_0 of the focal area can be estimated from:

$$w_0 \approx \frac{2\lambda}{\pi NA} \tag{2.1}$$

where λ is the laser wavelength and *NA* is the numerical aperture of the focalizing objective. Considering *NA* = 0.46 and λ = 780 nm, a focal radius of ~1 μm is obtained, leading to an intensity *I* on the order of:

$$I = \frac{P_{peak}}{\pi w_0^2} \approx 3 \ \frac{\mathrm{GW}}{\mathrm{cm}^2} \approx 10^{28} \ \frac{\mathrm{photons}}{\mathrm{cm}^2\mathrm{s}} \qquad (2.10)$$

Typical values[110] of β for UV lithography photoinitiators (such as the one used in this work) are on the order of 10 GM‡, while values for α average around 10^{-15} cm^2. This means that for the intensities reported above the ratio between the efficiencies is on the order of:

$$\frac{\alpha}{\beta I} \approx 10^5 \qquad (2.11)$$

As can be seen, one-photon absorption in much more efficient than the second-order process. During DLW this increased efficiency translates into shorter exposure times needed to induce polymerization, which in turn allows faster fabrication of large-area structures. Unfortunately this gain in time corresponds to a decrease in terms of resolution. One-photon processes are less intensity-dependant than non-linear ones, and so it is very difficult (if not outright impossible) to realize structures with dimensions under a few micrometers by simply reducing the laser power or the exposure time. Attempts to do so will usually result in no polymerization whatsoever. Despite this limitation, one-photon DLW would be quite useful for large area, low resolution tasks. For this reason, 10 μm and 20 μm step grids have been realized with frequency doubled laser light (wavelength 390 nm), 500 μW laser power on sample and 2000 μm/s and 1400 μm/s stage speeds, respectively. A microscope image showing the typical results is reported in Figure 2.15. Marked overpolymerization at line intersection can be seen in the image, and most of the corners show cracks. Attempts to lower the laser power, or

‡ The Goeppert-Mayer is a unit for the two-photon absorption cross section. 1 GM = 10^{-50} $\frac{\mathrm{cm}^4\mathrm{s}}{\mathrm{photon}}$

increase the stage speed resulted in no polymerization at all. This poor result is the product of two different factors. The strong absorption of the photoinitiator due to one-photon processes translates into a high local concentration of activated initiator, which in turn leads to fast polymerization (accentuating the risk of cracks) and to diffusion outside the target area (which degrades resolution). Moreover, the reduced stiffness of this hybrid material allows some accommodation of tensile stress due to shrinkage, but evidently not enough to realize crack-free structures with more than one dimension exceeding 1-2 μm (i.e. 1 μm thin lines can be hundreds of micrometers long, but 10 μm wide lines will usually crack). This means that this hybrid sol-gel material is unsuitable for bulk MFD fabrication. However, its other qualities make it an excellent candidate for channel internal sub-structuration. As an example, the desired features could be realized on a coverglass which is then used to seal a network of channels engraved on PDMS. A possible limit to this approach is the fact that this procedure requires a mask aligner or similar instrument to ensure that channel and sub-structuration are not misaligned.

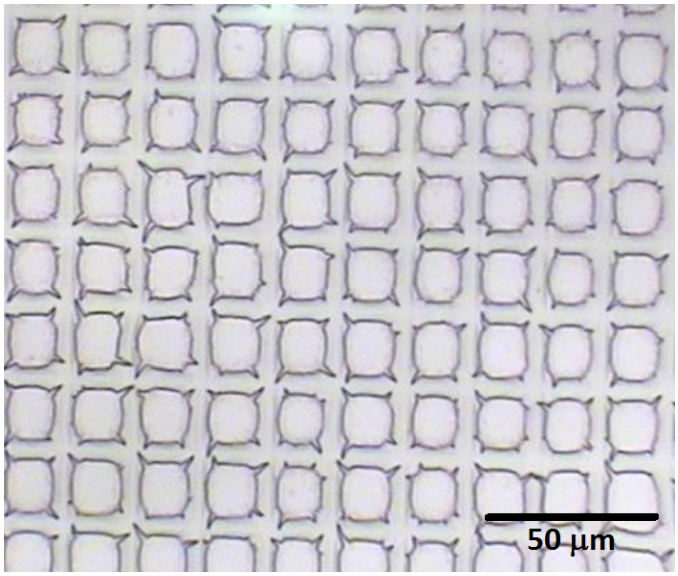

Figure 2.15: optical microscope image of a grid (step 20 μm) realized through one-photon DLW (power 0.5 mW; scanning speed 1400 μm/s). Cracks can be seen at corners, and line intersections are overpolymerized.

2.3.5 Biocompatibility

To further extend the potential usefulness of this material, the biocompatibility of the fully polymerized form was tested. This characterization is very important in light of the recent interest of the scientific community towards MFDs for biological applications

(see Section 1.1.4). The biocompatibility tests were performed by realizing a series of glass samples covered with a flat layer of the MPTMS blend. The sol-gel was kept under the UV lamp for 30 minutes, turned upside down and exposed for another 30 minutes to ensure complete polymerization of the film. After the thermal treatment, the samples were submerged in the development solution (hot 2-propanol) to remove any surviving non-polymerized part that could be present. Following this, the substrates were inserted at the bottom of the wells of a standard 24 multiwell plate (SGW) and then exposed again to UV light for two hours in order to sterilize the material. After sterilization the sol-gel surface was functionalized with a 0.5 μg/μL fibronectin solution. This molecule is a promoter for cellular adhesion, and is commonly used in most biologically oriented MFDs[111,112]. Finally, human umbilical vein endothelial cells (HUVEC) were seeded on the samples, and cultured in endothelial cell basal medium (EBM) supplemented with 10% fetal bovine serum (FBS), 100 IU/ml penicillin and 100 mg/l streptomycin. A microscope image of these cells attached on the sol-gel substrate is shown in Figure 2.16. HUVEC cells were chosen because they are primary cells and as such can be considered a good benchmark for biocompatibility of artificial materials. Indeed their proliferation and viability is more sensitive to the chemical and physical characteristic of the material on which they grow, with respect to cancer line cells or similar more sturdy cell cultures. HUVEC proliferation was tested using a colorimetric assay (Biosource International) based on the redox sensor alamarBlue. The alamarBlue

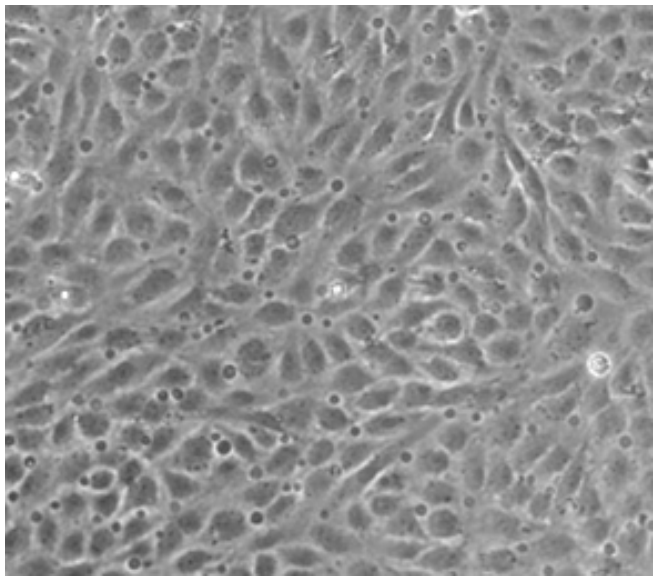

Figure 2.16: optical microscope image of HUVEC cells grown on a completely polymerized MPTMS sol-gel substrate.

reagent functions as a cell health indicator by using the reducing power of living cells to quantitatively measure their proliferation. Resazurin, the active ingredient of alamarBlue reagent, is a non-toxic, cell permeable compound that is blue in color. Upon entering cells, resazurin is reduced to resorufin, a compound that is red in color. The absorbance of alamarBlue reagent can be read on a spectrophotometer and the results are analyzed by plotting absorbance versus compound concentration. HUVEC grown on the sol-gel substrate were compared to cell cultured on a conventional microscope glass slide (coated with fibronectin). The results of this comparison are reported in Figure 2.17, and show that the cell proliferation is comparable between the two substrate, confirming the biocompatibility of the MPTMS sol-gel blend.

During these tests, an unforeseen negative feature of this material was discovered. Even if the film is subjected to long exposure times, some of the photoinitiator (4,4'-bis(diethylamino)benzophenone) will remain in its original, unreacted form. This compound absorbs light between 300 and 420 nm, and, once excited, the presence of both a local and a TICT (twisted intramolecular charge transfer) excited state causes the fluorescence emission profile to be very broad, covering the wavelength spectrum from 400 nm to 600 nm[113]. Both these ranges (absorption and emission) cover those of many common cells staining reagents, like DAPI (4',6-diamidino-2-phenylindole) or BrdU (5-bromo-2-deoxyuridine).

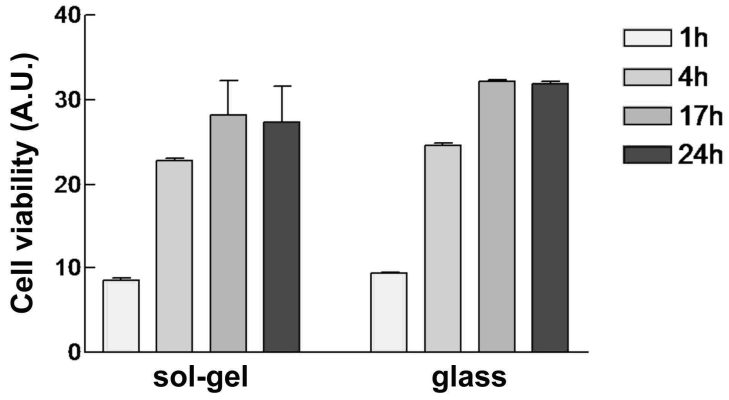

Figure 2.17: results of the alamarBlue tests on MPTMS (sol-gel) and control (glass) substrates. The cell proliferation and viability is, within experimental error, the same for both materials, confirming the biocompatibility of the MPTMS blend.

This means that many of the fluorescence-based tests commonly featured in biology-related works will suffer from a diffuse background that will degrade the signal to noise ratio of the measurement. While this problem is not

unsolvable (e.g. different fluorescent labels can be used), it poses certain limitations to biological applications in MFDs realized with this material.

2.3.6 Final remarks on MPTMS

Summarizing what has been assessed in this chapter, the MPTMS hybrid organic/inorganic sol-gel blend poses itself as a good candidate for the fabrication of microstructures that for any reason (e.g. shape or solvent incompatibility) cannot be made in PDMS or by replica molding. While attempting to realize big, large structures will usually result in cracked surfaces, small feature can be realized with excellent resolution (~600 nm) through two-photon direct laser writing. Being biocompatible, this material is also available for MFDs dedicated to biological applications. However, the native fluorescence of residual unreacted photoinitiator can cause a diffuse background in many fluorescence-based tests, degrading the measurement signal to noise ratio. Notwithstanding these limitations, this sol-gel blend can be very useful especially for the internal sub-structuration of microchannels.

Chapter 3

MICROFLUIDIC MIXER

3.1 Free diffusion mixing

As has already been stated in Section 1.3.3, efficient mixing of two fluids inside a microchannel can be extremely tricky to achieve due to the dominant laminar flow conditions. Without some form of specifically designed element acting as a mixer, the only effect that induces mixing in MFDs is free diffusion of molecules of the first liquid into the second (and vice versa). The time needed to complete this process depends on the molecular mobility of the involved fluids, but except for the very smallest channels it will usually be much to long to be realistically employed into a device. An example of mixing by free diffusion, made to verify that this kind of method is too slow for the typical channel dimensions used in this work, is reported in the following.

3.1.1 Device fabrication

To verify free diffusion mixing, a simple Y-shaped channel was designed. The master was realized in SU-8 on a silicon substrate using the procedure described before (see Section 2.1.2). The structure was obtained through one-photon direct laser writing (DLW) using light of 400 nm wavelength. The inlet channels (upper arms of the Y) are 55 μm wide, while the long channel is 95 μm wide. All channels are 25 μm high. After development the master was replicated in PDMS (see Section 2.1.3) and finally the

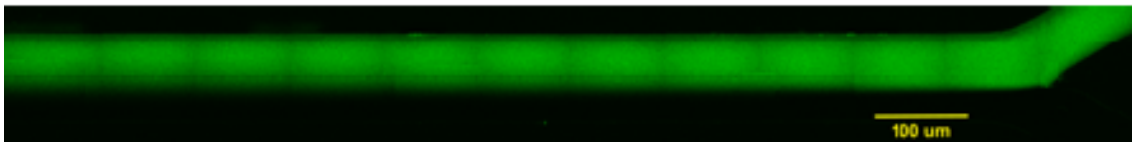

Figure 3.1: fluorescence image of the channel used for the free diffusion experiment. Only the upper half of the channel, where fluorescein is injected, is visible. The lower half is filled with a non-fluorescent KI solution. Diffusion mixing can be see as a slight blurring of the border between dark and bright flows on the far left.

replica was punched for inlets and sealed with a coverglass. Figure 3.1 reports an image of the channel. The choice of sealing the channel with glass means that it features two different materials, PDMS on three sides and glass on the last one, which could in principle induce flow conditions different from those inside a full-PDMS device. However, the thin (150 μm) glass was needed to permit fluorescence microscopy imaging. This material requirement is not due to PDMS being optically unsuitable, but simply to the fact that the high-NA objective necessary to achieve precise characterization has a very small working distance (280 μm). If a wall so thin was to be made of PDMS, it would deform at the slightest pressure inside the channel due to the low Young modulus of this material.

To verify the effective dimensions of the replicas with respect to the original masters, confocal fluorescence microscopy is employed. The devices are filled with an aqueous solution of fluorescein, and fluorescence images are recorded with the confocal microscope. Confocal microscopy allows a strict selection of the fluorescence emitted in the focal volume, excluding all signal from different areas of the optical axis[114]. This means that by moving the sample in the three dimensions it is possible to record multiple two-dimensional "optical slices" of the object, which can then be combined to obtain a three-dimensional image. The typical result of this technique is shown in Figure 3.2. The experimental set-up for this analysis is the same used for voxel characterization in chapter 2.3.1, that is a confocal microscope

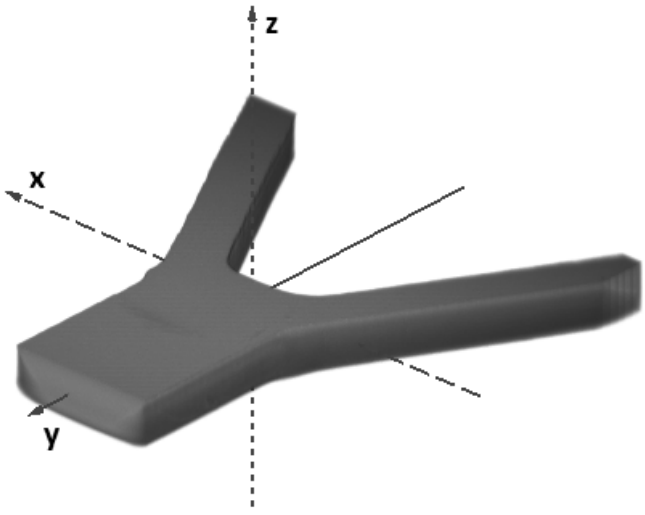

Figure 3.2: example of 3D reconstruction of a microfluidic channel. This image was realized by filling the channel with fluorescein and then recording multiple two-dimensional images in the xy plane at different z. The images were then combined into a single 3D representation using the bioView3D software.

(Olympus FV300) equipped with a water-immersion 60x (NA 1.4) objective (Olympus UPLSAPO60XW) used both to focus the exciting laser and to collect the fluorescence induced by said laser. Excitation at 488 nm from a CW Ar laser is used to map fluorescence intensity.

3.1.2 Diffusion mixing measurements

Once fabricated the device, polyethylene tubes were inserted into the punched inlets and connected to two syringes actuated by a dual syringe pump (KdScientific KDS 210). The syringes were used to inject in the two short branches of the device (the upper arms of the Y) an aqueous solution of fluorescein and an aqueous solution of potassium iodide (KI). Since both channels have the same dimensions, if the two solutions are pumped with the same flow rate (and this is assured by the use of a dual syringe pump), the fluids will meet at the junction and then proceed along side-by-side with the interface between the two exactly in the middle of the long channel (see Figure 3.1). The two chemicals (fluorescein and KI) were selected because fluorescein is a fluorescent molecule whose emission is strongly quenched in presence of I^- ions[115]. So, mixing between the two can be estimated by observing the progressive reduction in fluorescence from the center of the channel toward the lateral wall on the fluorescein side. Increasing distances from the junction correspond (via flow velocity) to increasing mixing times. To obtain this estimation, fluorescence intensity measurements were used to record channel cross-sectional profiles at increasing distances from the junction, allowing the localization of the "fluorescent ridge" where the fluorescein emission becomes quenched due to KI diffusion.

3.1.3 Results for free diffusion mixing

The measurement results are reported in Figure 3.3. The graph shows the variation of fluorescence intensity across the channel from the fluorescein side wall (x = 0) towards the KI side wall (x = 95). In this kind of representation a constant, horizontal line would

indicate perfect mixing, with no difference in composition across all the channel. Conversely, a vertical step in the center of the channel would indicate no mixing whatsoever. It should be noted that the sharp decrease on the left side of the graph (x < 20) is an artifact due to the nearness of the channel wall which perturbs and deforms the incoming laser beam. The data show indeed some kind of mixing that slightly increases at greater distances (i.e. times) from the junction. However, it is quite clear that even after 2 mm of travel the mixing is very slight, since a very marked difference in fluorescence intensity persists between the two sides of the channel. It is thus confirmed that for the channel dimensions used in our devices (i.e. around 100 μm wide) simple free diffusion mixing is not enough, and some sort of specifically designed functionality must be included if efficient mixing is required by the device.

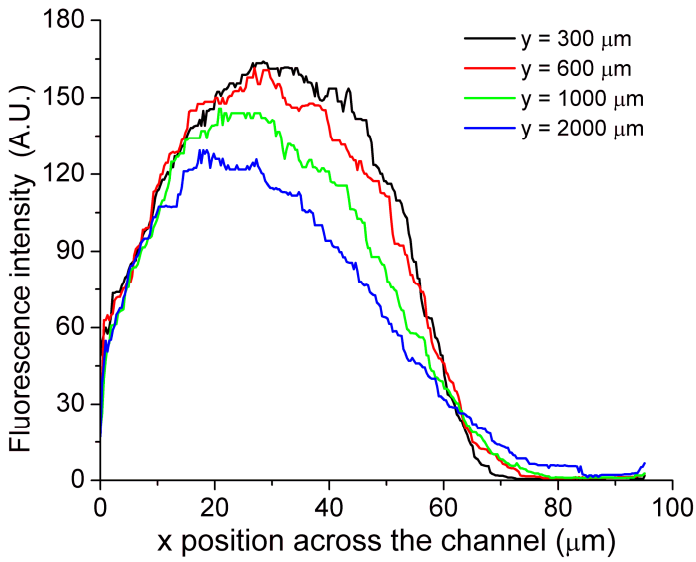

Figure 3.3: fluorescence intensity measurements for free diffusion. The data show an increase in mixing (less sharp step) with increasing distances from the junction. However, after 2 mm the mixing is still markedly incomplete.

3.2 Pillars passive mixer

In Section 1.3.3 a division was made between active and passive mixers, the former requiring external input and/or power to work while the latter are always active without the need for off-chip equipment. Active mixers are often more efficient and have the advantage of been able to be switched on and off as needed, but for device simpleness and portability reasons the mixer realized for this work is of the passive variety.

3.2.2 Mixer design

To be able to mix different fluids inside a MFD, a mixer module must be able to overcome the dominating laminar conditions. One way to do that is to locally perturb the system to relax laminar constrains. Vectorially speaking, laminar motion means that the velocity of any infinitesimally small volume of fluid has only one component, parallel to the channel axis (which is usually dubbed the y axis), and this fact is the reason why mixing in laminar conditions is so difficult. Regardless of this, if there is an obstacle inside the channel, so that the fluid physically cannot maintain its straight-on direction, the flow will necessarily bend around the obstacle. This bending means that laminar conditions are locally relaxed and mixing can be achieved.

Unfortunately, building an obstacle inside a microchannel will formally perturb laminar condition, but most often the perturbation will be limited in both magnitude and spatial extension, meaning that very little mixing will be achieved before the fluid restores itself to its preferred laminar motion. However, such perturbation can be extended and magnified if multiple, carefully placed obstacles are used instead of a single one. With this consideration in mind, the attention was posed to the design of a microfluidic mixing module based on a channel featuring multiple internal obstacles. To help tune design parameters such as number, size and position of obstacles, a preliminary screening of tentative device designs was performed through numerical simulations with the aid of the commercial COMSOL 3.5 software. The simulated devices feature a T junction where two fluids are injected with a flow speed of 1 mm/s from the two short arms and meet at the junction. Both then flow along a straight channel containing various obstacles. The first fluid is pure solvent, while the second is a solution of a given chemical species. Considering the laminar conditions inside the channel, the Navier-Stokes and convective-diffusive equations for the species to be mixed can be expressed as[116]:

$$\rho u_j \frac{\partial u_i}{\partial r_j} - \mu \hat{\nabla}^2 u_i + \frac{\partial p}{\partial r_i} = 0 \qquad (3.1)$$

$$\frac{\partial u_i}{\partial r_i} = 0 \tag{3.2}$$

$$u_j \frac{\partial c}{\partial r_j} - D\hat{\nabla}^2 c = 0 \tag{3.3}$$

where $\boldsymbol{u} = (u_x, u_y, u_z)$ is the velocity field (i, j = x, y, z), ρ is the density, p is the pressure, μ is the dynamic viscosity, c is the species concentration and D the diffusion coefficient of said species.

For all these parameters (except c and D), value typical for the solvent (water) are assumed, considering that the nanomolar concentration of the solute does not modify them significantly. The solute is the fluorophore Alexa488, and the considered D is the diffusion coefficient of this molecule in water at room temperature (295 K, $D = 3.9 \cdot 10^{-10}$ m^2/s). One such simulation result is reported in Figure 3.4 as an example. It should be noticed that the simulation took into account both convective (via the Navier-Stokes equation) and diffusive (via the Fick law) contribution to mixing. This means that increasing flow velocities will provide reduced mixing due to the reduced time available for diffusion. The convective component is by comparison constant with the fluid speed. A greater velocity will cause a greater Reynolds number (see Section 1.1) which in turn means less strict laminar conditions. This would promote mixing, but its final weight is minimal, and this

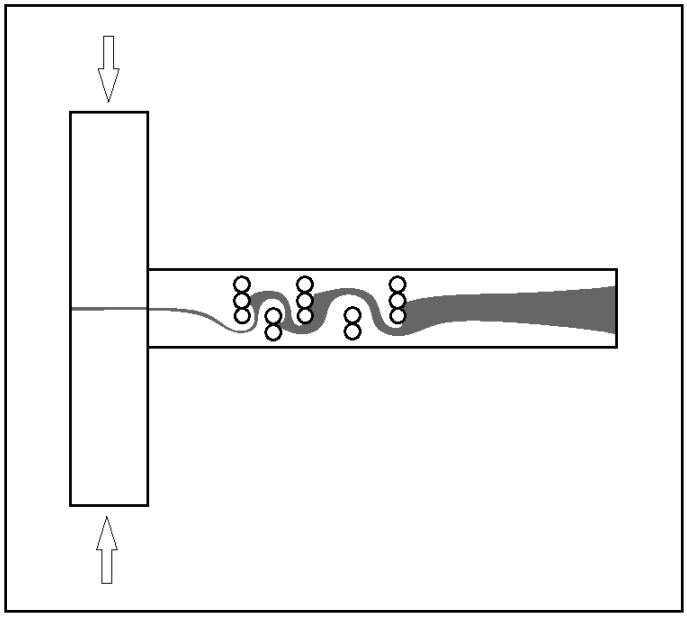

Figure 3.4: mixing simulation for a 5-obstacle channel. Alexa488 in water and pure water are injected for the channels marked with arrows. Shown in grey is the area where the relative concentration of Alexa488 is between 45% and 55%, i.e. almost perfect mixing.

effect is swallowed by the much greater (and opposite) diffusion component.

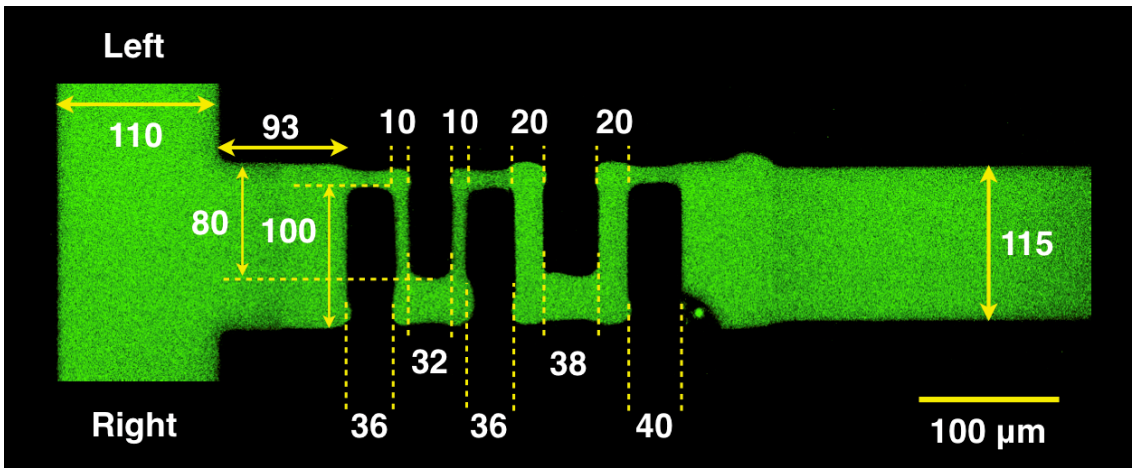

Figure 3.5: fluorescence image of the first mixer (bigger pillars). The image was obtained by filling the channel with fluorescein. Black area inside the channel are the microfabricated pillars. During mixing efficiency measurements, aqueous alexa488 is injected from the "Right" inlet, and pure water from the "Left" inlet. All dimensions are in micrometers.

At the end of numerical simulation screening, two mixer designs where selected. A first one (Figure 3.5) features five big pillars that occupy most of the channel width and all its height, floor to ceiling. The second design (Figure 3.6) still features five pillars, but

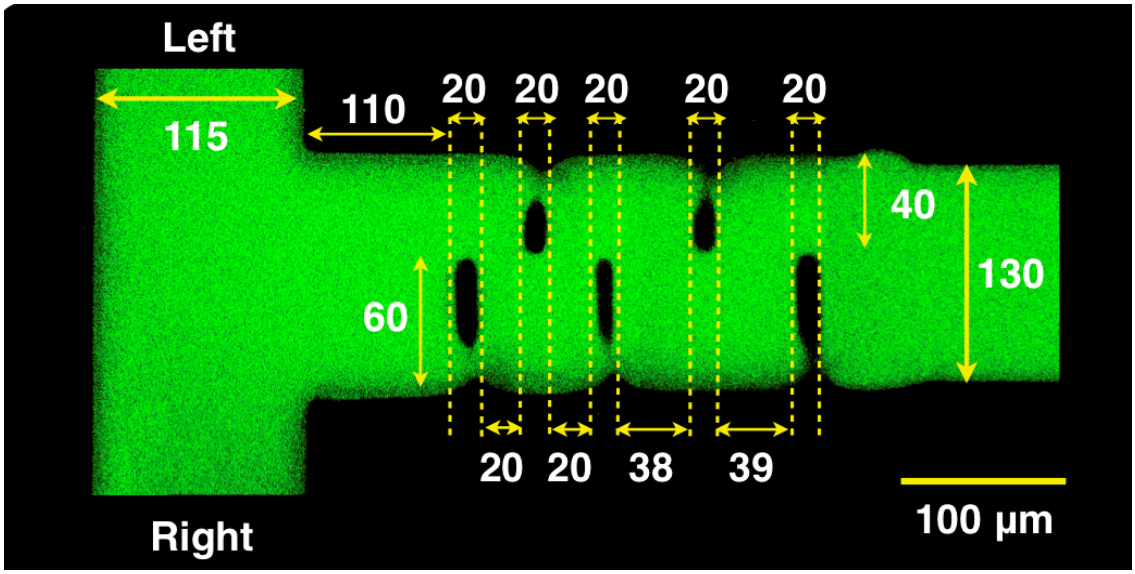

Figure 3.6: fluorescence image of the second mixer (smaller pillars). As before, the image was obtained by filling the channel with fluorescein. Black area inside the channel are the microfabricated pillars. During mixing efficiency measurements, aqueous alexa488 is injected from the "Right" inlet, and pure water from the "Left" inlet. All dimensions are in micrometers.

these are much smaller. Also these obstacles do not reach the ceiling of the channel (33 μm from the bottom), but are instead 20 μm (first two pillars) and 10 μm high (last three pillars). Both devices were fabricated as described above (Sections 2.1.2 and 2.1.3) in PDMS replicated from SU-8 masters realized with one-photon DLW, and were sealed with a coverglass.

3.2.3 Mixing measurements

The efficiency of these modules was quantified with a method similar to that used for free diffusion mixing, but somewhat simplified. Pure water and an aqueous solution of Alexa488 were injected from the two short arms of the T junction. The flow rate was adjusted so that the flow speed inside the channel was 1 mm/s, in accordance with the simulation parameter. Fluorescence imaging microscopy was then used to record images of the channel beyond the pillars at increasing distances from the junction. These images were then elaborated with the ImageJ software to obtain the (one-dimensional) fluorescence intensity profile across the channel cross section. Such a measurement can be used to quantify mixing, since a sharp step in fluorescence intensity in the middle of the channel would indicate negligible mixing, while a constant intensity across all the cross section would signal perfect mixing of the two fluids. This concept is quantified by the parameter *M*, which ranges from 0 (no mixing) to 1 (perfect mixing). The parameter *M* is defined as[116]:

$$M = 1 - \sqrt{\frac{1}{n}\sum_{i=1}^{n}\left(\frac{k_i - \bar{k}}{\bar{k}}\right)^2} \qquad (3.4)$$

where n is the number of pixels in the linear cross section, k_i is the fluorescence intensity of pixel i and $\bar{k}$ is the average fluorescence intensity across all the linear cross section. It should be noticed that these measurements are not directly comparable with those in the previous section due to different channel shape (Y- vs T-junction), different

reagents (fluorescein/KI vs alexa488/water) and different method for fluorescence reduction (quenching vs dilution).

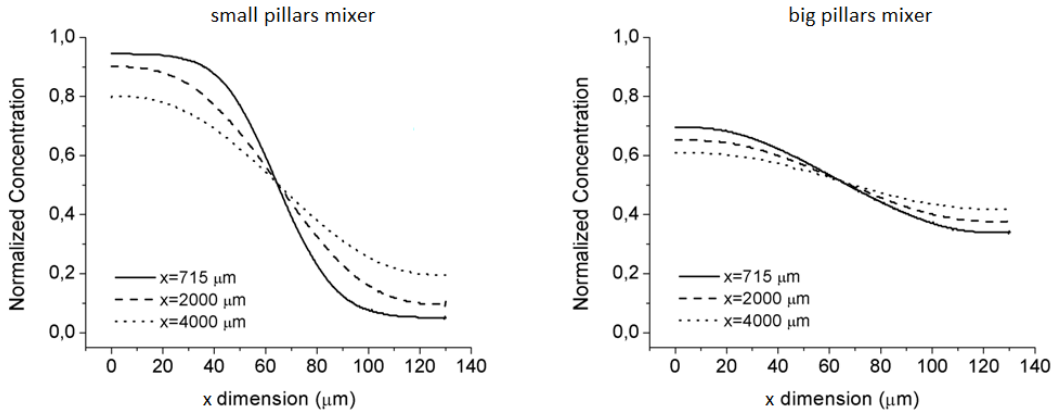

Figure 3.7: numerical simulations results for both mixers. The normalized concentration profile across the channel cross section at different distances from the T-junction is reported. Lesser variation in concentration across the channel indicate better mixing.

Figure 3.7 shows the simulated concentration profiles for the two channels. It can be immediately noticed that the channel with bigger obstacles is markedly more efficient in inducing mixing. Also, increasing the measurement distance from the junction causes a better mixing. This effect was expected since greater distances mean longer mixing times, which increase the effect of the free diffusion contribute. The simulated M parameters for both modules are reported in Figure 3.8, and confirm the previous analysis. The same figure also shows the experimental values for M obtained in this work. All experimental values are lower (less efficient) than the simulated ones. This fact is explained considering that the module design for the simulations was the one that was found to be the most efficient. Thus, any variation due to the fabrication process (such as slightly bigger pillars, or small variations in the distances between them) will necessarily degrade the mixer performances. Notwithstanding this differences, the trend of the M parameter is the same between simulation and experiment. It can then be stated that the mixer with bigger (and higher) obstacles is indeed more efficient. Concentrating on this module, another consideration can be made. After a distance of 2 mm from the inlet, about 50% mixing can be achieved even with the imperfect

	Simulated M	Experimental M
Small pillars mixer		
x = 715 μm	0.25	0.24
x = 2000 μm	0.39	0.32
x = 4000 μm	0.55	0.45
Big pillars mixer		
x = 715 μm	0.74	0.51
x = 2000 μm	0.79	0.48
x = 4000 μm	0.86	0.64

Figure 3.8: simulated and experimental values for the M parameter for both mixers at different distances from the T-junction. Differences between simulated and experimental results are attributed to small differences in channels layout due to imperfection in the fabrication process.

experimental device. A module of better quality could approach the 80% mixing obtained in the simulations. Both these results are quite good compared to those of other passive mixers like, for example, Whitesides' herringbone mixer that needs 2-3 cm to achieve good mixing between two fluids[30].

3.2.4 Final remarks on the passive mixer

The work reported in this chapter was aimed at realizing a passive microfluidic mixer module. The choice to work on a passive mixer, as opposed to an active one, was due to the desire of realizing a device as simple as possible and, more importantly, nondependent on external instrumentation. To induce mixing in a laminar environment, multiple obstacles were placed inside a microchannel to force the flow to wind around them, breaking pure laminar motion. A number of module designs, different in term of number, dimension and position of obstacles, were tested through numerical simulations, and two promising modules where realized in PDMS/glass. Fluorescence intensity profiling allowed the quantification of the mixing efficiency of these devices, and confirmed the better performance of the mixer with bigger obstacles. This mixer is

highly efficient regardless of the quite simple design and production technique, and without the need for any additional equipment can be readily added to any modular MFD that requires a mixing functionality.

Chapter 4

OPTOFLUIDIC OPTICAL SWITCH

4.1 Module realization

Section 1.5 provided a number of examples of microfluidic application approaching the tasks of generating, guiding and focalizing light. The high interest surrounding optofluidics has caused many such devices to be proposed and realized. However, the majority of these works confine themselves to those three specific issues (i.e. light generation, waveguides or lenses). Conversely, many other useful optical elements like polarizers, choppers, irises, etc. still lack optofluidic development. In this work, one of such elements is proposed: an optofluidic module to control the transmission and reflection of light.

4.1.1 Module fabrication and working principles

This module exploits a water/air segmented flow to alternatively transmit or reflect a laser beam intersecting it. The device has been realized through UV photolithography in SU-8 2050 followed by replica molding in PDMS, and all channels are 1 mm wide and 140 μm thick. The channel layout is made by a T-junction followed by a long channel (folded in a serpentine to ensure device compactness). A scheme of the layout is given in Figure 4.1. The inlets are connected to a couple of syringes, one filled with air and the other with water. Both syringes are actuated by the same syringe pump, ensuring that the flow rate of both gas and liquid are the same. Flow rates are varied between 0.2 ml/min and 1.5 ml/min. In this conditions, once the two flow (air and water) are brought into contact at the T-junction there is no chaotic mixing nor parallel flow of the two fluids. Instead, a segmented flow is generated[117,118]. In other words, periodic segments of air or water alternate inside the long channel as they flow towards the outlet. Once the flow is stable, the beam generated by a He-Ne laser (Melles Griot 05-LHP-991; λ = 633 nm) is expanded to a radius *w* of 5 mm and focalized by a lens with focal distance *f*

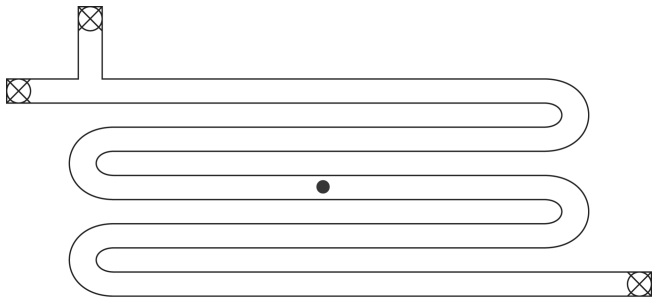

Figure 4.1: Scheme of the channel layout of the optofluidic module. Water and air are injected from the top inlets and collected at the bottom outlet. The dark circle indicates the place where the laser beam intersects the channel. All channels are 1 mm wide and 140 μm high.

of 20 cm on the channel. This lens arrangement is chosen to guarantee that the beam is small enough to easily fit the channel width. Due to the higher refractive index of PDMS with respect to both air and water, if the incident angle is chosen correctly the beam will be alternatively transmitted or total-reflected depending on the segment (water or air) currently transiting inside the channel under the laser spot. This behavior is due to the total internal reflection effect. When a light beam meets the interface between the medium in which it is currently transiting and another material with lower refractive index, if the angle of incidence upon the interface is greater than a certain critical angle the beam will not be refracted in the second medium but instead totally reflected inside the first. This critical angle θ_c is defined by the formula[109]:

$$\theta_c = \arcsin \frac{n_2}{n_1} \qquad (4.1)$$

where n_1 and n_2 are the refractive index of (respectively) the first and second media. It should be noticed that, in accordance with optics conventions, incidence angles are measured with respect to the surface normal, so that an angle of 0° indicates perpendicular incidence.

Considering that the refractive indexes for PDMS, water and air are respectively n_{PDMS} = 1.412, n_{water} = 1.33 and $n_{air} \sim 1$, incident angles between 45.1° and 70.4° will be sub-critical for a PDMS-water interface, but beyond θ_c for a PDMS-air interface. In light of this, in our device an incident angle of 60° is chosen, keeping in mind that the vast range of viable angles means that fine goniometric control is not needed. The final

effect is that the inbound laser light is periodically sent in one of two well-defined directions (see Figure 4.2). In this set-up the beam is focalized and not collimated, but the long focal distance of the lens ensures that the beam radius is not only small enough

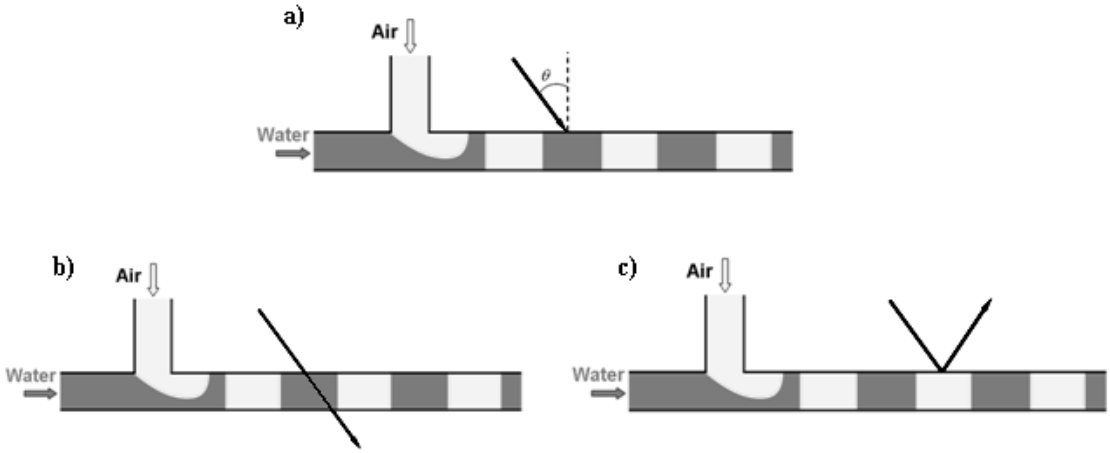

Figure 4.2: a) scheme of the optofluidic module. Laser light is shone through the surrounding PDMS and impacts on the channel with an angle $\theta = 60°$; b) if a water segment is flowing under the laser, $\theta_c > 70°$ and the beam is transmitted; c) if an air segment is flowing under the laser, $\theta_c < 50°$ and the beam is reflected.

to fit the channel, but also almost constant through all the device. The spatial distribution of the He-Ne beam intensity can satisfactorily be assumed to be a TEM_{00} Gaussian mode. According to the laws of Gaussian optics, the beam radius in the focal plane (w_0) is[109]:

$$w_0 = \frac{\lambda f}{w\pi} \qquad (4.2)$$

where f is the focal distance of the lens, λ is the laser wavelength and w is beam radius just before the lens.

By this formula, our beam will have a focal radius of 8 μm, much smaller that the channel width (1 mm). The length of the beam path inside the channel (if the beam is not reflected) can be calculated considering the channel thickness (140 μm) and the angle of refraction which stems from the Snell's law:

$$n_1 \sin\theta_1 = n_2 \sin\theta_2 \qquad (4.3)$$

where n_1, n_2 are the refractive indexes of PDMS and water (respectively 1.412 and 1.33), θ_1 is the incidence angle (60°) and θ_2 is the angle of the refracted beam.

From this, simple geometry gives a beam path inside the channel of approximately 360 μm. Considering that the focal point falls on the first wall encountered by the beam, the radius of the beam exiting the channel on the other side can be calculated from[109]:

$$w(z) = w_0 \left[1 + \left(\frac{\lambda z}{\pi w_0^2} \right)^2 \right]^{\frac{1}{2}} \qquad (4.4)$$

where $w(z)$ is the beam radius at a distance z from the focal point (360 μm in this case), w_0 is the beam radius in the focal plane and λ is the laser wavelength.

The result is 12 μm, still quite close to the original 8 μm, which guarantees that the beam still fits the channel width and that the divergence of the beam is small (< 1°). This low divergence is of paramount importance, since in tight focusing (i.e. highly divergent) conditions the wide angle spread around the focal plane would cause a possibly large part of the incident light to fall short of critical angle condition, and so be continuously transmitted and never reflected (and vice versa, see Figure 4.3).

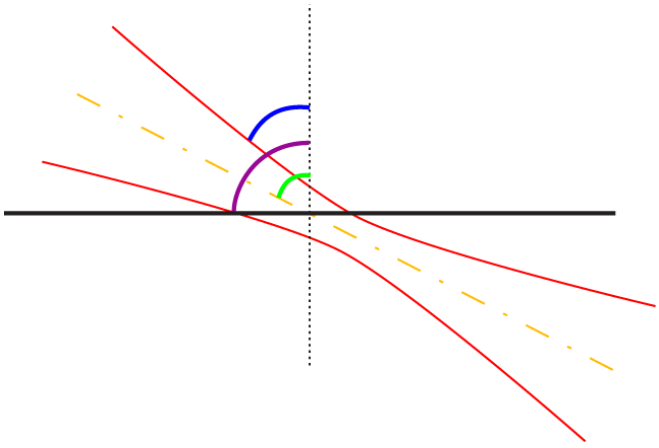

Figure 4.3: simplified representation of a tightly focused light beam impacting on an interface (refraction in the transmitted beam is ignored). The average (geometric optics) angle of incidence is shown in green. Half the beam will have a greater angle (purple) possibly being total-reflected even when the "average beam" is not. The other half has a smaller incidence angle (blue) possibly being transmitted even when the "average beam" is total-reflected.

4.2 Module characterization

The optofluidic module behavior regarding differences in injection flow rate has been characterized. Also, a method to modulate the device duty cycle by means of a temperature increase is proposed and tested. These tests are performed by using a photodiode to measure the intensity traces in time of the reflected beam and an oscilloscope to record them.

4.2.1 Duty cycle characterization

The first characterization performed has been that of duty cycle. The duty cycle of this device is defined as the fraction of the total period spent by the laser beam in the reflecting state, that is the ratio of the transit time of one air segment and the transit time of the sum of one air and one water segment. The results are shown in Figure 4.4. Each data point in the graph is an average calculated on sequences of 10 reflection-transmission periods measured at least at five different times during the experiment. The error bars are estimated through standard deviation. These data indicate that regardless of flow rate, the duty cycle is constant at 50%, which means that water and air segments have the same length. It should be noticed that this also means that the gas phase is not increasingly compressed as the flow rate increases.

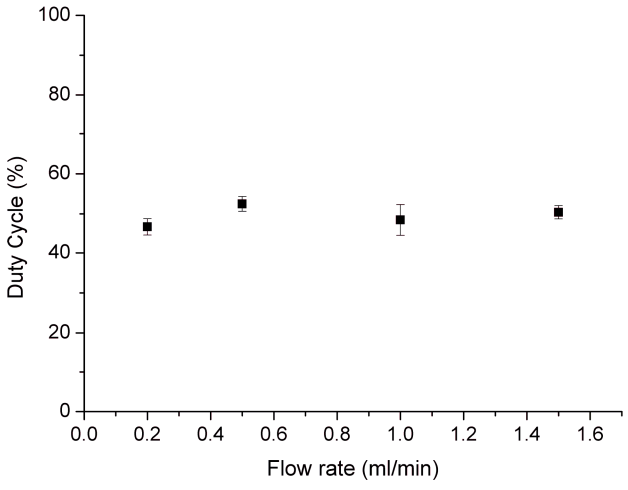

Figure 4.4: duty cycle of the device at different flow rates. The constancy of duty cycle at 50% means that for all flow rate the water and air segments have the same relative dimension.

4.2.2 Duty cycle modulation

The constancy of duty cycle with flow rate is directly related to the fact that in this device a single syringe pump is used to inject both fluids, which in turn means that said fluids always share the same relative flow rate. For some applications, however, it would be useful to be able to modulate the duty cycle of this module. A simple way to do that would be to implement a second syringe pump and inject the fluids with different flow rates, thus generating segments of different length. However, this would also double the external equipment required by this module, reducing both its compactness and its portability. For this reason, another method to modulate the duty cycle was tested: an increase in viscosity of the liquid phase. In a first attempt, water was replaced with an aqueous solution of glycerol. Unfortunately, all tested concentrations (from 10% v/v to 50% v/v) induced a very strong instability in the segmented flow which made measurements impossible. To date it is not clear whether this effect is due to specific interactions of glycerol with the PDMS walls, or to the increased viscosity making the segmented flow much more sensible to the roughness of said walls. In the second case, higher quality channels could possibly solve the problem, but once again at the price of increased device (production) complexity. Thus, a different approach was tried. The viscosity of the liquid phase has been reduced by means of an increase in temperature. This effect was achieved by submerging the water inlet tubing in an hot bath, so that the liquid phase flowing from the syringe to the device is heated just before reaching the module inlet. On

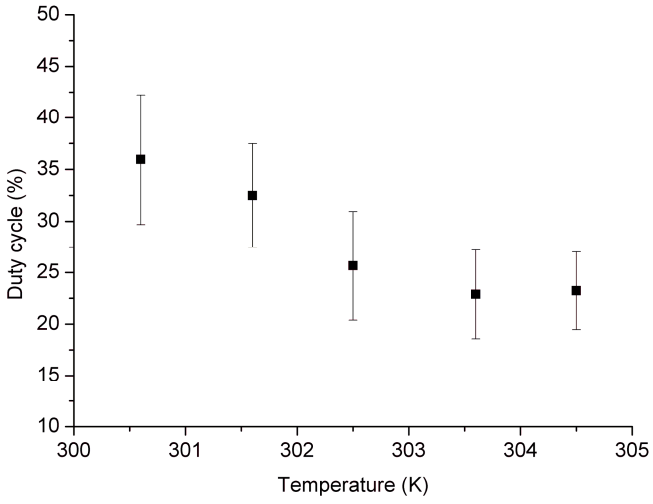

Figure 4.5: duty cycle variation as a function of increased temperature of the water phase. At higher water temperatures, water and air segments no longer share the same relative length.

the contrary the gas phase is not heated in any way before entering the device, and therefore it can be safely assumed that its temperature is constant, since the experiments is carried on in a thermally controlled laser laboratory. Temperatures are measured after all data are collected by inserting a spherical thermocouple (radius < 1 mm) through the PDMS into the channel at the point where the laser beam impacts, and then reproducing the same water flow conditions as during the actual data measurements. This method is destructive, since a hole must be punched to allow the sensor to reach the channel. The effect of increasing the liquid temperature (at a fixed flow rate) is reported in Figure 4.5.

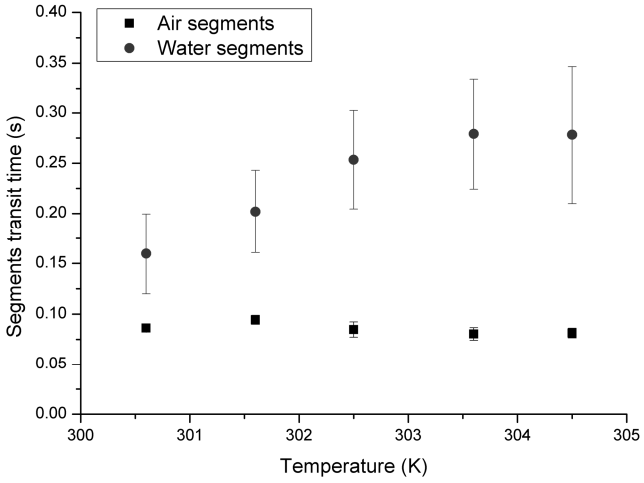

Figure 4.6: segment length (reported as time needed to clear the laser spot area) of both water and air phases at increasing temperatures. Air segments are not modified in any way by the increased temperature, but are generated with lower frequency, leading to longer water segments.

It can be easily seen that a variation in viscosity has a marked impact on the duty cycle. Interestingly, by comparing the water and air segment lengths at increasing water temperature (Figure 4.6) it appears that while the liquid segments are increasingly longer, the air ones have always the same length. In other words, the air segments are not modified in any way, but are generated with a lower frequency. This effect is tentatively attributed to the fact that a reduced liquid viscosity causes a reduced shear stress applied on the liquid/gas interface at the T-junction and thus a longer time is necessary to completely detach a new air segment. A similar effect is predicted from numerical simulations by de Menech et al. According to this work[119], a decrease in the capillary number *Ca* of the carrier phase (water in our case) correspond to a (non-linear) reduction in frequency of droplet generation. Since *Ca* depends on the fluid viscosity as:

$$Ca = \frac{\mu v}{\gamma} \qquad (4.5)$$

where μ is the dynamic viscosity of the fluid, v its velocity and γ the interfacial tension between the two phases, our results are in accordance with these predictions. However, it should be noticed that de Menech's work treated a liquid/liquid system, as opposed to the liquid/gas one proposed here. Also, a number of published results[119–121], both theoretical and experimental, show that a reduced generation frequency should be matched by the generation of progressively longer segments for both fluids, a result that we did not observe, possibly due to differences in channels geometry.

From Figures 4.5 and 4.6 it can be seen that the experiments with increased temperatures feature a noticeably lower reproducibility compared with those at room temperature. This is likely caused by the fact that water has been heated just before being introduced in the device, but considering the very large surface/volume ratio inside the microchannels it is inevitable that a gradient in liquid temperature will be generated inside the module. This gradient is a source of instability that degrades the reproducibility properties of the experiment. Another remarkable point is that while a relatively small change in liquid temperature will cause a variation of the duty cycle, during the previous room temperature experiments the 50% duty cycle shown in Figure 4.4 was nonetheless highly reproducible for long times (up to 90 minutes). This can be explained considering two facts. First of all, all experiments are performed in a thermally controlled laser laboratory with variations in room temperature not exceeding ±2 K. Secondarily, PDMS is a very poor heat conductor. As such, it takes a long time for a slight increase in room temperature to actually increase the temperature inside the device, under several millimeters of PDMS. A similar reasoning can be made for the water reservoir that provides the liquid for the device, since water itself is a quite poor heat conductor. These properties help to dampen the temperature fluctuation that can happen during the experiment, and can be extremely advantageous if the device is to be used "on the field". The measurements at increasing temperatures have been repeated

with a different prototype of identical design, and while the absolute duty cycle values were slightly different, the trend was the same. Thus, small differences in channel production require each device to be calibrated, but once a couple of data point are recorded, the rest of the duty cycle – temperature curve can be readily deduced.

4.2.3 Frequency characterization

The next feature to be characterized has been the reflecting/transmitting switching frequency of the device, at room temperature and for different flow rates. The results are summarized in Figure 4.7 and demonstrate good reproducibility with variations averaging around 10% across different experiments with different replicas of the prototype device. The graph shows a non-linear increase of switching frequency with increasing flow rates. To understand this behavior, it must be considered that two distinct phenomena occur inside the channel when the flow rate is increased: an increase in (segmented) flow velocity and the generation of shorter segments. Regarding the first effect, an increase in flow rate will cause an increase of the (segmented) flow velocity. From the constancy of duty cycle at all flow rate it can be assumed that the air segments are not increasingly compressed at greater flow rate (see Section 4.2.1). Since the liquid phase is (by definition) also uncompressed, mass conservation requires the relationship between flow rate and (segmented) flow velocity to be linear. The non-linear behavior must then be ascribed to the second effect, i.e. the generation of smaller segments.

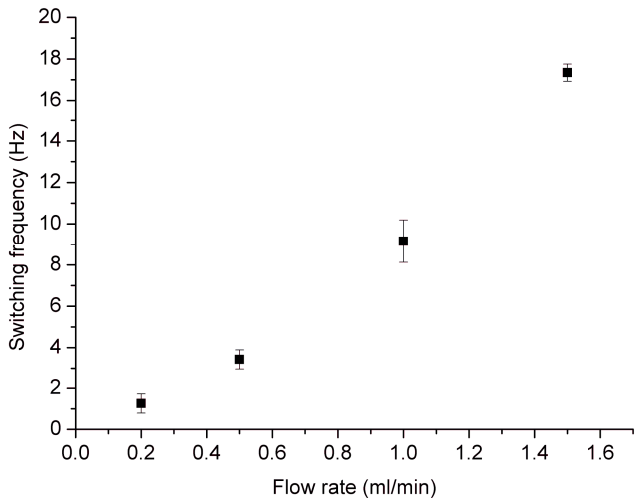

Figure 4.7: switching frequency of the device as a function of air/water flow rate. The non-linear increase is due to the simultaneous presence of two effects: an increase in (segmented) flow velocity and the flow rate induced generation of smaller air and water segments.

While this effect can be clearly seen experimentally, this component is difficult to model, and so channels with different geometries will have to be experimentally calibrated.

Regardless of the quite simple production processes used to fabricate this module, the device features a very good stability in time for flow rates up to 1.5 ml/min. In these conditions the capacity of the employed syringes is usually the limiting factor for maximum measurement time. At very high flow rates (greater than 2 ml/min) the segmented flow becomes unstable after a few minutes. This is likely caused by the microscopic roughness of the channel walls, that becomes critical at high flow velocities. Literature evidences[122,123] suggests that this problem could be mitigated (if not outright solved) by fabricating higher quality devices or by functionalizing the channels interiors, but as before these improvements would be to the detriment of production simplicity. Moreover, flow rates up to 1.5 ml min^{-1}, corresponding to a switching frequency of almost 18 Hz, have been deemed sufficient for most applications. Considering (as an example) a device for recording light absorption spectra which uses this module to implement a two beam geometry with 0.5 nm spectral resolution, a switching frequency of 10 Hz (equal to a flow rate of 1 ml/min, well below the device limit) would be enough to achieve a scanning speed of 300 nm/min, which is a typical value for commercial, macroscopic spectrophotometers.

4.2.4 Final remarks on the optofluidic light switch

In this chapter an optofluidic module for the control of light has been proposed and characterized. This device exploits a segmented flow to alternatively and periodically transmit or reflect a laser beam shone on the channel. The frequency of operation depends only on the liquid/air flow rate, and thus can be easily controlled. Also, a variation in liquid phase viscosity can be used to tune the duty cycle of the device. While the construction process is very simple, the device response is reproducible. If greater stability becomes a requirements, additional processes can be implemented (like

channel functionalization) by partially sacrificing ease of production. This module is quite straightforward in its use, and requires minimal external equipment, making it a good candidate for inclusion in any modular optofluidic arrangement that currently lack a light switching or chopping functionality. This module can also work as a sort of beam splitter that, instead of dividing the total energy of the inbound beam, sends all the available energy alternatively (and periodically) toward one direction or the other. This particular feature can be extremely beneficial for applications where the available light power is low, as is typically the case for MFDs where the light is generated on-chip.

Chapter 5

WATER-CORE PDMS WAVEGUIDE

5.1 Porous PDMS claddings

The importance of waveguiding light inside microfluidic devices has already been mentioned in Section 1.5.4, in particular concerning the possibility of making the fluid-carrying microchannels double as waveguides. This arrangement would not only allow a reduction of the physical dimensions of the involved modules, but also (and more importantly) guarantee long interaction paths between fluid and light. Unfortunately, the typical MFD bulk materials (PDMS and glass) feature a greater refractive index than the fluid commonly carried inside the device (i.e. water). This means that microchannels cannot usually work as conventional, total-reflection-confined waveguides, and other strategies must be implemented.

5.1.1 Limits of existing liquid-core waveguides

Two of the most common optofluidic waveguides, ARROWs and L^2, have been described in Section 1.5.4. Both these strategies have been successfully employed, but suffer also from some limitation. Starting with ARROWs, antiresonant reflecting optical waveguides are quite efficient in keeping the light in the channel, but require very fine micro- or nanofabrication methods to precisely tune the thickness of the layer providing the antiresonant effect. Moreover, these guides require the integration of at least two different materials. This fact not only complicates the design of the involved modules, but if the second material is not elastic, it also hampers the deformation capabilities of PDMS modules. Considering that a great number of tunable MFDs achieve tunability thanks to said deformations (see Sections 1.5.3 and 1.5.5), this last drawback is non-negligible. The second kind of guiding geometry, L^2 waveguides, doesn't have the strict fabrication requirements of ARROWs, but still present limitations. First of all, since the guiding flow is usually stratified and not annular, light is confined only in one

transverse direction, but free to escape in the other. Also, chemical diffusion will in time blur the interface between core and cladding layers (degrading the guiding properties) and/or reduce the concentration of target molecules in the core.

Considering these limits of the most widespread optofluidic waveguides, another strategy to confine light inside microchannels is here presented.

5.1.2 Low-index porous PDMS

Since PDMS is the material of choice for all the microfluidic modules presented in this work, a waveguide made with this polymer would be greatly beneficial. Unfortunately, PDMS features a refractive index *n* of 1.412, sensibly greater than that of water (*n* = 1.33). A possible solution would be to change the flowing liquid to another fluid with higher refractive index, but this would pose several problems. First of all, most liquid chemical species with $n > 1.33$ are organic compounds that are incompatible with PDMS. Moreover, the substitution of water would severely limit the field of applicability of these waveguides.

Another possibility is that of decreasing the refractive index of the PDMS surrounding the channel down to the point where light can be confined by water through total internal reflection. According to Bruggeman[124], the dielectric constant of a biphasic material can be expressed as a function of the refractive indexes of the single substances that compose the two phases, as long as the phase domains are sensibly smaller than the wavelength of the involved light. This effective dielectric constant ε_{eff} is given by:

$$f\frac{\varepsilon_1-\varepsilon_{eff}}{\varepsilon_1+2\varepsilon_{eff}}+(1-f)\frac{\varepsilon_2-\varepsilon_{eff}}{\varepsilon_2+2\varepsilon_{eff}}=0 \qquad (5.1)$$

where f is the volumetric fraction of the first phase and ε_1 and ε_2 are the dielectric constants of the first and second phase, respectively.

Considering that (neglecting absorption) $n \approx \sqrt{\varepsilon}$, equation (5.1) provides a way[125] to reduce the refractive index of any given material by mixing it with another substance

with lower *n*. In the work here reported, PDMS ($n = 1.413$) has been mixed with air ($n \approx 1$) in the attempt to achieve an effective refractive index n_{eff} lower than that of water ($n = 1.33$). To be able to work with the light wavelength commonly used in waveguides ($\lambda \approx 1.5\ \mu m$) the air pores must have a diameter not exceeding a few hundred nanometers, or tens of nanometers to extend the range of applicability to the visible frequencies. The volume fraction of air needed to lower the effective refractive index to 1.33 can be calculated by rearranging equation (5.1):

$$f = -\frac{\dfrac{n_2^2 - n_{eff}^2}{n_2^2 + 2n_{eff}^2}}{\left(\dfrac{n_1^2 - n_{eff}^2}{n_1^2 + 2n_{eff}^2}\right) - \left(\dfrac{n_2^2 - n_{eff}^2}{n_2^2 + 2n_{eff}^2}\right)} \qquad (5.2)$$

and inserting $n_1 = n_{air} = 1$, $n_2 = n_{PDMS} = 1.413$ and $n_{eff} = n_{water} = 1.33$. The result is $f = 0.195$, which means that to achieve an effective refractive index slightly lower than that of water the volumetric fraction of air pores must be around 20%.

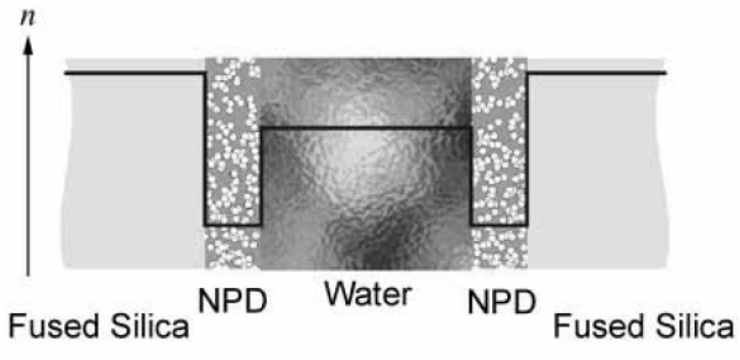

Figure 5.1: Cross section of a water-core waveguide. The channel walls are covered with a nanoporous dielectic (NPD) material with lower refractive index than water. Light injected along the channel will be confined in the water core by total internal reflection. (reproduced from [128])

This kind of approach is commonly used to tune the refractive index of nanoporous silicon[125–127], and has also been applied to realize a water-core, silica-cladding waveguide. In this last work[128], a nanoporous silica layer was deposited on the walls of a microchannel engraved in bulk silica to lower the refractive index and confine light in the water-filled channel (see Figure 5.1). Realizing a similar structure in PDMS would maintain the waveguiding effect without harming any existing tunability property of the module.

5.1.3 Refractive index step tunability

There is another advantage in employing porous PDMS claddings. The effective refractive index can be finely tuned by varying the volumetric fraction of air included in the material, increasing or reducing as needed the refractive index step between core and cladding. This possibility is highly beneficial, since the magnitude of this step in refractive index controls the properties of the waveguide by setting the critical angle for total internal reflection (see equation (4.1)). This means that waveguides with a high index step will be able to confine in the core light coming to the entrance of the guide from a wide range of angles, facilitating alignment and reducing coupling losses. On the other hand, inside the waveguide different light rays will travel markedly different paths, leading to signal blurring. Also, the exit cone of the light will be symmetrical to the entrance one, meaning that the exiting light will be highly divergent. All of this reasoning is reversed for a low index step waveguide, which require a finer alignment but provides lower divergence for the exiting light.

Once a reliable method to generate nanoporous PDMS is established, the magnitude of refractive index step between core and cladding could be selected during module design depending on the requirements of the final device.

5.2 Experimental attempts

This Section reports the experimental attempts made as part of this thesis work to fabricate a porous PDMS with refractive index lower than that of water. To date, this efforts have not been completely successful due to the fact that the generated pores are still too big to allow the effective medium approximation described by equation (5.1).

5.2.1 Sample preparation

Porous PDMS has been prepared with a procedure similar to that described in Section 2.1.3. PDMS prepolymer and iniziator (Dow Corning Sylgard 184) are mixed in a 10:1 ratio, and water is added to the blend in proportion variable from 5% to 15% (v/v) with respect to PDMS prepolymer. Finally, Triton X-100 surfactant (Sigma Aldritch) is added in proportion variable from 1% to 5% (v/v) with respect to PDMS prepolymer. The mixture is then stirred vigorously and degassed in mild vacuum to remove trapped air bubbles. Next, the blend is poured in a mould previously heated to 90°C on a hotplate and kept at that temperature for 1 hour to trigger the polymerization of PDMS which traps the tiny water droplets inside the material. Finally, the now solid sample is removed from the mould and subjected to a second thermal treatment in an oven at 120°C in mild vacuum for 1 to 4 hours. This second bake promotes the evaporation of water, leaving air bubbles in the PDMS. The presence of Triton X-100 surfactant makes this material a ternary mixture, and thus different from the case considered by equation (5.1). In an attempt to remove the surfactant through evaporation, the samples have been subjected to a third thermal treatment on a hotplate at 300°C for 1 hour. However, upon characterization this additional step did not modify in any way the measured refractive index. On the other hand, the samples appeared slightly browned in color, suggesting thermal oxidative degradation of the surfactant instead of evaporation. According to Mitsuda et al.[129], performing this last step in an inert atmosphere should lead to efficient removal.

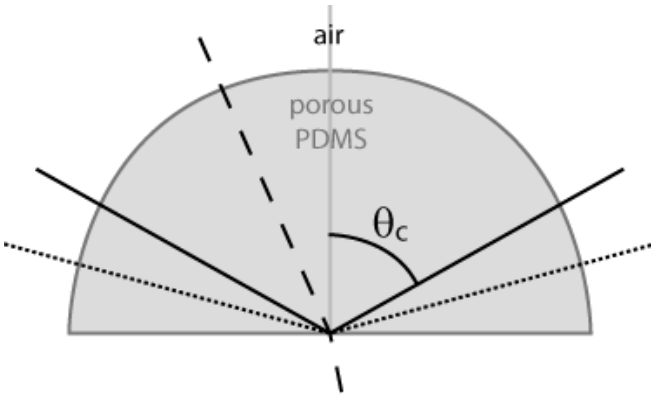

Figure 5.2: Refractive index measurement. When the laser beam impacts the flat side with a small angle, it is transmitted (dashed line), while if the angle is high the beam is total-reflected (dotted line). The transition between the two is set by the critical angle θ_c (solid line).

5.2.2 Sample characterization

Samples have been characterized with two different methods. In the first, porous PDMS half-disks are used to measure the critical total reflection angle θ_c of the material by shining the beam of a He-Ne laser through the sample and measuring the incident angle at which the beam is no longer transmitted (see Figure 5.2). From this angle, the refractive index can be calculated rearranging equation (4.1) to give:

$$n_{PDMS} = \frac{1}{\sin\theta_c} \qquad (5.3)$$

The second method makes instead use of a thin (~1 mm) layer of porous PDMS whose refractive index is measured with an Abbe refractometer (Officine Galileo).

5.2.3 Results

All tested samples, regardless of the volumetric fraction of water and/or surfactant present in the mixture, feature the same refractive index of pure PDMS. This results are attributed to the fact that the generated bubbles are too big, meaning that the incident light does not treat the mix as a single material, but is instead simply scattered by the

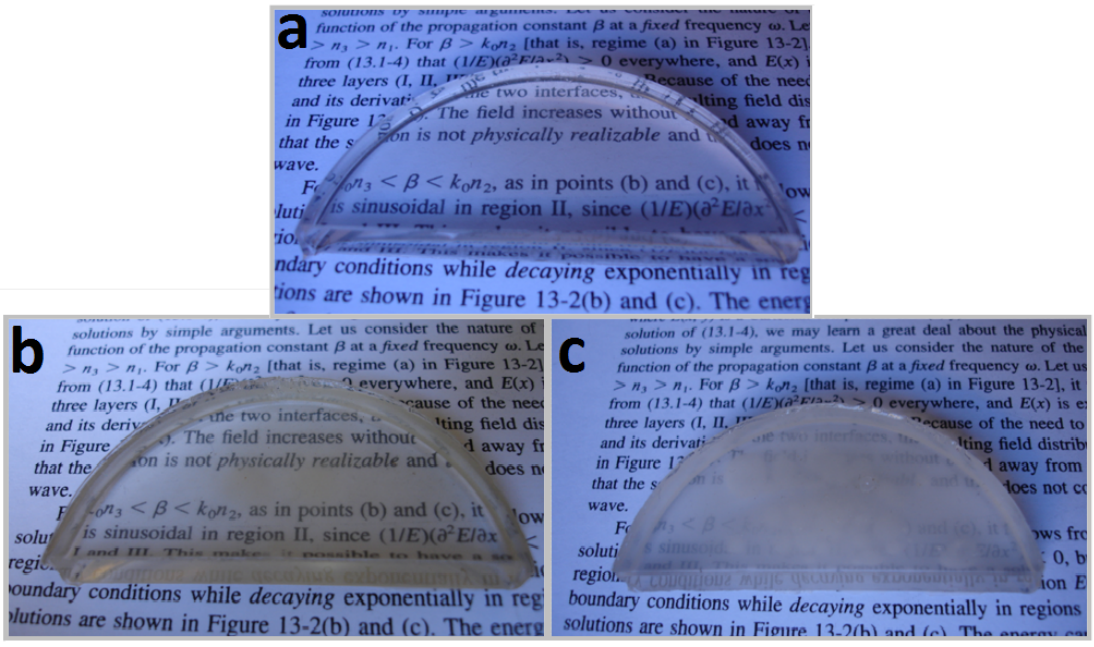

Figure 5.3: Samples of porous PDMS prepared with increasing water content: a) 5%; b) 10%; c) 15%.

pores. Supporting this explanation is the fact that all samples appear opaque under white light, and the opacity increases with increasing water content (see Figure 5.3). This appearance suggests that the air bubbles inside the PDMS have a diameter on the order of hundreds of nanometers to a few micrometers, so to efficiently scatter visible light.

The difficulty in obtaining small pores is related to the hydrophobicity of PDMS, which makes the generation of small water droplets strongly energetically unfavorable, even when a surfactant is added to the mix. This limit can be mitigated by using a different, more affine, species as templating liquid. Unfortunately, a too strong affinity will usually translate in actual mixing between liquid and (unpolymerized) PDMS, preventing the formation of two distinct phases. Thus, a balance must be stroke so that droplets are formed, but the surface energy between the two phases is low enough to keep the emulsion stable until PDMS polymerization.

Following this reasoning, an attempt was made to substitute water with acetonitrile. An emulsion was formed with unpolymerized PDMS as described in Section 5.2.1 except for the first bake temperature that was reduced to 70°C to prevent acetonitrile from boiling. The resulting samples show a noticeable degrade in terms of elasticity and appear not completely polymerized even after several days, probably due to unfavorable interactions between acetonitrile and PDMS. Moreover, the refractive index was still that of pure PDMS.

5.2.4 Future prospects

Future experiments concerning this part of the work will concentrate on the identification of a suitable templating fluid to generate nanometric pores in PDMS. Also, different surfactants and will be tested, as well as different processes to generate the initial emulsion. If a porous material of suitable refractive index can be generated, liquid-core waveguides will be tested by depositing a thin layer of this material on the inside walls of a microchannel engraved in bulk PDMS. While this will bring the porous

material in direct contact with the flowing water, it is expected that the hydrophobicity of PDMS will inhibit the fluid from entering the nanometric pores.

Conclusions

The work in this thesis was aimed at the realization of single-function modules ready for inclusion into modular microfluidic devices (MFDs). The rationale behind this aim in that once a suitable collection of different modules has been created, MFDs for a great number of different applications can be realized by simply combining the modules that carry out the required functionalities.

The modules have been realized through PDMS replica molding, a well-established technique frequently employed in literature. The masters to be replicated have been realized in the commercial photoresist SU-8 with masked UV photolithography or direct laser writing (DLW). While UV-photolithography is a fast method to structure large areas, the better resolution of DLW allows the realization of smaller features. This benefit is further enhanced by the employment of laser writing mediated by two-photon processes, since the strong dependency of non-linear absorption on incident light intensity allows a very fine control on the photopolymerization process.

The use of PDMS as bulk material for microdevices has several advantages, including optical transparency, good resistance to water and a marked elasticity that facilitate the detachment of the PDMS replica from the SU-8 master. Unfortunately, this same elasticity also causes some limitations on the shapes that can be created, since high aspect ratio structures will usually collapse under their own weight. For this reason, a new photopolymerizable hybrid organic/inorganic sol-gel material was proposed and characterized. This blend has better mechanical properties and chemical resistance than PDMS. It also allows two-photon DLW with good resolution (down to 600 nm), and shows a clear relation between diameter of the polymerized area, exposure time and laser power. However, results from different batches of the same blend are only reproducible within ~500 nm, so if submicrometric resolutions are required, the exact response of each batch of material will have to be calibrated before use. Another limiting factor of this sol-gel blend is that, while its hybrid nature confers it a reduced

stiffness compared to fully inorganic materials, still the shrinkage occurring during polymerization produces cracks in structures with more than one dimension exceeding 1-2 μm. This limit translates into the fact that this blend cannot be used as bulk material for MFDs, but it is an excellent candidate for the realization of specific internal sub-structurations that PDMS cannot replicate. To extend the field of applicability of this material, the biocompatibility of flat, fully polymerized sol-gel substrates was tested by growing primary HUVEC cells and comparing their proliferation to that of a control sample grown on a glass substrate. The results confirmed the biocompatibility of this blend, but also revealed another potential problem. Even for the fully polymerized material, a small fraction of the photoinitiator remains unreacted. This species is fluorescent in a range overlapping that of some fluorescent labels commonly used in biology-related work (mainly DAPI and BrdU). This means that a number of typical tests performed on this substrate will suffer from a diffuse background that will degrade the signal to noise ratio of the measurement.

The first microfluidic module that has been realized is a mixer. Fluids inside micrometric channel are subjected to laminar conditions, i.e. their vectorial velocity has only one component, parallel to the channel axis. This means that two different miscible liquids brought into contact inside a microchannel will only mix through chemical diffusion, a slow process compared to the residence time of the fluid inside the MFD. To increase the mixing efficiency, and thus the time required to blend the different fluids, specific microfluidic elements must be designed. In this work one such element was realized by inserting multiple obstructions inside a microchannel to locally perturb the laminar conditions and thus favor mixing. A preliminary screening of different designs was performed by means of numerical simulations, and two promising layouts were tested experimentally. To quantify the mixing efficiency, a fluorophore solution and pure solvent were injected in the upper arms of a T-shaped channel and brought into contact at the junction. Fluorescence intensity profiles were recorded across the channel at different distances from the junction and the degree of mixing was estimated

considering a flat, uniform intensity profile as 100% and a vertical drop from maximum to zero as 0%. The results were in good agreement with the simulation predictions, and demonstrated that the channel with bigger and higher obstacles was the most efficient. Slight deviations of the measured mixing efficiencies from the simulated ones were attributed to fabrication imperfections.

The second microfluidic module that has been realized is a light switch for optofluidic applications. This device exploits a water/air segmented flow to alternatively transmit and reflect a laser beam incident on the channel. This behavior is due to the difference in refractive index between the two fluids composing the segmented flow. For the selected light incidence angle (60°), the refractive index of air triggers total internal reflection inside the bulk PDMS that surrounds the channel, preventing the light from being transmitted. On the contrary, the higher refractive index of water is too similar to that of PDMS to achieve the same phenomenon, and the light can pass through the channel. The result is a periodic deflection of the inbound laser towards one of two well-defined directions. The duty cycle of the device (the fraction of the total period spent by the laser beam in the reflected state), was found to be constant at 50% for all tested injection flow rates. Since some applications would benefit from a variable duty cycle, a method for its modulation was proposed and tested: an increase in the water phase temperature. This method proved effective, causing a reproducible decrease in duty cycle from 50% to 25% with a temperature variation of less than 10 K. The dependency of the switching frequency of the device on injection flow rate was also characterized, and showed a nonlinear increase at higher flow rates. This effect was attributed both to the faster movement of segments inside the channel and to the generation of shorter segments at higher flow rates. Notwithstanding the simple design and realization of this device, the module proved to be stable for very long times for flow rates up to 1.5 ml/min. It is probable that higher flow rates could be supported if the fabrication technique was improved to achieve better quality channels. However,

flow rates up to 1.5 ml/min have been deemed sufficient for most applications, and so to preserve ease of fabrication this further modifications were not explored.

Finally, a number of attempts to realize a nanoporous, low refractive index PDMS have been reported. Water and a surfactant have been mixed to unpolymerized PDMS and forced to generate an emulsion of water droplets, which is then fixed by thermal polymerization of the continuous phase (PDMS). Finally, water is removed by evaporation to give the final porous PDMS. The generation of nanometric pores would reduce the refractive index of the whole material, allowing its employment as cladding for water-core waveguides (e.g. microfluidic channels). Unfortunately, up to date it has been impossible to generate sufficiently small water droplets. This fact is attributed to the high surface energy of the PDMS-water interface, which makes small droplets energetically unfavorable. This limit could be overcome employing a more affine liquid, a more efficient surfactant or a different method to generate the emulsion. Future works will concentrate on these strategies.

Bibliography

[1] G. M. Whitesides, *Nature* **2006**, *442*, 368–73.

[2] O. Reynolds, *Philosophical transactions of the Royal Society* **1883**, *174*, 935–982.

[3] N. Rott, *Annual review of fluid mechanics* **1990**, *24*, 1–11.

[4] R. Wootton, R. Fortt, A. DeMello, *Organic process research & development* **2002**, *6*, 2000–2002.

[5] X. Zhang, S. Stefanick, F. Villani, *Organic process research & development* **2004**, *8*, 455–460.

[6] R. A. Maurya, C. P. Park, J. H. Lee, D.-P. Kim, *Angewandte Chemie international edition* **2011**, *50*, 5952–5955.

[7] J. McMullen, K. Jensen, *Organic process research & development* **2010**, *107*, 1169–1176.

[8] A. D. Beaton, V. J. Sieben, C. F. A. Floquet, E. M. Waugh, S. Abi Kaed Bey, I. R. G. Ogilvie, M. C. Mowlem, H. Morgan, *Sensors and actuators B: Chemical* **2011**, *156*, 1009–1014.

[9] P. Liu, J. R. Scherer, S. a Greenspoon, T. N. Chiesl, R. a Mathies, *Forensic science international: Genetics* **2011**, *5*, 484–492.

[10] D. Voicu, C. Scholl, W. Li, D. Jagadeesan, I. Nasimova, J. Greener, E. Kumacheva, *Macromolecules* **2012**, *45*, 4469–4475.

[11] J. Sun, Y. Zheng, X. Feng, W. Du, B.-F. Liu, *Analytica chimica acta* **2012**, *721*, 104–109.

[12] W.-Y. Lin, Y. Wang, S. Wang, H.-R. Tseng, *Nano today* **2009**, *4*, 470–481.

[13] P. K. Yuen, *Lab on a chip* **2008**, *8*, 1374–1378.

[14] C. B. Kennedy, *Multiplexed Microfluidic Devices and Systems*, **2000**, U.S. Patent 6,086,740.

[15] S. D. O'Connor, C. D. Karp, E. Dantsker, M. Pezzuto, *Modular Microfluidic Systems*, **2004**, U.S. Patent 6,827,095 B2.

[16] P. Zhou, L. Young, *Reconfigurable Modular Microfluidic System and Method of Fabrication*, **2006**, U.S. Patent 7,011,793 B2.

[17] N. L. Jeon, D. T. Chiu, C. J. Wargo, H. Wu, I. S. Choi, J. R. Anderson, G. M. Whitesides, *Biomedical microdevices* **2002**, *4*, 117–121.

[18] Y. S. Song, *Carbon* **2012**, *50*, 1417–1421.

[19] M. A. Unger, H.-P. Chou, T. Thorsen, A. Scherer, S. R. Quake, *Science* **2000**, *288*, 113–116.

[20] K. W. Oh, C. H. Ahn, *Journal of micromechanics and microengineering* **2006**, *16*, R13–R39.

[21] D. D. Nolte, *Review of scientific instruments* **2009**, *80*, 101101.

[22] J. Ducrée, S. Haeberle, S. Lutz, S. Pausch, F. von Stetten, R. Zengerle, *Journal of micromechanics and microengineering* **2007**, *17*, S103–S115.

[23] J. Kim, H. Kido, R. H. Rangel, M. J. Madou, *Sensors and actuators B: Chemical* **2008**, *128*, 613–621.

[24] B. D. Iverson, S. V. Garimella, *Microfluidics and nanofluidics* **2008**, *5*, 145–174.

[25] Z. Chen, P. Wang, H.-C. Chang, *Analytical and bioanalytical chemistry* **2005**, *382*, 817–824.

[26] X. Niu, Y.-K. Lee, *Journal of micromechanics and microengineering* **2003**, *13*, 454–462.

[27] D. Ahmed, X. Mao, J. Shi, B. K. Juluri, T. J. Huang, *Lab on a chip* **2009**, *9*, 2738–2741.

[28] B. He, B. J. Burke, X. Zhang, R. Zhang, F. E. Regnier, *Analytical chemistry* **2001**, *73*, 1942–1947.

[29] J. Knight, A. Vishwanath, J. Brody, R. Austin, *Physical review letters* **1998**, *80*, 3863–3866.

[30] A. D. Stroock, S. K. W. Dertinger, A. Ajdari, I. Mezic, H. A. Stone, G. M. Whitesides, *Science* **2002**, *295*, 647–651.

[31] C.-Y. Lee, C.-L. Chang, Y.-N. Wang, L.-M. Fu, *International journal of molecular sciences* **2011**, *12*, 3263–3287.

[32] M. Toda, T. Otake, H. Miyashita, Y. Kawai, T. Ono, *Microsystem technologies* **2012**, DOI 10.1007/s00542-012-1698-3.

[33] Z.-R. Xu, Z.-L. Fang, *Analytica chimica acta* **2004**, *507*, 129–135.

[34] A. Evstrapov, N. Esikova, *Optica applicata* **2008**, *38*, 31–38.

[35] L. Zhu, L. Hou, W. Zhang, *Sensors and actuators B: Chemical* **2010**, *148*, 135–146.

[36] P. K. Yuen, V. N. Goral, *Journal of chemical education* **2012**, *89*, 1288–1292.

[37] H. Löwe, W. Ehrfeld, *Electrochimica acta* **1999**, *44*, 3679–3689.

[38] J. Brandner, in *Microreactors in Organic Synthesis and Catalysis* (Ed.: T. Wirth), Wiley-VCH, **2008**.

[39] H. Becker, L. E. Locascio, *Talanta* **2002**, *56*, 267–287.

[40] S. K. Sia, G. M. Whitesides, *Electrophoresis* **2003**, *24*, 3563–3576.

[41] J. C. McDonald, G. M. Whitesides, *Accounts of chemical research* **2002**, *35*, 491–9.

[42] J. C. McDonald, D. C. Duffy, J. R. Anderson, D. T. Chiu, H. Wu, O. J. A. Schueller, G. M. Whitesides, *Electrophoresis* **2000**, *21*, 27–40.

[43] W. Schrott, M. Svoboda, Z. Slouka, M. Přibyl, D. Šnita, *Microelectronic engineering* **2010**, *87*, 1600–1602.

[44] Y. Xia, G. M. Whitesides, *Angewandte Chemie international edition* **1998**, *37*, 550–575.

[45] J. N. Lee, C. Park, G. M. Whitesides, *Analytical chemistry* **2003**, *75*, 6544–6554.

[46] T. C. Merkel, V. I. Bondar, K. Nagai, B. D. Freeman, I. Pinnau, *Journal of polymer science B: Polymer physics* **2000**, *38*, 415–434.

[47] T. Zhu, K. H. Row, *Journal of separation science* **2012**, *35*, 1294–1302.

[48] F. Mammeri, L. Rozes, E. Le Bourhis, C. Sanchez, *Journal of the european ceramic society* **2006**, *26*, 267–272.

[49] M. Sajjad, B. Feichtenschlager, S. Pabisch, J. Svehla, T. Koch, S. Seidler, H. Peterlik, G. Kickelbick, *Polymer international* **2012**, *61*, 274–285.

[50] A. Ershad- Langroudi, C. Mai, G. Vigier, R. Vassoille, *Journal of applied polymer science* **1998**, *65*, 5–11.

[51] V. Purcar, I. Stamatin, O. Cinteza, C. Petcu, V. Raditoiu, M. Ghiurea, T. Miclaus, A. Andronie, *Surface and coatings technology* **2012**, *206*, 4449–4454.

[52] C. Sanchez, B. Lebeau, F. Chaput, J.-P. Boilot, *Advanced materials* **2003**, *15*, 1969–1994.

[53] Y. Wang, H. Kim, *Organic electronics* **2012**, *13*, 2997–3003.

[54] S. Dirè, V. Tagliazucca, G. Brusatin, J. Bottazzo, I. Fortunati, R. Signorini, T. Dainese, C. Andraud, M. Trombetta, M. L. Di Vona, et al., *Journal of sol-gel science and technology* **2008**, *48*, 217–223.

[55] J. S. Mecomber, D. Hurd, P. a. Limbach, *International journal of machine tools and manufacture* **2005**, *45*, 1542–1550.

[56] M.-S. Huang, Y.-C. Chiang, S.-C. Lin, H.-C. Cheng, C.-F. Huang, Y.-K. Shen, Y. Lin, *Polymers for advanced technologies* **2012**, *23*, 57–64.

[57] A. a Tseng, *Journal of micromechanics and microengineering* **2004**, *14*, R15–R34.

[58] A. A. Evstrapov, I. S. Mukhin, I. V. Kukhtevich, A. S. Bukatin, *Technical physics letters* **2011**, *37*, 956–959.

[59] H.-W. Li, D.-J. Kang, M. G. Blamire, W. T. S. Huck, *Nanotechnology* **2003**, *14*, 220–223.

[60] C. M. Kolodziej, H. D. Maynard, *Chemistry of materials* **2012**, *24*, 774–780.

[61] D. M. Koller, A. Hohenau, H. Ditlbacher, N. Galler, A.-L. Baudrion, F. Reil, S. Schausberger, F. R. Aussenegg, A. Leitner, J. R. Krenn, *Microelectronic engineering* **2008**, *85*, 1639–1641.

[62] C. Iliescu, B. Chen, J. Miao, *Sensors and actuators A: Physical* **2008**, *143*, 154–161.

[63] X. Li, T. Abe, M. Esashi, *Sensors and actuators A: Physical* **2001**, *87*, 139–145.

[64] H. H. Solak, *Journal of physics D: Applied physics* **2006**, *39*, R171–R188.

[65] M. Goeppert-Mayer, *Annalen der Physik* **1931**, *9*, 273–295.

[66] S. Maruo, S. Kawata, *Journal of microelectromechanical systems* **1998**, *7*, 411–415.

[67] K. K. Seet, V. Mizeikis, S. Juodkazis, H. Misawa, *Applied physics letters* **2006**, *88*, 221101.

[68] T. Baldacchini, *Journal of applied physics* **2004**, *95*, 6072–6076.

[69] C. N. LaFratta, J. T. Fourkas, T. Baldacchini, R. A. Farrer, *Angewandte Chemie international edition* **2007**, *46*, 6238–6258.

[70] J. Fischer, M. Wegener, *Laser & photonics reviews* **2012**, *23*, 1–23.

[71] S.-H. Park, D.-Y. Yang, K.-S. Lee, *Laser & photonics review* **2009**, *3*, 1–11.

[72] S. Bhattacharya, A. Datta, J. M. Berg, S. Gangopadhyay, *Journal of microelectromechanical systems* **2005**, *14*, 590–597.

[73] C. N. LaFratta, T. Baldacchini, R. a. Farrer, J. T. Fourkas, M. C. Teich, B. E. a. Saleh, M. J. Naughton, *Journal of physical chemistry B* **2004**, *108*, 11256–11258.

[74] C. Monat, P. Domachuk, B. Eggleton, *Nature photonics* **2007**, *1*, 106–114.

[75] U. Levy, R. Shamai, *Microfluidics and nanofluidics* **2007**, *4*, 97–105.

[76] W. Song, A. E. Vasdekis, D. Psaltis, *Lab on a chip* **2012**, *12*, 3590–3597.

[77] M. Oelgemöller, O. Shvydkiv, *Molecules* **2011**, *16*, 7522–7550.

[78] S. E. Chung, W. Park, H. Park, K. Yu, N. Park, S. Kwon, *Applied physics letters* **2007**, *91*, 041106.

[79] D. Cialla, A. März, R. Böhme, F. Theil, K. Weber, M. Schmitt, J. Popp, *Analytical and bioanalytical chemistry* **2012**, *403*, 27–54.

[80] E. Le Ru, E. Blackie, *Journal of physical chemistry C* **2007**, *111*, 13794–13803.

[81] C. Lim, J. Hong, B. G. Chung, A. J. DeMello, J. Choo, *The analyst* **2010**, *135*, 837–844.

[82] I. M. White, S. H. Yazdi, W. W. Yu, *Microfluidics and nanofluidics* **2012**, *13*, 205–216.

[83] J. Zhou, K. Ren, Y. Zhao, W. Dai, H. Wu, *Analytical and bioanalytical chemistry* **2012**, *402*, 1601–1609.

[84] W. Wang, C. Yang, X. Q. Cui, Q. L. Bao, C. M. Li, *Microfluidics and nanofluidics* **2010**, *9*, 1175–1183.

[85] K. D. Kihm, S. Cheon, J. S. Park, H. J. Kim, J. S. Lee, I. T. Kim, H. J. Yi, *Optics and lasers in engineering* **2012**, *50*, 64–73.

[86] N. Zhang, H. Liu, W. Knoll, *Biosensors & bioelectronics* **2009**, *24*, 1783–1787.

[87] C. Huang, K. Bonroy, G. Reekmans, W. Laureyn, K. Verhaegen, I. De Vlaminck, L. Lagae, G. Borghs, *Biomedical microdevices* **2009**, *11*, 893–901.

[88] A. Hemmi, T. Usui, A. Moto, T. Tobita, N. Soh, K. Nakano, H. Zeng, K. Uchiyama, T. Imato, H. Nakajima, *Journal of separation science* **2011**, *34*, 2913–2919.

[89] R. Hall, G. Fenner, J. Kingsley, T. Soltys, R. Carlson, *Physical review letters* **1962**, *9*, 366–368.

[90] W. Song, D. Psaltis, *Applied physics letters* **2010**, *96*, 081101.

[91] Z. Li, Z. Zhang, A. Scherer, D. Psaltis, *Optics express* **2006**, *14*, 10494–10499.

[92] H. Schmidt, A. R. Hawkins, *Microfluidics and nanofluidics* **2007**, *4*, 3–16.

[93] M. A. Duguay, Y. Kokubun, T. L. Koch, L. Pfeiffer, *Applied physics letters* **1986**, *49*, 13–15.

[94] T. Baba, Y. Kokubun, *Photonics technology letters* **1989**, *1*, 232–234.

[95] W. Huang, R. M. Shubair, N. Arokia, Y. L. Chow, *Journal of lightwave technology* **1992**, *10*, 1015–1022.

[96] G. Testa, Y. Huang, L. Zeni, *Photonics technology letters* **2012**, *24*, 1307–1309.

[97] D. B. Wolfe, R. S. Conroy, P. Garstecki, B. T. Mayers, M. a Fischbach, K. E. Paul, M. Prentiss, G. M. Whitesides, *Proceedings of the National Academy of Sciences* **2004**, *101*, 12434–12438.

[98] D. B. Wolfe, D. V. Vezenov, B. T. Mayers, G. M. Whitesides, R. S. Conroy, M. G. Prentiss, *Applied physics letters* **2005**, *87*, 181105.

[99] S. Kuiper, B. H. W. Hendriks, *Applied physics letters* **2004**, *85*, 1128–1130.

[100] N. Chronis, G. Liu, K.-H. Jeong, L. Lee, *Optics express* **2003**, *11*, 2370–2378.

[101] W. H. Teh, U. Dürig, U. Drechsler, C. G. Smith, H.-J. Güntherodt, *Journal of applied physics* **2005**, *97*, 054907.

[102] A. Del Campo, C. Greiner, *Journal of micromechanics and microengineering* **2007**, *17*, R81–R95.

[103] H. J. Kong, S. W. Yi, D.-Y. Yang, K.-S. Lee, *Journal of the korean physical society* **2009**, *54*, 215–219.

[104] S. Keller, G. Blagoi, M. Lillemose, D. Haefliger, A. Boisen, *Journal of micromechanics and microengineering* **2008**, *18*, 125020.

[105] K. K. Seet, S. Juodkazis, V. Jarutis, H. Misawa, *Applied physics letters* **2006**, *89*, 024106.

[106] W. F. Schroeder, S. L. Asmussen, W. D. Cook, C. I. Vallo, *Polymer international* **2011**, *60*, 1362–1369.

[107] V. McGinniss, T. Provder, C. Kuo, A. Gallopo, *Macromolecules* **1978**, *11*, 393–404.

[108] J. Serbin, A. Egbert, A. Ostendorf, B. N. Chichkov, R. Houbertz, G. Domann, J. Schulz, C. Cronauer, L. Fröhlich, M. Popall, *Optics letters* **2003**, *28*, 301–303.

[109] E. Hecht, *Optics*, Addison Wesley, **2002**.

[110] K. J. Schafer, J. M. Hales, M. Balu, K. D. Belfield, E. W. Van Stryland, D. J. Hagan, *Journal of photochemistry and photobiology A: Chemistry* **2004**, *162*, 497–502.

[111] M. L. B. Palacio, B. Bhushan, *Philosophical transactions of the Royal Society A* **2012**, *370*, 2321–2347.

[112] Z. L. Zhang, C. Crozatier, M. Le Berre, Y. Chen, *Microelectronic engineering* **2005**, *78-79*, 556–562.

[113] E. van Veldhoven, H. Zhang, W. Rettig, R. G. Brown, J. D. Hepworth, *Chemical physics letters* **2002**, *363*, 189–197.

[114] T. Wilson, *Journal of microscopy* **2011**, *242*, 111–116.

[115] M. Miki, C. G. dos Remedios, *Journal of biochemistry* **1988**, *104*, 232–235.

[116] I. Fortunati, N. Rossetto, R. Signorini, C. Ferrante, S. Carlotto, A. Polimeno, *La houille blanche* **2011**, *4*, 79–85.

[117] L. Wang, Y. Zhang, L. Cheng, *Chaos, solitons & fractals* **2009**, *39*, 1530–1537.

[118] V. van Steijn, M. T. Kreutzer, C. R. Kleijn, *Chemical engineering science* **2007**, *62*, 7505–7514.

[119] M. De Menech, P. Garstecki, F. Jousse, H. a. Stone, *Journal of fluid mechanics* **2008**, *595*, 141–161.

[120] T. Fu, Y. Ma, D. Funfschilling, C. Zhu, H. Z. Li, *Chemical engineering science* **2010**, *65*, 3739–3748.

[121] P. Garstecki, M. J. Fuerstman, H. a Stone, G. M. Whitesides, *Lab on a chip* **2006**, *6*, 437–446.

[122] C. P. Ody, *Microfluidics and nanofluidics* **2009**, *9*, 397–410.

[123] R. Dreyfus, P. Tabeling, H. Willaime, *Physical review letters* **2003**, *90*, 1–4.

[124] D. A. G. Bruggeman, *Annalen der Physik* **1935**, *416*, 636–664.

[125] E. V. Astrova, V. a. Tolmachev, *Materials science and engineering: B* **2000**, *69-70*, 142–148.

[126] S. Setzu, R. Romestain, V. Chamard, *Thin solid films* **2004**, *460*, 53–57.

[127] V. Torres-Costa, R. J. Martín-Palma, *Journal of materials science* **2010**, *45*, 2823–2838.

[128] W. Risk, H. Kim, R. Miller, H. Temkin, S. Gangopadhyay, *Optics express* **2004**, *12*, 6446–6455.

[129] K. Mitsuda, H. Kimura, T. Murahashi, *Journal of materials science* **1989**, *24*, 413–419.

Ringraziamenti

Tre anni di lavoro significano necessariamente un buon numero di collaborazioni e contributi, e per diretta conseguenza un certo numero di doverosi ringraziamenti.
Il primissimo ringraziamento va sicuramente al mio supervisore di dottorato, prof. Camilla Ferrante, il cui contributo è stato sicuramente determinante sia per il lavoro qui riportato che per la mia crescita scientifica. Un grazie va anche alla dr. Raffaella Signorini, al prof. Danilo Pedron e al prof. Renato Bozio per le utilissime discussioni e per la disponibilità che hanno sempre dimostrato.
Un ringraziamento sentito va poi a Simone Crivellaro e a tutti i miei vecchi e nuovi colleghi di laboratorio (Alessandro, Alessia, Caterina, Eleonora, Elisabetta, Francesco, Ida, Ilaria, Luca, Lucio, Maria Chiara, Roberto, Verena) che si sono sempre dimostrati molto disponibili nel dare una mano qualora fosse necessario. Tra tutti merita una menzione d'onore la dr. Ilaria Fortunati, senza il cui contributo questo lavoro e in generale la mia esperienza scientifica sarebbero stati assai più poveri.
Fuori dai confini del gruppo di ricerca meritano un ringraziamento per l'aiuto che mi hanno dato anche il dr. Davide Ferraro e il dr. Simone Silvestrini, assieme al dr. Matteo Pierno, al prof. Giampaolo Mistura e al prof. Michele Maggini.
Per il lavoro riportato nel capitolo due, un ringraziamento è dovuto alla dr. Gioia Della Giustina, alla prof. Giovanna Brusatin e alla prof. Sandra Dirè per la sintesi dei materiali ibridi, e alla dr. Elisa Sorato e alla prof. Giovanna Albertin per le prove di biocompatibilità. Un grazie va anche al dr. Francesco Todescato per le immagini SEM delle strutture prodotte.
Per il lavoro riportato nel capitolo tre, un ringraziamento sentito va alla dr. Silvia Carlotto (per le simulazioni teoriche) e alla dr. Ilaria Fortunati (per le caratterizzazioni di fluorescenza).
Per il lavoro riportato nel capitolo cinque, un ringraziamento va al prof. Danilo Pedron per l'aiuto nella determinazione dell'indice di rifrazione dei campioni ottenuti.
Infine, poiché una vita serena fuori dal laboratorio contribuisce in modo determinante ad una proficua esperienza lavorativa, un particolare ringraziamento, collettivo ma sincero, va ai miei familiari, ai miei amici, ai miei coinquilini e soprattutto, più di tutti, ad una certa scienziata dei materiali adottiva di nome Antonella.